# U.S. Coast Guard Research and Development Center

### 1082 Shennecossett Road, Groton, CT 06340-6096

## Report No. CG-D-12-01

## DYNAMIC SIMULATION OF A FUEL
## CELL-POWERED ELECTRIC-DRIVE SHIP

**FINAL REPORT**
**FEBRUARY 2001**

This document is available to the U.S. public through the
National Technical Information Service, Springfield, VA 22161

Prepared for:

U.S. Department of Transportation
United States Coast Guard
Operations (G-O)
Washington, DC 20593-0001

**20010711 100**

# NOTICE

This document is disseminated under the sponsorship of the Department of Transportation in the interest of information exchange. The United States Government assumes no liability for its contents or use thereof.

The United States Government does not endorse products or manufacturers. Trade or manufacturers' names appear herein solely because they are considered essential to the object of this report.

This report does not constitute a standard, specification, or regulation.

Marc B. Mandler, Ph.D.
Technical Director
United States Coast Guard
Research & Development Center
1082 Shennecossett Road
Groton, CT 06340-6096

ii

| 1. Report No.  CG-D-12-01 | 2. Government Accession Number | 3. Recipient's Catalog No. | |
|---|---|---|---|
| 4. Title and Subtitle  Dynamic Simulation of a Fuel Cell-Powered Electric-Drive Ship | | 5. Report Date  February 2001 | |
| | | 6. Performing Organization Code  Project No. 3310.2 | |
| 7. Author(s)  Z. Karni, H. Ghezel, M. Lucas, A. Shecter, G. Rossi | | 8. Performing Organization Report No.  R&DC 441 | |
| 9. Performing Organization Name and Address  John J. McMullen Associates, Inc.  4300 King Street, Suite 400  Alexandria, VA 22302 | U.S. Coast Guard  Research and Development Center  1082 Shennecossett Road  Groton, CT  06340-6096 | 10. Work Unit No. (TRAIS) | |
| | | 11. Contract or Grant No.  DTCG39-95-D-E99010 T.O. 98FE00260 | |
| 12. Sponsoring Organization Name and Address  U.S. Department of Transportation  United States Coast Guard  Operations (G-O)  U.S. Coast Guard Headquarters  Washington, DC 20593-0001 | | 13. Type of Report & Period Covered  Final Report | |
| | | 14. Sponsoring Agency Code  Commandant (G-OCU-1)  U.S. Coast Guard Headquarters  Washington, DC 20593-0001 | |

15. Supplementary Notes

The R&D Center's technical point of contact is Robert D. Sedat, 860-441-2684, email: rsedat@rdc.uscg.mil.

16. Abstract (MAXIMUM 200 WORDS)

This report describes a dynamic simulation model (DSM) of an electrically propelled ship with power provided by four 625 kW fuel cells. The model allows prediction of transient responses, and allows design modifications to be made inexpensively prior to hardware construction. Simulations are performed for extreme acceleration and deceleration maneuvers, and the responses are compared to those of diesel and turbine-powered ships. It is concluded that a fuel cell-powered ship can achieve transient responses comparable to those of conventionally powered vessels.

The report documents refinements to the existing DSM model of Fuel Cell Energy (FCE) Corporation's diesel-fueled molten carbonate fuel cell module. The DSM is based on principles of mass and energy balance, and incorporates dynamic characteristics of the fuel cell, all balance-of-plant components, the controller, electric bus, AC propulsion motors, shafting and propellers. Recent changes in FCE's design improve the power module's transient response. Rapid accelerations and crash stop maneuvers were simulated. Results showed the need for careful coordination between available power, the torque absorption of the AC motors, and total system load requirements. For crash stops, shaft brakes were used to reduce propeller RPM. Resistance banks, included in the model, can also be used to absorb excess power, and some fuel cell venting may be required. It is shown that a fuel cell-powered ship can achieve starting and stopping distances considered acceptable under current practice.

| 17. Key Words  fuel cell, electric drive, dynamic simulation, ship maneuvering, ship acceleration, head reach parameter | 18. Distribution Statement  This document is available to the U.S. public through the National Technical Information Service, Springfield, VA 22161 | | |
|---|---|---|---|
| 19. Security Class (This Report)  UNCLASSIFIED | 20. Security Class (This Page)  UNCLASSIFIED | 21. No of Pages  106 | 22. Price |

Form DOT F 1700.7 (8/72) Reproduction of form and completed page is authorized

# EXECUTIVE SUMMARY

Compared to conventional prime movers, fuel cells offer significantly lower emissions, improved fuel economy, lower thermal and noise signatures, and more flexible arrangements. The U.S. Navy and the U.S. Coast Guard are investigating shipboard fuel cell applications including ship service generators and main propulsion using electric drives. Various fuel cell systems have been investigated, and Fuel Cell Energy (FCE) Corporation's molten carbonate fuel cell module powered by standard diesel fuel has been selected for further development. While the steady-state performance of this system is well understood, questions remain about its ability to react to changing load requirements in marine service. It was decided that simulation of dynamic system performance was needed to design systems that could meet these anticipated requirements.

This report describes a dynamic simulation model (DSM) of an electrically propelled ship with power provided by four 625 kW fuel cells. Simulations are performed for extreme acceleration and deceleration maneuvers, and the responses are compared to those of diesel and turbine-powered ships. It is concluded that a fuel cell-powered ship can achieve transient responses comparable to those of conventionally powered vessels.

This report documents refinements to the existing DSM model of FCE's diesel-fueled molten carbonate fuel cell module. The DSM is based on principles of mass and energy balance, and incorporates dynamic characteristics of the fuel cell, all balance-of-plant components, the controller, electric bus, AC propulsion motors, shafting and propellers. Recent changes in FCE's design improve the power module's transient response. Rapid accelerations and crash stop maneuvers were simulated. Results showed the need for careful coordination between available power, the torque absorption of the AC motors, and total system load requirements. For crash stops, shaft brakes and resistance banks were used to absorb excess power, and the need for some fuel cell venting was indicated. It is shown that a fuel cell-powered ship can achieve starting and stopping distances considered acceptable under current practice.

The algorithms for the individual components of the ship powering system were integrated into a SIMSMART™ platform. The SIMSMART™ simulation model includes a ship, electric motors for propulsion, fuel cells, ship controls and auxiliary systems to support the fuel cell. Various variables and parameters can be followed as the model is executed. These variables and parameters include:

1) Propeller RPM, pitch and torque
2) Electric motor current and voltage
3) Flow rates and pressures in the auxiliary support systems
4) Ship speed
5) Fuel cell flow parameters, and
6) System and ship controls.

The main finding of the simulation is that both acceleration and deceleration maneuvers can be performed as rapidly by a fuel cell-powered vessel as by conventional prime movers. Appendices A through E provide detailed explanations of the dynamic simulation of the fuel cell, maneuvering requirements and standards, mathematical formulations developed to run the dynamic simulation, and the user interface to the DSM model. Appendix A contains sections describing the dynamic simulation of the molten carbonate fuel cell (MCFC). This material was primarily provided by Fuel Cell Energy (FCE) based on work done at the University of Pennsylvania under a subcontract to FCE. These sections contain the description of the building components of the MCFC. Mathematical descriptions of these components were used to develop the time stepping, dynamic simulation. The criteria used to evaluate responsiveness of the propulsion system are based on a survey of maneuvering requirements and standards. This report is included as Appendix B to this report. Appendix C contains the detailed description of the response curve generation and mathematical formulations used in the dynamic simulation. The detailed description of the building components of a marine propulsion system in mathematical formulation is described in Appendix D. This integrated ship and fuel cell propulsion system dynamic simulation was produced by John J. McMullen Association (JJMA) using Matlab$^{TM}$ and Simulink$^{TM}$ algorithms. In addition to the MCFC, the modeled ship power system components include the propeller, the AC motor and the complex control system to govern the required changes in ship's speed at maneuvering. Icons and computer monitor displays used in the dynamic simulation are presented in Appendix E. These are the user interfaces to the DSM.

The simulation tool developed is sufficiently generic and can be used to optimize the control scheme for maneuvering for any other vessel with an integrated electric power system. Further ship maneuvering simulations are needed to determine optimum system configuration and control settings for using fuel cells for ship propulsion. Maneuvering performance of a fuel cell-powered ship is expected to be acceptable. The current simulation model will be used in future work to assess the system's ability to meet ship service requirements.

# TABLE OF CONTENTS

# LIST OF FIGURES

# LIST OF FIGURES

# 1.0  INTRODUCTION

The U.S. Navy is currently under contract to the U.S. Coast Guard (USCG) to develop a Marine Fuel Cell Module.  The U.S. Coast Guard is supporting this development for marine propulsion applications.  The Fuel Cell Module is a complete and independent power plant delivering 625 kW of 60 Hz AC power at 450 volts.  This power plant, a molten carbonate fuel cell (MCFC), uses diesel fuels from NATO F-76 with one percent sulfur to distillates with lower end points and lower sulfur levels.  The MCFC design is based on FCE's commercial Direct Fuel Cell (DFC) technology adapted for marine application.  The MCFC utilizes a mixture of alkaline metal carbonates as the electrolyte and operates at 1050-1250 °F where internal reformation of methane is feasible.  By capturing the process waste heat through endothermic fuel reforming reaction, the DFC stack provides overall power plant efficiency of greater than 50% over a load range from 30% to full-rated power.  To more fully evaluate the feasibility of utilizing this powering system in USCG vessels and to assist in the development of the fuel cell module, John J. McMullen Associates, Inc. (JJMA) developed a dynamic computer simulation model of the integrated powering system of a vessel utilizing a Molten Carbonate Fuel Cell power plant.

## 1.1  Dynamic Simulation Modeling

A dynamic computer simulation model of the MCFC power plant was developed by JJMA in cooperation with FCE, the fuel cell developer.  The model was designed to simulate fuel cell power plant operation and electrical distribution system integration, and was developed using a variety of software tools including: SIMSMART$^{TM}$ dynamic simulation software, Matlab$^{TM}$ analytical software, and the Visual Basic programming language.  The dynamic simulation model includes functional relationships and associated time rate derivatives for the preconverter and the fuel cell stacks.  It was assumed that the largest time delay is produced by the fuel processing system, in particular, the preconverter.  As an intermediate step, a stand-alone program was created to simulate the performance of the preconverter and the fuel stacks.  The user interactive program is written in Visual Basic, and provides the time record from a power demand instruction to the provision of the power.  Graphic results such as time records for gas component concentration were created using a spreadsheet.  These stand-alone programs were translated into a C++ language subroutine, which was then integrated with SIMSMART$^{TM}$ simulation software to depict propulsion system components and simulate the dynamics of the propeller and the vessel.

## 1.2  Modeling the Fuel Cell Module and Load Demand Simulation

The fuel cell module consists of a multi-cell stack of individual fuel cells. Each cell consists of an anode and cathode, separated by a porous ceramic matrix filled with carbonate electrolyte. The reforming catalyst is strategically placed both in the anode gas flow field and in special individual reforming units inside the fuel cells.

The DC current produced is proportional to the extent of the electrochemical reaction in accordance with Faraday's Law.  There are also process time delays associated with the flow of material and energy in the MCFC system.  The simulation model incorporates the appropriate time delays for the oxidant delivery subsystem, heat recovery units, fuel pump and other major pipes and valves in the system.

1

The realistic evaluation of the electric load demand for a vessel requires consideration of the primary elements of the integrated electric power plant. These elements consist of the AC ship service loads and the AC/DC propulsion loads, both of which are fed from a common power bus.

While the largest demand load elements are the propulsion loads associated with the propulsion motors, 800 hp in case of a T-AGOS 3 Class ship, the transient response of the propulsion system acting alone does not always place the most stringent response requirements on the power source. This is due to the hull form design characteristics and the inherent load limiting capability of the propulsion drive controllers. The more stringent step load requirements of IEEE 45 require rates of response that even most modern diesel generators are unable to satisfy. The current work scope concentrated on the propulsion load demand, which includes the hull resistance and inertia characteristics, including the shafting, propulsion motors and the propeller four quadrant characteristics. Simulation results show that the fuel cell-powered ship can accelerate and decelerate as rapidly as the conventionally powered vessels surveyed in Appendix B.

## 2.0 BACKGROUND AND APPROACH

### 2.1 Past Marine Fuel Cell Dynamic Simulation Effort

During FY99, USCG Fuel Cell simulation efforts were suspended per USCG direction due to funding issues and the pending selection of the technology, Proton Exchange Membrane (PEM) or Molten Carbonate (MC), for the demonstration Marine Fuel Cell. However, during that time, relevant simulation experience was gained through other U.S. Navy and commercial projects, such as the development of a SIMSMART$^{TM}$ model of the U.S. Navy's Plasma Arc Waste Destruction System (PAWDS), which incorporates similar mathematical and simulation principles as the Fuel Cell model.

The development of a SIMSMART$^{TM}$ dynamic simulation model for the USCG Fuel Cell system involves the combination of several SIMSMART$^{TM}$ sub-networks (e.g., compressible flow and incompressible flow), that must be combined into a single network to facilitate conservation of mass, momentum and energy. However, standard SIMSMART$^{TM}$ library icons and section models were not originally designed to allow mixing of different stream or fluid types into a fully interactive and coupled SIMSMART$^{TM}$ network. As a result, new SIMSMART$^{TM}$ components must be developed in order to simulate this type of system.

Such simulation models were recently developed for other projects by creating customized icon components. These models are based on the fact that the SIMSMART$^{TM}$ solver models are applied to each section in a SIMSMART$^{TM}$ model bounded by pressurized nodes, and the fact that input stream icon pressure can be adjusted dynamically so that mass, momentum and energy can be conserved across different network types.

A brief summary of the Dynamic Simulation Model (DSM) for the Molten Carbonate, Coast Guard Fuel Cell (MCFC) power plant, which was developed during FY98 was documented in a December 1999 report to the USCG titled, "Fuel Cell Advanced Concept Development for USCGC VINDICATOR - Dynamic Simulation Model Summary Report." The computer programs and software coding of the DSM were outlined, as well as the vessel's electric propulsion system and the vessel's hydrodynamics characteristics. The fuel cell dynamic response was attributed to the time lag during the pre-conversion process of liquid fuel to gaseous fuel. The electrochemical process equations were detailed in the "Dynamic Simulation Model Technical Report" that was delivered to the USCG in October 1998.

### 2.2 Simulation Tools

There are numerous commercial dynamic simulation software packages in the market today. Many of these simulation software packages cater to one specific application such as process control, aviation, mechanical design, and etc. A few software packages provide a general-purpose dynamic simulation platform with additional strength in specific areas. The "Review of Simulation Tools Report" dated July 31, 1998 depicts and compares an extensive list of commercially available software tools. This report was delivered to the USCG during August 1998.

JJMA developed the earlier version DSM using SIMSMART™, Matlab™, and Visual Basic. Fuel Cell Energy, Inc. (FCE), formerly Energy Research Corporation (ERC), provided the functional relationships and associated time rate derivatives for the preconverter and the fuel cell's voltage, current and fuel consumption relationships.

The present integrated system's DSM development builds upon the work by the University of Pennsylvania and Fuel Cell Energy Corporation, which is described in detail in Appendix A of this report. The stand-alone program that was created to simulate the performance of the preconverter and the fuel stacks has been replaced by a stand-alone Simulink™ presentation that provides data for the integrated SIMSMART™ simulation. At this time, the stand-alone program does not solve the electrochemical equations in real time. The stand-alone program may later be translated into a "C" language subroutine which will be integrated with the Balance of Plant (BOP) comprising of the ship's auxiliary fluid systems, propulsion system components, and hydrodynamics of the propeller and the vessel. The SIMSMART™ integrated simulation uses curve interpolation to retrieve data required for system dynamic simulation rapidly.

## 2.3  Maneuvering Performance Standards

An essential criterion for the successful application of fuel cells as prime movers in the marine industry is preserving or improving the maneuvering performance of the ship. A survey of maneuvering performance standards and regulations for the marine industry was performed and reported in "Marine Fuel Cell — Maneuvering Survey Report." This report, which was provided to the USCG in March 2000, sets performance recommendations based on ship size and propulsion system type. Detailed results of a survey of standards for maneuvering performance are reported in the report, which is contained within its entirety in Appendix B. This report documents a survey of U.S. and international regulatory bodies, commercial, and military sources for existing requirements, ship simulation and model test data, and ship full-scale trial data for ship acceleration and stopping capabilities. The data were then used in various regression analyses to determine a correlation between the applicable ship capability and one or more of the ship's characteristics, and to establish maneuvering requirements for the candidate ship.

Due to the limited amount of data made available to the authors of the Maneuvering Survey Report, the curves in the report were preliminary in nature. Therefore, the report recommended that the curves be updated and refined as more data points were gathered.

In the meantime, to formulate a set of requirements which ship designers may use, the following performance guidelines were recommended, listed in order from the most general, representing minimum acceptable requirements, to the most specific, representing additional, owner-driven requirements:

1) Minimum acceptable stopping distance based on the International Maritime Organization (IMO) requirement. No minimum requirement for acceleration can be established.

2) Stopping distance based on "good ship" maneuvering characteristics, as ascertained in the analysis. No acceleration requirement can be established.

3) More stringent requirements based on ships of similar type or on the specific ship the candidate ship is replacing.

4) Additional requirements based on a need for higher performance than in previous ships to address a maneuvering deficiency or based on a specific mission requirement.

As an example, in the absence of existing trial data and any overriding mission requirements for a T-AGOS 3 class ship, subparagraph no. 2) above and Figure 2-1 are used to establish a stopping requirement. For a 2295-ton ship with diesel-electric drive and FP propellers a minimum requirement of <u>ten ship lengths</u> for stopping distance is set. Based on the same criteria and changing from FP to CPP, a minimum requirement of <u>four ship lengths</u> is set.
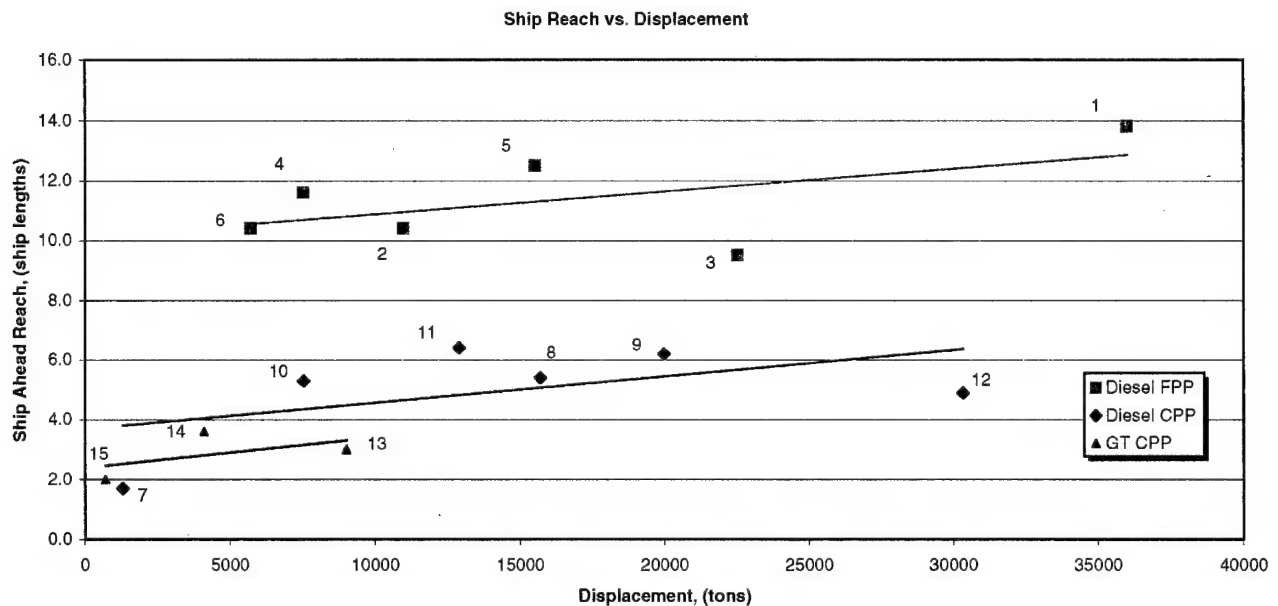


Figure 2-1. Ship Reach vs. Displacement

## 2.4 Marine MCFC System Dynamic Model

### 2.4.1 Purpose

The purpose of the simulation described herein is to assess the applicability of fuel cells as a power source for electric propulsion plants for ships. The criteria for the successful applicability of fuel cells are pre-selected maneuvering performance requirements or standards from the ship, as discussed in section 2.3.

For the purpose of this work, a maneuver is defined as the operation of changing the speed of the ship from an initial value to a prescribed terminal value within a prescribed distance (usually, number of ship lengths).

5

The propulsion actuator considered for the application is an electric AC synchronous motor. The motor is expected to deliver torque for the range of angular speeds spanning from zero to the maximum speed allowed for the propeller (e.g., due to cavitation). Existing synchronous motor models have the major shortcoming of not allowing for finite torque at zero rotational speed. A new synchronous motor model that has been developed overcomes this inconsistency.

In the following sections, the models utilized and/or developed for each of the components of the propulsion system are described. Also, the procedures used in the execution of the maneuvers are detailed.

### 2.4.2 Ship Component Models

The models used to represent the ship and its propulsion system components are described in detail in the following subsections.

### 2.4.3 Fuel Cell

The simulation is performed on the real-time simulator SIMSMART$^{TM}$. Therefore, the fuel cell model has to be incorporated into the SIMSMART$^{TM}$ network model of the ship propulsion and maneuvering systems. However, the fuel cell model cannot be integrated in a real time mode due to the time consuming computation it requires. Therefore, the temporal responses of its principal variables with respect to various characterizing inputs were extracted and used to define the fuel cell behavior. Nevertheless, for the sake of generality, a wide range of initial and terminal states has to be covered. This implies that a very large number of runs of the fuel cell model have to be carried out and the results input to SIMSMART$^{TM}$.

### 2.4.4 Integrated Fuel Cell System Block Diagram

Figure 2-2 shows a simplified block diagram of the marine fuel cell power plant including the overall organization and inter-relationships of the key electric/control components and the power and information signal flows. The major components consist of:

- Fuel Cell Direct Current (DC) Block

- Power Conditioning System (PCS)

- Control System (CS)

- Motor Control Center (MCC)

The MCFC power plant is designed to carry its own auxiliary load. The auxiliary power to the plant is provided by the PCS through a Motor Control Center (MCC). The MCC provides the on-and-off switching for starting the motors for the blowers and pumps in the power plant. It also houses the variable speed controls for certain blowers and step-down transformers for 600-208/120 VAC circuits.

6

During all operating modes, the CS will provide the coordination and control required for fuel flow, steam flow, fuel utilization, process temperatures and pressures, and electric power load generation. The amount of power/current that can be drawn from the fuel cell is directly proportional to the concentration and flow of reactants ($H_2$, $CO$, $CO_2$) within the fuel cell stacks which are continuously monitored and controlled by CS.
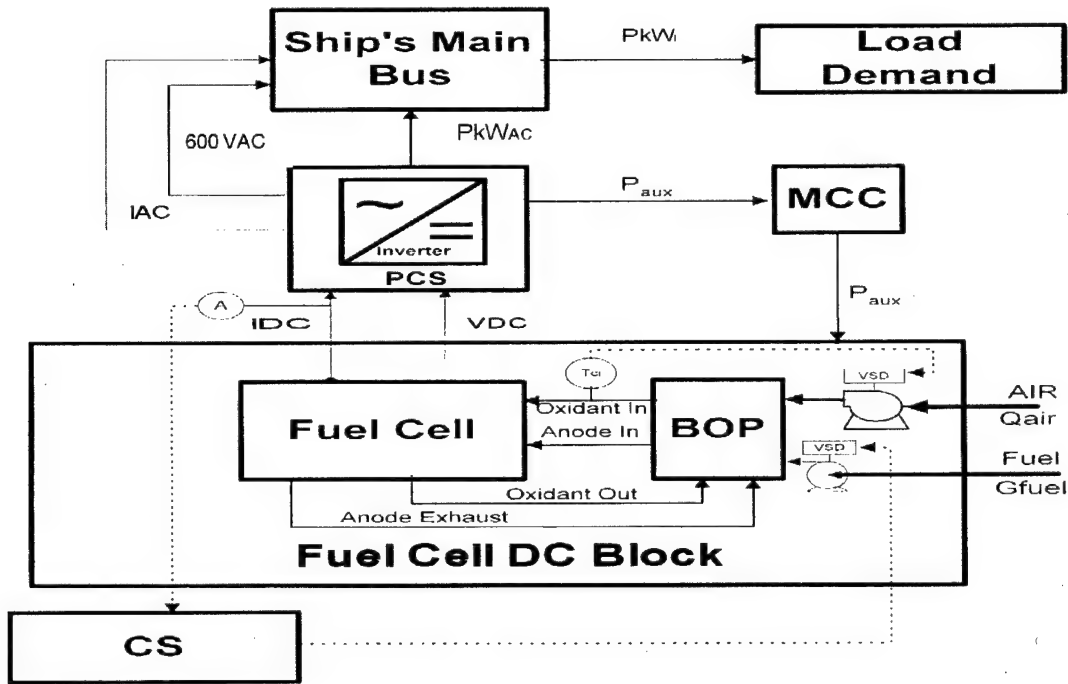


Figure 2-2. Simplified Power Control Diagram of CGFC Power Plant

Fuel cells by themselves are very quick in responding to outside stimuli if the reactants (anode and cathode gases) are delivered promptly. The most important factor in DSM is to formulate the fuel processing response characteristics. The key equipment in the fuel processing subsystem is the preconverter. Figure 2-3 shows a schematic block diagram of the fuel cell and preconverter. Past simulation work considered the preconverter to be the only component causing a delayed power production. The present simulation considers all the other system components.
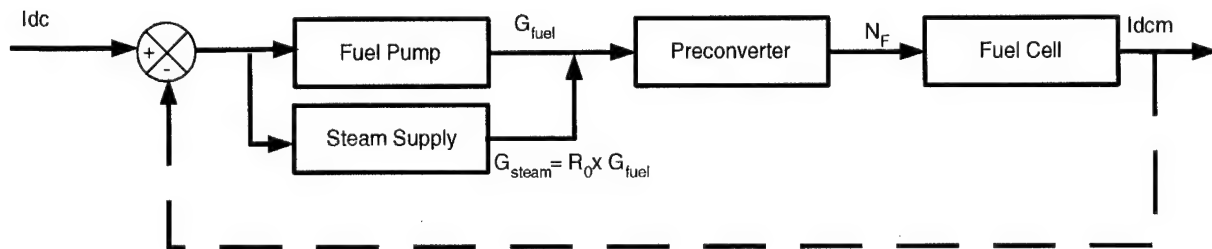


Figure 2-3. Schematic of DC Current Generation Block Diagram

2.4.5    Load Demand Simulation

The integrated electric power plant consists of the AC ship service load module and the AC/DC propulsion load module, both of which normally are fed from a common power bus. The realistic evaluation of the electric load demand for a vessel requires consideration of both.

The propulsion load demand, which includes the hull resistance and inertia characteristics, including the shafting, propulsion motors and the propeller four quadrant characteristics, was simulated even though it may not represent the most stringent operating requirement for the power source.

The second element of the electric load demand consists of the aggregate loads of the constant voltage, constant frequency ship service power system. This element, acting alone, while the ship is in port or at anchor, or in combination with the propulsion loads at sea, may be required to comply with the electrical distribution system interface characteristics described in DOD-STD-1399 Section 300, IEEE-STD-45, and Classification Society Rules to ensure acceptable operation of shipboard electrical and electronics equipment. This element places the most stringent demand for dynamic response characteristics on the power source, since tightly controlled transient voltage and frequency variations and rapid recovery times are mandatory for successful system operation. Other power generating systems such as high-speed diesels have difficulties meeting these requirements.

These stringent requirements were not selected for simulation and modeling at this time. Ultimately, the transient response characteristics of the existing diesel generator sets and the proposed fuel cell system must be simulated to ensure system performance that is in compliance with the interface standards.

Results from simulation of ship's maneuvering can be compared to maneuvering times from conventionally powered vessels deemed acceptable by their operators and used by the designers of the fuel cell for system design. Energy accumulators designed into the system can meet the very short transient requirements. The current load demand simulation includes the vessel's resistance and inertia characteristics, shafting, the propulsion motors and the propeller's four quadrant characteristics.

## 2.5    Response Curve Generation

The fuel cell subsystem Simulink$^{TM}$ model was provided by FCE. The model is designed to generate the fuel cell internal flow time histories as well as the corresponding DC and AC electric output power histories. The diagrams of the actual Simulink$^{TM}$ model are depicted in Figure 2-4. It can be subdivided into four sub-models:

1) The Inverter Control model

2) The 625 kW SSFC Module model

3) The Process Control model, and

4) The Process Measurement model.

Appendix C contains the detailed description of the response curve generation and mathematical formulations used in the dynamic simulation.

## SIMULINK ™ MODEL OF THE 625 kW FUEL CELL SYSTEM



Dynamic Simulation Model for Ship Service Fuel Cell
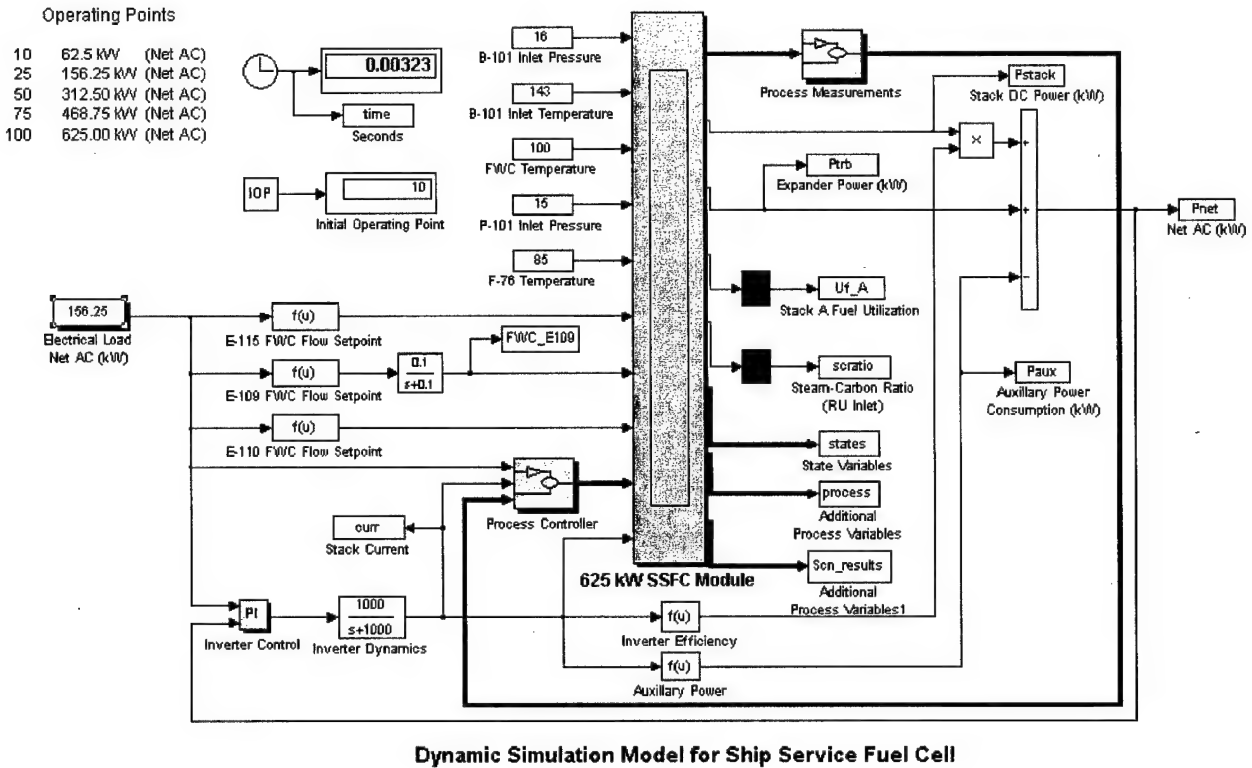
Figure 2-4.  Simulink™ Model Modules

## 2.6   The Motor and Its Control

The propulsion system is a direct drive power train consisting of 3-phase AC synchronous motors.  The propulsion motor is a torque source whose torque characteristics are determined by a Variable Speed Drive Control Unit (VSDCU).  The propeller uses the motor torque to produce thrust; however, this can be accomplished only if change in the torque of the motor is applied in conjunction with a change in the propeller rotational speed.  Figure 2-5 illustrates the equivalent electric circuit corresponding to one phase of the motor.

9
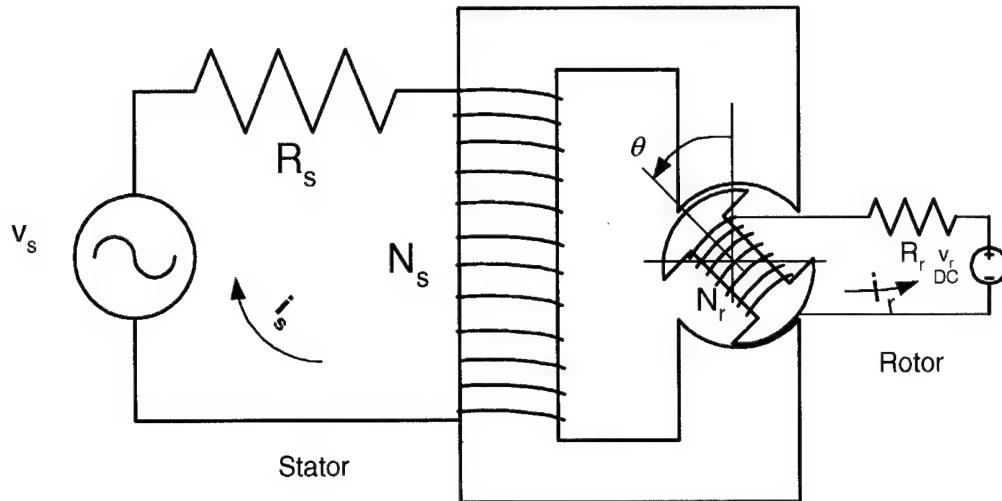
Figure 2-5. Equivalent Circuit of One Phase of a Y-Connected Synchronous Motor

## 2.7 Ship Dynamics

The ship is assumed to be equipped with "$n$" number of motors/propellers, which operate simultaneously and identically. This implies that the dynamics of the ship is one-dimensional. Additionally, the model assumes two degrees of freedom for the ship system: the ship location, $x$, and the rotational position of a shaft, $\theta$.

## 2.8 Maneuvering Computations

In developing algorithms for maneuvering computations, only ship maneuvers involving acceleration of the ship and crash stop deceleration were considered for simulation at this time. In the acceleration maneuvers, the ship is assumed to initially be cruising at a given constant speed and it is desired to increase it by raising the power to the motors. In the deceleration maneuvers, the ship is crash stopped from a given speed to a ship speed of zero.

From the motor torque equation, it is clear that the torque is only related to the amplitude of the current supplied to the motor. On the other hand, the torque developed by the propeller depends on its rotational speed. These two variables are independent, as far as both the source and the motor are concerned; however, they are connected through the dynamics of the system, which serves as a constraint for the controller. The propeller requires change in rotational speed in order to change the torque it delivers, the change time history is determined by the solution to the equations of motion with the torque of the motor being the driving force. Any other change in rotational speed will either not take advantage of the fuel cell capability when using a slower rate of motor rotation acceleration or, will stall the motor if faster motor rotation acceleration is used.

Due to the fact that the time constant of the ship is much larger than the time constant of the propulsion system, the determining factor in the maneuver is the capability of the fuel cell to provide current.

10

The fuel cell voltage is assumed to be constant throughout the maneuvers; therefore, the power output is proportional to the torque of the motor.

Figure 2-6 depicts maneuvering parameters that are simulated mathematically to evaluate ship dynamic characteristics.
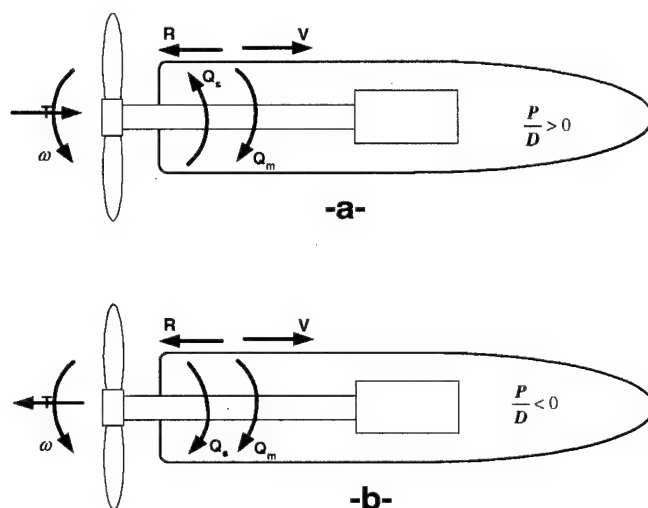


Figure 2-6.  Ship Maneuvering Parameters

## 2.9   The Integrated Ship Model

The ship system is modeled as a power network.

### 2.9.1   Data Flow Diagram

The network comprises three blocks:

1) The Fuel Cell Power Unit – the unit is composed of two sub-units:

- The Fuel Cell and its Controller – provides the transient power-up/power-down characteristics of the fuel cell unit given the initial and terminal power levels,

- The Inverter and its Controller – converts the DC power output of the fuel cell into 3-phase AC power instantaneously and with high efficiency (~98%),

2) AC Motor and its Controller – provides torque and mechanical power at various rotational speeds without exceeding power limitations,

3) The Ship Model –

- Provides the dynamics of the ship and the propeller,

- Defines the maneuver demand curve.

11

Figure 2-7 provides the Data Flow Diagram (DFD) for the simulation network, which specifies the routes of data flow between the major blocks of the fuel cell powered propulsion system.
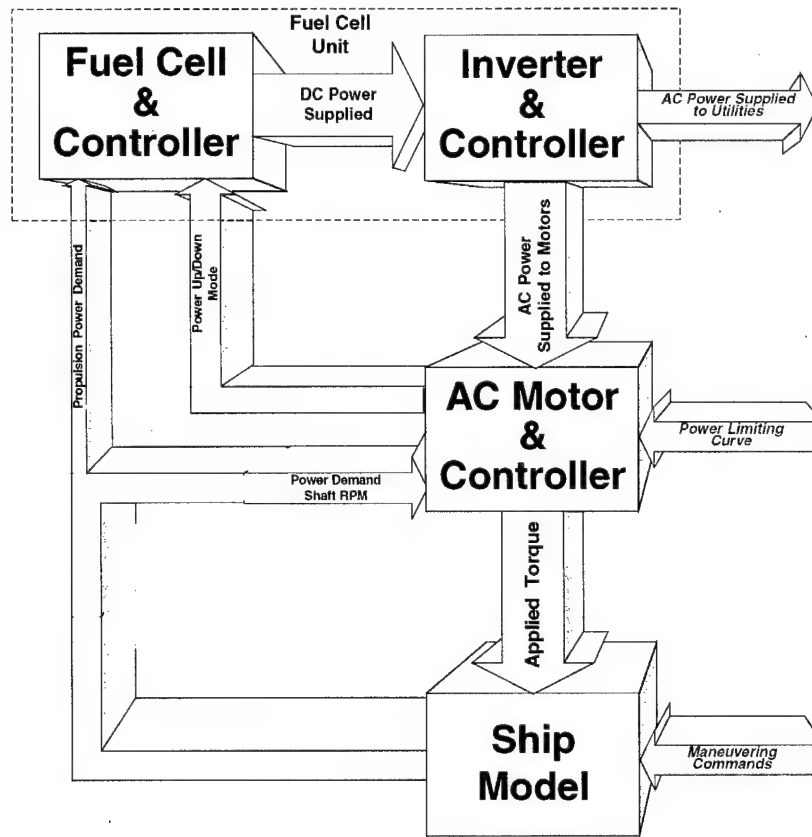
Figure 2-7.  DFD of the Propulsion System

# 3.0 AC SYNCHRONOUS MOTOR OPERATIONAL CONTROL SCHEMES

The development of a control scheme that will enable the incorporation of new types of power producers, i.e., fuel cells and the variable speed AC propulsion motors, has been a major challenge. The products described in this report and the simulation program can be utilized for other AC, variable speed drives intended to be used in marine vessels, independent of the prime mover type.

The major characteristic of an AC synchronous motor is that it is designed to operate under no-slip condition. In other words, the frequency of rotation of the rotor and the frequency of rotation of the magnetic field in the armature are identical. This characteristic allows the motor to be operated and controlled precisely at different rotor speeds. In order to operate an AC synchronous motor under variable speed conditions, the frequency of the AC electrical source must be variable. At the same time, other motor parameters, such as line voltage, current and DC excitation voltage, must be controlled during the operation of an AC synchronous motor. For a full discussion of these concepts, see Appendix D.

Two control schemes can be used to achieve maximum instantaneous motor power demand throughout a complete ship maneuver:

> Scheme 1: Instantaneous source power available is equal or larger than the instantaneous motor power demand. This control scheme is applied when the instantaneous power demanded by the motor is smaller or equal to the instantaneous power available from the source. In this control scheme, the source frequency and the AC voltage should be increased correspondingly so that the motor torque angle and the instantaneous current drawn from the source are maintained constant to their respective maximum allowable values.

> Scheme 2: Instantaneous source power available is less than the instantaneous motor power demand. This control scheme is applied when the instantaneous power demanded by the motor is larger than the instantaneous power available from the source. In this control scheme, the AC source frequency and voltage should be increased correspondingly so that the motor torque angle is kept constant and close to its maximum allowable value, while matching the electrical source instantaneous available power.

Both schemes are used automatically to enable maneuvering from any initial status of the vessel and its instantaneous available power resources.

# 4.0 MANEUVERING SIMULATION EXERCISES

This section provides a description of the execution of maneuvering exercises of the Dynamic Simulation Model (DSM) for the Molten Carbonate, Coast Guard Fuel Cell (CGFC) powered ship. The computer programs and software coding of the DSM were described in previous sections. The vessel's electric propulsion system's is treated as a controlled large-electrical load typical to ships with an integrated electric propulsion system as described in earlier sections. This section discusses the maneuvering exercises performed with the integrated simulation program, and is used to access acceptability of ship maneuvering performance using fuel cells as the prime mover.

## 4.1 Simulation Activities

The development of a SIMSMART™ dynamic simulation model for the USCG Fuel Cell system involves the combination of several SIMSMART™ sub-networks into a single network to facilitate conservation of mass, momentum and energy. The first phases of this effort took place in 1998 and involved the creation of simplified ship, DC motor, and fuel cell models. Recommendations resulting from this effort were incorporated in the molten carbonate fuel cell design.

While previous simulation efforts included the fuel cell pre-reformer, the major time lag contributor to the system's dynamics and a DC simple load control system, the simulation model now includes sophisticated variable AC motors, load centers and a comprehensive control system. The fuel cell model includes most of the building blocks of the power unit. Although the execution of load exercises is done as a preparatory step, the results are an integral part of the ship's power system simulation exercised herein. This is done in order to enable real time execution. The ship model also was upgraded to include a CPP.

## 4.2 Maneuvering Simulation

### 4.2.1 Load Demand Simulation

The simulation was exercised on a ship modeled using the main hydrodynamic characteristics of a TAGOS-3 class ship. The propulsion system was modified to include four molten carbonate fuel cell units, 625 kW each. The realistic evaluation of the electric load demand for such a ship requires consideration of both elements of the integrated electric power plant. These elements consist of the AC ship service loads and the propulsion loads, both of which are fed from a common power bus. Simulation of the ship maneuvering characteristics such as forward acceleration and crash stops provide ship performance parameters that can be compared to those of conventional vessels judged acceptable by their operators. A "new" feature that was found to be necessary in a fuel cell power system and AC propulsion is the ability to either burn excess power by having, for example, resistance banks or a carefully controlled slow down system. This feature can be illustrated in maneuvering simulations that include fast accelerations and slow downs.

The current load demand simulation includes the vessel's resistance and inertia characteristics, the shafting including the propulsion motors and the propeller's four quadrant operational characteristics. The parameters of each component in the simulation model

can be modified to represent various other vessels, different size propellers, other ship auxiliary loads, or AC motors.

### 4.2.2   User Interfaces

The parameters associated with components that are represented in the dynamic simulation of the fuel cell–powered ship are embedded within icons. The icons are interconnected functionally by connectivity icons such as piping and electrical and control cables. The time stepping through the simulated process is performed by SIMSMART$^{TM}$'s inherent "engine." Integration for processes such as ship reach ahead is done internally to the icon.

Some parameters can be changed any time throughout the simulation, thus enabling user interaction. Samples of icons that were developed for this dynamic simulation of the fuel cell–powered ship and screen displays are provided in detail in Appendix E. The Marine Fuel Cell Powered Electrical System Assembly is depicted in Figure 4-1. Four fuel cell icons, two AC motors and a ship icon are interconnected electrically via a power and distribution bus. Control buttons allow for the application of individual components, for example, only one electrical motor can get power and less than four fuel cells can be on-line.



**REAL TIME DYNAMIC SIMULATION MODEL OF A SHIP**
**MARINE FUEL CELL POWERED ELECTRICAL PROPULSION SYSTEM**
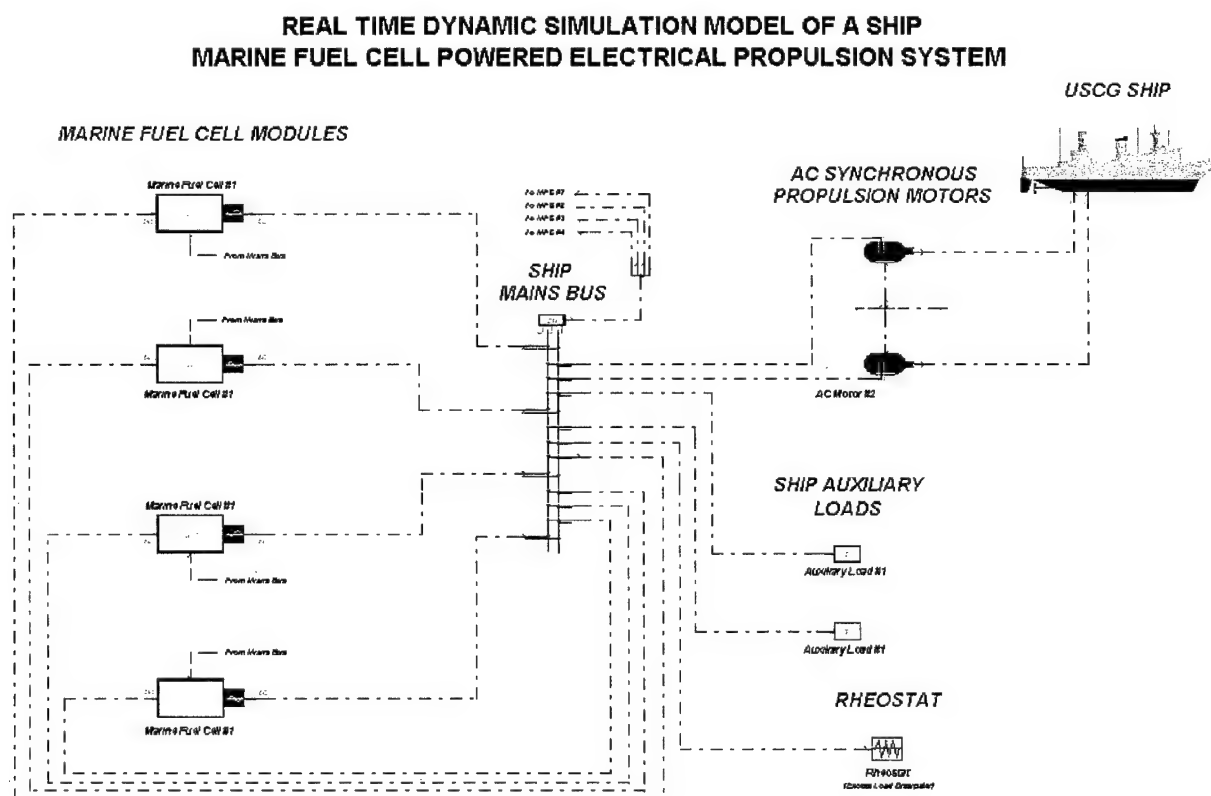
Figure 4-1.  Dynamic Simulation - Marine Fuel Cell Powered Electrical System Assembly

### 4.2.3   Dynamic Simulation Results

The results of several runs of the dynamic simulation model covering various maneuvering simulations are presented in Figures 4-2 through 4-7. In general, there are three simulation result plots each for the acceleration maneuver simulations and crash stop maneuver simulations. Figures 4-2 through 4-4 show the dynamic simulation results for rapid ship acceleration maneuver starting from zero speed conditions to full speed conditions. Figures 4-5 through 4-7 present the results of a dynamic simulation of crash stop maneuvers from full speed conditions to zero speed conditions. Two plots show the power supplied by the fuel cell and consumed by the ship propulsion and auxiliary loads (Figures 4-2 and 4-5). Two other plots show the transient response of AC synchronous motor control voltage and control current, one for acceleration (Figure 4-3) and one for deceleration (Figure 4-6). The final two plots show the transient response of the ship's dynamic parameters such as shaft RPM, velocity, and position (Figures 4-4 and 4-7).

The crash stop maneuver simulation results show that the 80-meter ship stops within four (4) ship lengths. This was achieved by applying a shaft braking torque to reduce the propeller shaft's rotational speed to zero, and then by reversing the motor shaft rotational speed to minimize ship stopping distance. A similar performance could be achieved by reversing the CPP propeller, however, this generates many possible control scheme permutations. To simplify the presentation and the assessment of the fuel cell powered ship, the crash stop maneuver was achieved using a shaft braking system.

The dynamic simulations of the fuel cells, AC propulsion motors, and auxiliary loads for both ship acceleration and crash stop maneuvers were performed without the need to dissipate excess fuel cell energy. If excess fuel cell energy had been developed during any of the maneuvers, this excessive energy could be vented as a gas prior to its conversion to electrical energy or "wasted" on the resistor bank after conversion to electricity. In the dynamic simulation the ship acceleration and crash stop maneuvers were achieved by changing the fuel cell power demand to match the instantaneous load requirement. This careful control of the fuel cell and propulsion plant allowed the maneuvers to be performed without the need for venting or burning excess power. In practice, since other power users such as large fire pumps or winches could be operating at the same time, a realistic ship system configuration will probably require having means for excess power dumping.

**Acceleration Power Simulation Results**
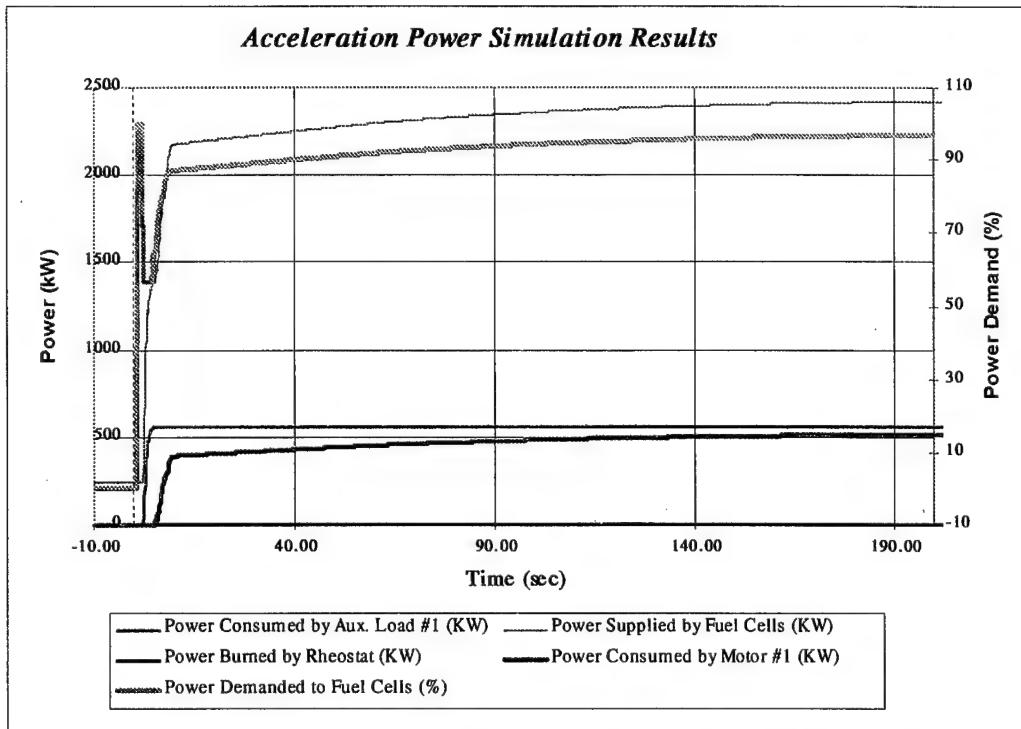
Figure 4-2.  Dynamic Simulation Results – Acceleration Power

**Acceleration Motor Simulation Results**
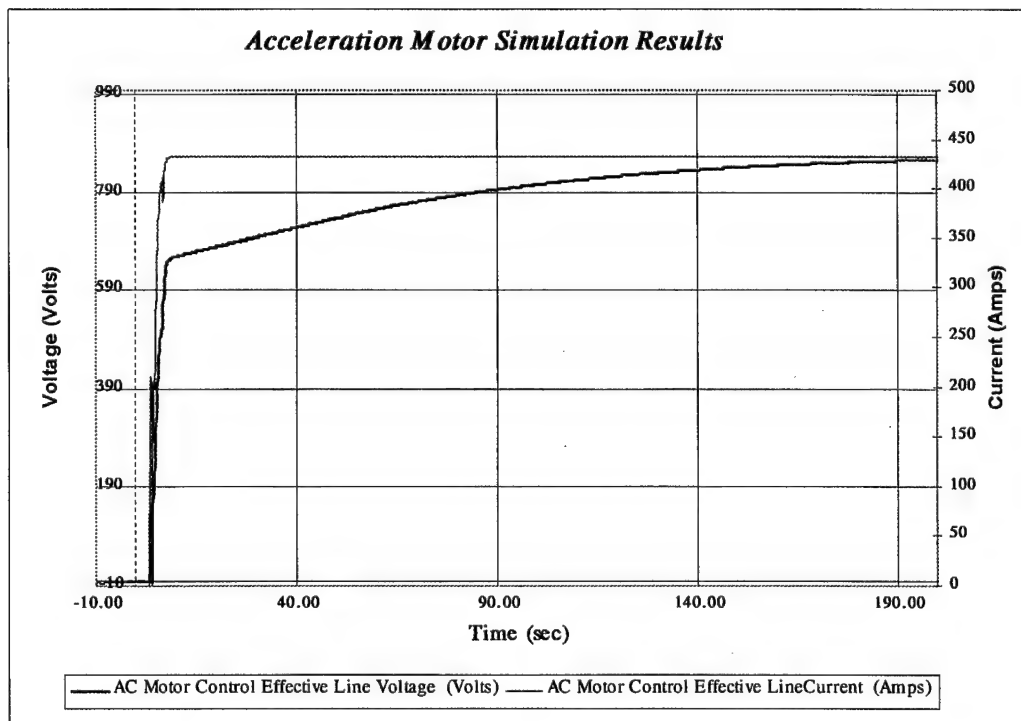
Figure 4-3.  Dynamic Simulation Results – Motor Data
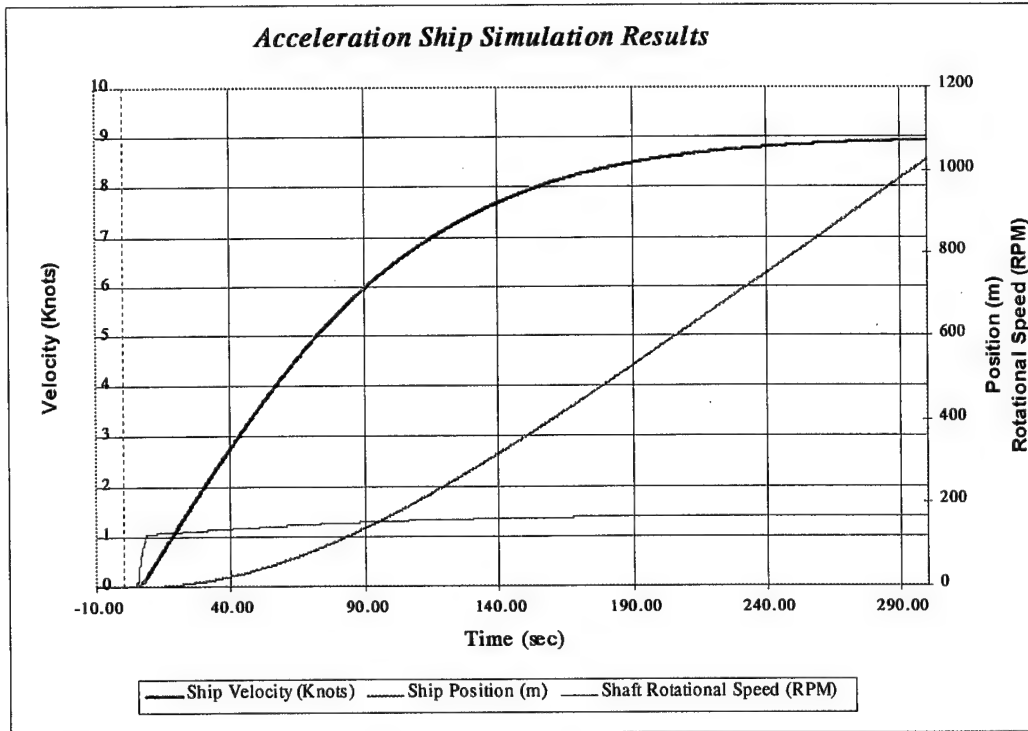
Figure 4-4.  Dynamic Simulation Results – Ship Speed, RPM, and Ahead Reach
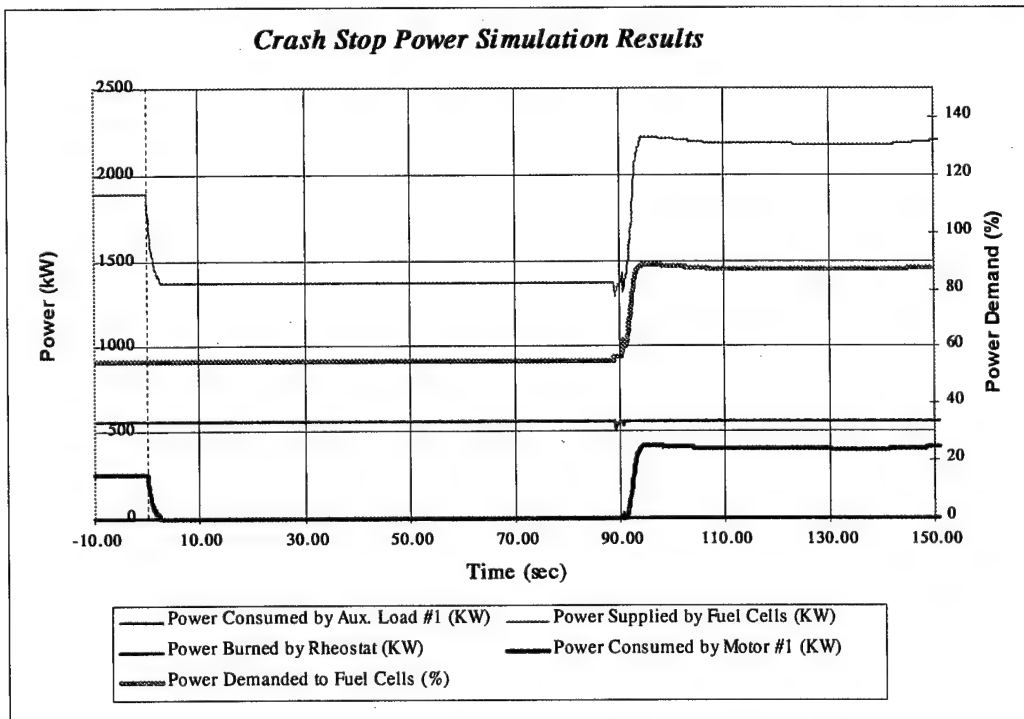


Figure 4-5.  Dynamic Simulation Results – Crash Stop Power
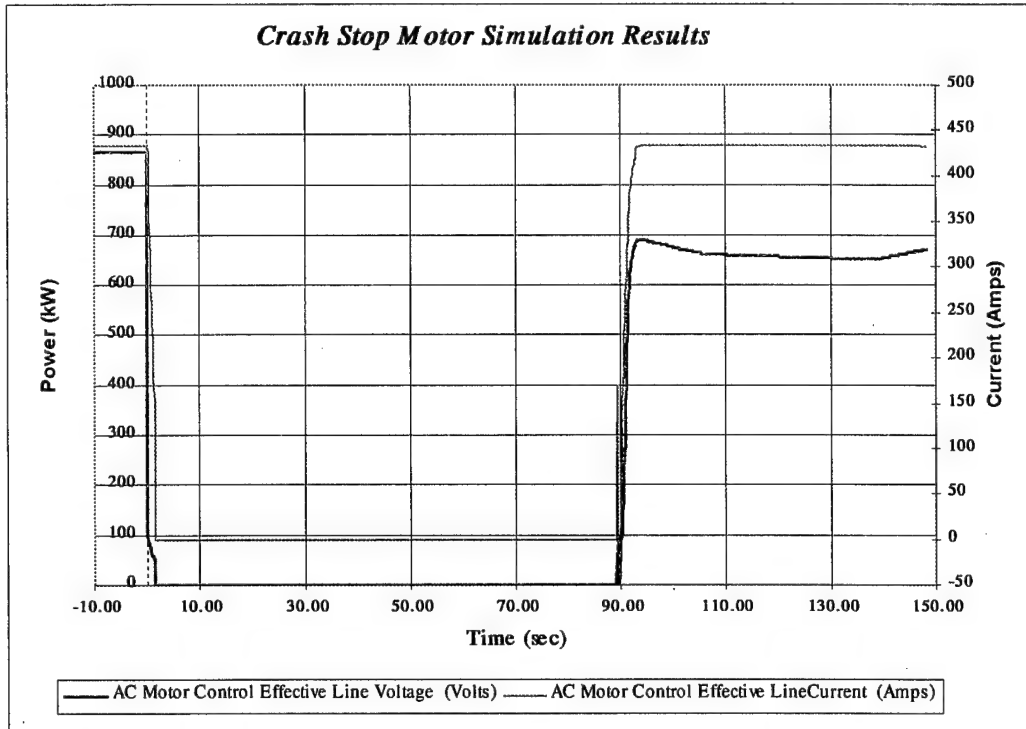
Figure 4-6.  Dynamic Simulation Results – Crash Stop Motor Data
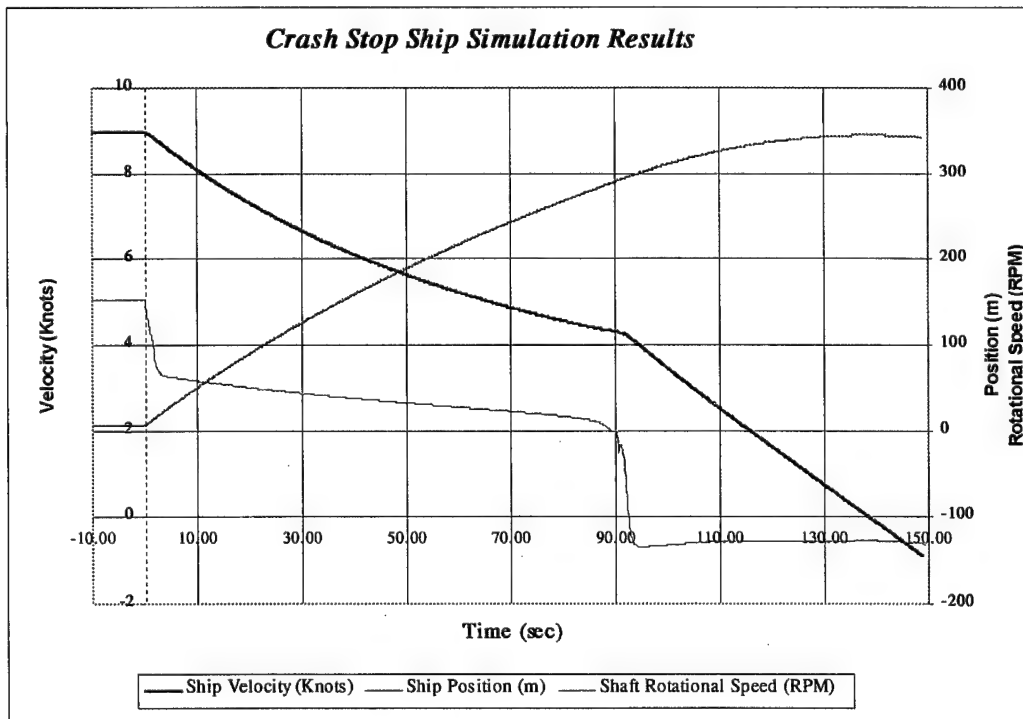


Figure 4-7.  Dynamic Simulation Results – Crash Stop Ship Speed, RPM, and Ahead Reach

# 5.0 CONCLUSIONS AND RECOMMENDATIONS

The physics-based dynamic simulation model was developed to simulate the entire ship's propulsion system. This includes the: marine fuel cells; the ship's main bus; auxiliary and hotel loads; AC synchronous motors; and reflects ship, shaft and propeller dynamics. The model was developed as individual separate components. As each component was developed, it was tested and simulation runs were conducted. As more and more components were developed, they were tested and then added to earlier completed components for more simulation runs. In this manner many of the conclusions presented by the model were realized during the model development. This process of individual component development, testing, and conducting simulation runs utilizing an increasing number of components and then feeding back into the development process requirements and information determined from the model, allowed real-time improvements during the dynamic simulation model design and development.

## 5.1 Conclusions

Based on the dynamic simulation results, the following observations and findings are noted:

1) The Molten Carbonate Fuel Cell (MCFC) Provides Linear Output Power. The MCFC model used in this study exhibits linear output power characteristics. A linear output power means that initial conditions of the fuel cell parameters do not affect the path between two power demand levels. This was not the same result derived from earlier simulations of the power generating system. According to FCE, this change in behavior is a result of changes in sub-component design. These changes produce a faster system response to sharp loading changes.

   In addition, it was observed that the transient response of the marine fuel cell between two power demand levels is relatively small compared to the time constant of the dynamics of the ship and its propulsion system. This last observation implies that marine fuel cells in principle are a suitable power plant alternative for ship propulsion applications.

2) The ship main-bus simulation model can effectively imitate all requirements of the power distribution task. The ship main-bus simulation-object, developed to simulate the ship power distribution management, was required to imitate accurately the dynamic response of the ship and its propulsion system. It was also required to imitate the dynamic response of all marine fuel cells that are on line at any given time when other loads, such as ship hotel and auxiliary loads, change their power requirements. In addition, the main-bus simulation-object, which provides an instantaneous power supply and demand balance between all power plants and loads, facilitates identifying potential operational problems in the balance of plant, such as excess or deficiency of power. The power distribution task can be handled effectively by programming the main bus to add and subtract power resources in response to actual demand.

3) <u>The AC Synchronous Motor Simulation Model can be used to develop safe system operational control parameters.</u> The AC synchronous motor simulation model was developed from physics-based principles to simulate and analyze the interaction between all the electrical motor control parameters (such as AC electrical source frequency, voltage and current, and DC excitation voltage and current), and the dynamics of the ship and its propulsion system. This model was utilized in this simulation to establish motor control strategies that allow the ship to adequately perform different desired maneuvers without interfering with the operation of other loads connected to the ship's main bus; and/or exceeding permissible operational parameters of the power distribution management system. Two electrical motor control algorithms, scheme 1 and scheme 2, were developed and tested for maximum ship acceleration. Scheme 1 is used when the instantaneous source power available is equal or larger than the instantaneous motor power demand, and Scheme 2 is used when the instantaneous source power available is less than the instantaneous power demanded by the motor. The AC synchronous motor simulation model, in conjunction with all the other simulation models described in this report, can be utilized to develop other electrical motor control algorithms to match specific propulsion system and/or balance of plant requirements. These models can also be used to establish safe system operational envelopes for all control parameters.

4) <u>Utilization of Excess System Electrical Power Needs Resolution.</u> Using AC synchronous motors for ship propulsion application requires matching between the motor and its electrical source. Because of the characteristics of an AC synchronous motor there is a limit in the amount of power it can consume at any given time. The amount of power that can be consumed by an AC synchronous motor at any given instance directly corresponds to the speed of the frequency change of the motor controller that can be reached without creating motor pullout conditions. In turn, this rate of change is affected by the inertia of the ship and its propulsion system. When the power supplied by the electrical source exceeds the maximum allowable power that the motor can consume, an excess of power will be generated in the ship's main-bus, and this excess of power must be used or burned by an external ship load. This situation may occur if ship deceleration or crash stop is attempted too rapidly.

## 5.2 Recommendations

1) <u>Use the fuel cell dynamic simulation model to model propulsion systems of other USCG vessels.</u> The simulation models developed and described in this report can be further utilized to simulate and perform system integration and design, control strategies development, and trade off studies of electrical propulsion systems of other USCG ships that use propulsion plants different than marine fuel cells. In addition, because each propulsion system component was simulated and developed as an independent object, other propulsion system configurations and/or arrangements can be easily created and simulated.

2) <u>Further study of propulsion system crash stops required.</u> Crash stop strategy using CPP has to be investigated and established. This is to resolve an optimum

21

rate of pitch balance in conjunction with AC variable speed motor torque and fuel cell power availability. An additional constraint in this case is the propeller shaft allowable stress.

3) <u>Normal Stopping of the Ship Requires Additional Study.</u> The optimal strategy for normal stopping of the ship has not been developed within the model due to the infinite possible combinations of torque angle, current, voltage, and propeller pitch. This will include a solution to matching AC variable speed motors with a power source that has a less than optimal change in power production.

4) <u>Full Ship Acceleration and Crash Stop Deceleration Can Match Conventional Powered Ships.</u> The simulation results show that control strategies can be developed which allow a fuel cell-powered ship to be accelerated as rapidly as most conventionally powered ships.

# APPENDIX A.

# DYNAMIC MODEL OF FUEL CELL AND BALANCE OF PLANT

# DYNAMIC MODEL OF FUEL CELL AND BALANCE OF PLANT

## EXECUTIVE SUMMARY

This report documents the status of the dynamic simulation task as of 9 June 2000. This material was primarily provided by Fuel Cell Energy (FCE) Corporation based on work done at the University of Pennsylvania under a subcontract to FCE. This is an abridged version of the original report with commercially sensitive, company proprietary data having been removed. Materials included in the full report are the full Marine Fuel Cell operating specifications and a description of the integrated system dynamic simulation. The sections concerning the dynamic simulation were produced by JJMA and are based on the Matlab$^{TM}$ and Simulink$^{TM}$ algorithms.

The algorithms are presently integrated into a SIMSMART$^{TM}$ platform. The SIMSMART$^{TM}$ platform contains a presentation of a maneuverable ship with an electric propulsion system. The work is based on the Marine Fuel Cell simulation work done in previous years with enhancements that include AC motors and CPP.

## TABLE OF CONTENTS

## 1.0 INTRODUCTION

The Marine Fuel Cell Module presently under development by Fuel Cell Energy Corporation is a complete and independent power plant, which delivers 625 kW of 60 Hz AC power at 450 volts. This power plant operates on diesel fuels as heavy as NATO F-76 with one percent sulfur, as well as a range of distillates with lower end points and lower sulfur levels. The design is based on adapting FCE's commercial Direct Fuel Cell (DFC) technology for marine application. This fuel cell system utilizes a mixture of alkaline metal carbonates as the electrolyte and operates at 1050-1250 °F where internal reformation of methane is feasible. Because the process waste heat is

unsurpassed overall power plant efficiency.

The 625 kW module has an efficiency greater than 50 percent over the load range from 30 percent to rated power, as shown in Figure A-1. Efficiency characteristics based on the fuel's lower heating valve (LHV) of typical gas turbine generator sets and high-speed diesel generator sets are also shown in Figure A-1 for comparison. The corresponding specific fuel consumption rate of the fuel cell module over the load range is shown in Figure A-2. The characteristic of high efficiency over the entire load range suggests that multiple modules installed on a ship be continuously connected to the ship service bus and share the load over the entire load range rather than shutting down modules at reduced power demand.
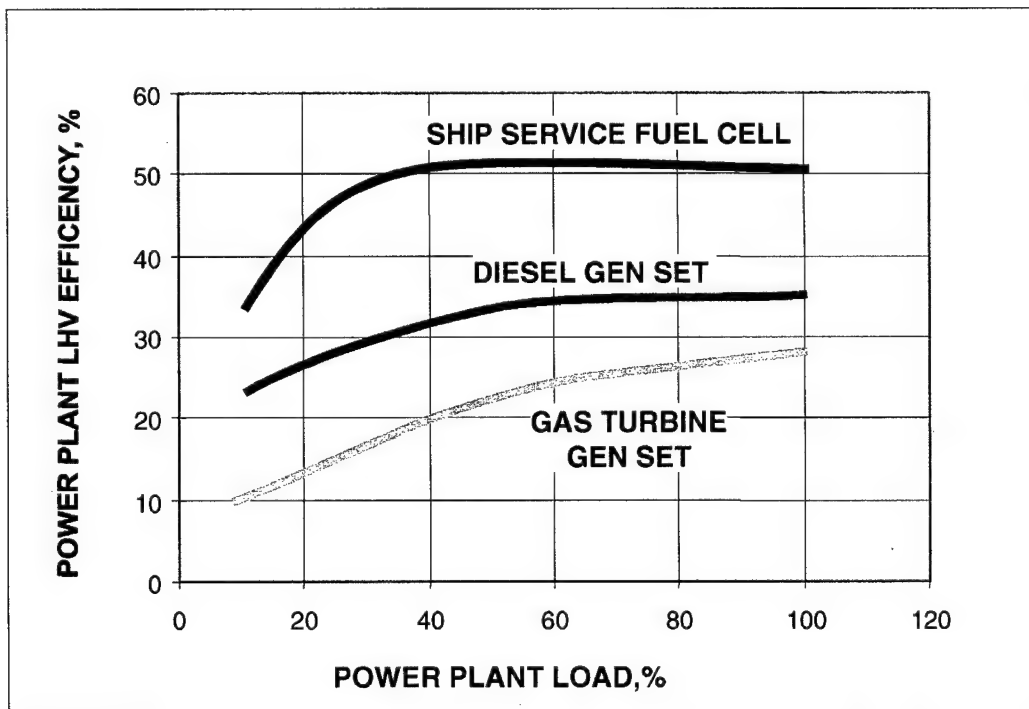


**Figure A-1. 625 kW MODULE EFFICIENCY OVER THE LOAD RANGE**
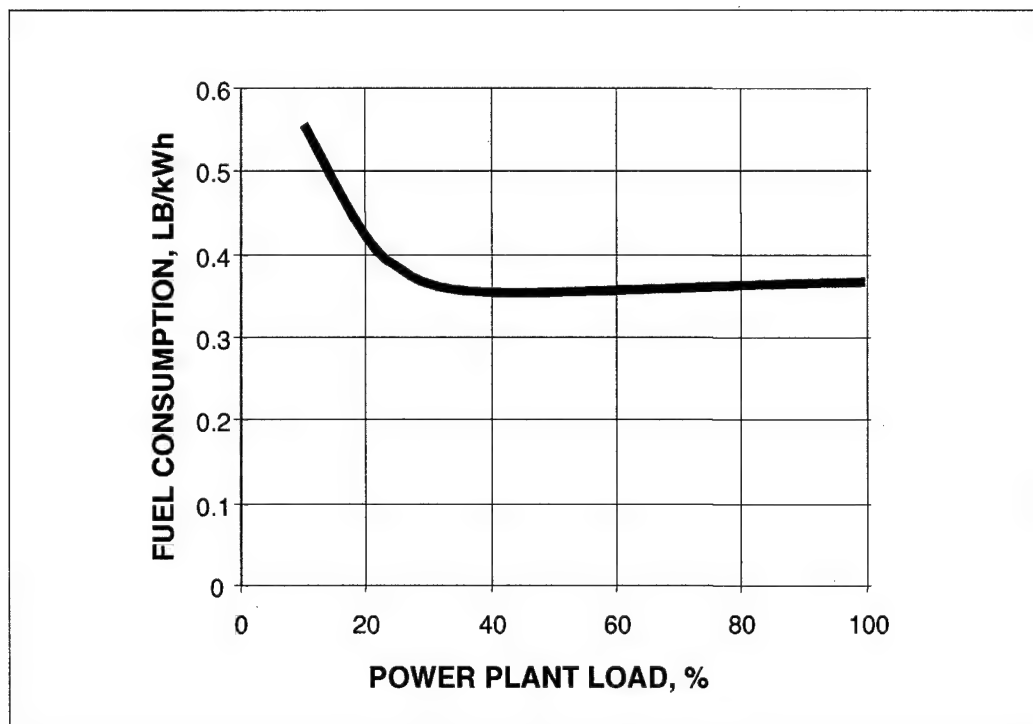
**Figure A-2. 625 kW MODULE FUEL CONSUMPTION VERSUS LOAD**

## 2.0 ELECTRICAL SYSTEM

An electrical one-line diagram for the 625 kW module is shown in Figure A-3. The module includes two direct fuel cell (DFC) stacks, generating a total of 661 kW, some of which is used in the BOP. Each cell stack employs 300 of FCE's commercial fuel cells with nominal dimensions of 27" x 50". At rated power the two fuel cell stacks deliver 1486 amps DC at 445 volts.

The power conditioning system (PCS) converts DC power from the fuel cells to three-phase, three-wire, 450 VAC 60 Hz power. The power control system (PCS) includes a no-load DC disconnect switch, a DC/AC converter, uninterruptible power supply (UPS) and PCS control system. The DC/AC converter is designed to meet MIL-STD-1399 (section 300) and IEEE45 standards for power quality requirements.

The module uses about 40 kW for balance of plant system auxiliaries. Power to the auxiliaries is provided from the motor control center (MCC), which includes switchgear, transformers and motor starters for the balance of plant auxiliaries. The MCC includes blower speed controls for a number of the blowers. A transfer switch is included to power auxiliaries from an external source during start-up.
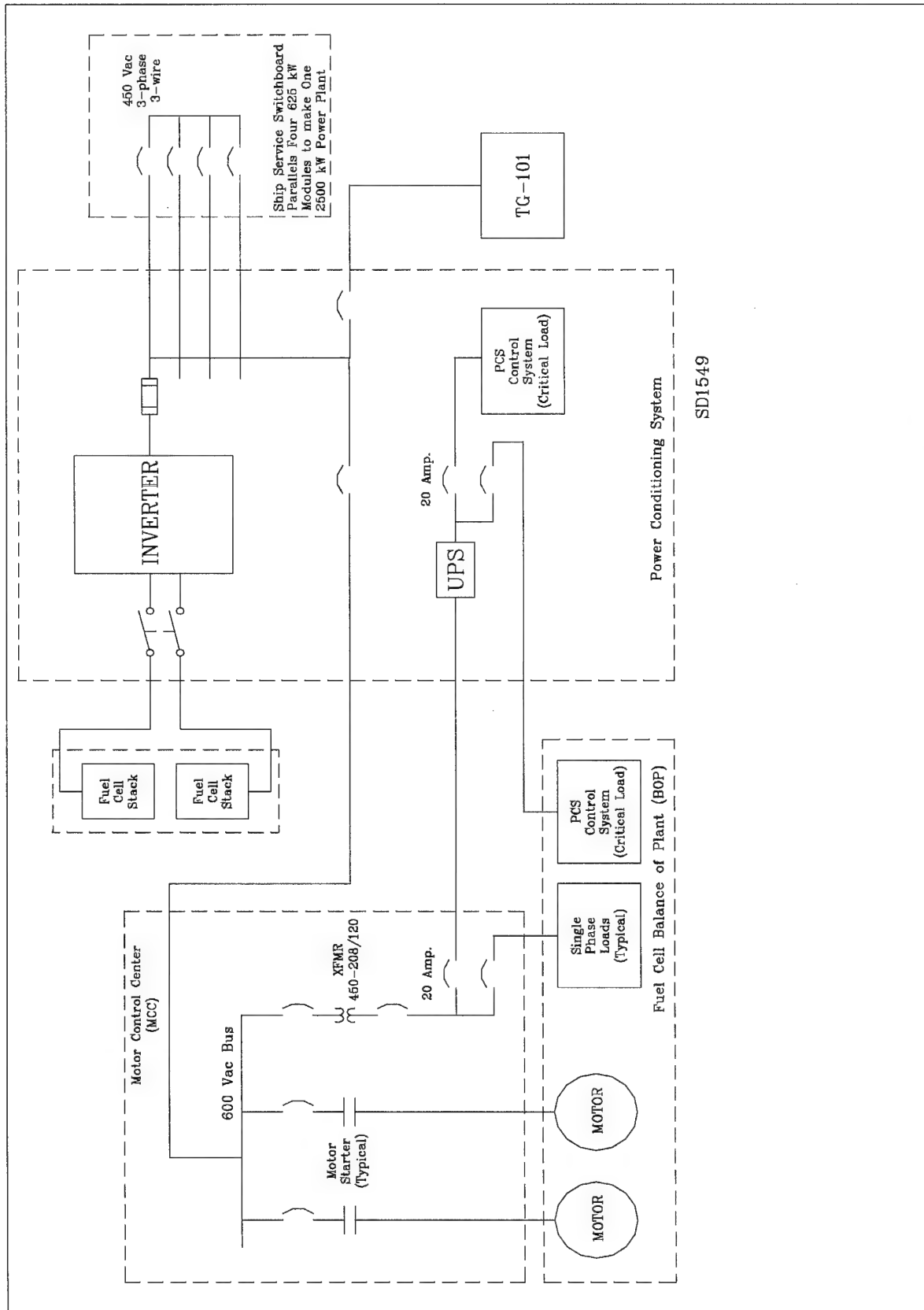
**FIGURE A-3. 625 kW MODULE ELECTRICAL ONE-LINE DIAGRAM**

The electrical system includes a turbo expander generator, TG-101, which delivers an additional 50 kW of AC power using the energy available in the expansion of 325 psig processed fuel from the prereformer down to the fuel cell pressure at 25 psig. The turbo expander includes a 3600-rpm generator delivering 60 Hz AC power at 450 volts.

An electrical one-line diagram of the power converter in the PCS is shown in Figure A-4. The power converter uses isolated gate bipolar transistor (IGBT) power semiconductors and pulse width modulation (PWM) to convert the fuel cell dc voltage to the regulated 450 VAC 60 Hz output. The converter has input filtering of the DC from the fuel cells followed by a DC boost stage. The DC/DC boost stage raises the unregulated 445-600 VDC voltage from the fuel cells to regulated 750 VDC and provides reverse current protection without diodes. Fuses are provided in series with the input boost chopper inductors. The boosted DC voltage is then converted to AC by the inverter. The boost stage uses two power electronics drawers. Each power electronics drawer uses six 1000 amp IGBTs. The inverter uses four of the same power electronics drawers.

The design of the PCS for the developed module has IGBTs with water-cooled cold plates. Closed-loop air circulation to a fresh water-cooled heat exchanger is included for cooling the other components and wiring in the PCS. The inverter also includes AC capacitors and electro-magnetic interference (EMI) filters and an output breaker.

The power conditioning system can provide power factor correction. The PCS control monitors the phase angle between the output voltage and current on all three phases and can adjust the phase angle to change the power factor. The power conditioner is designed to deliver power at ±0.8 power factor. If inductive loads on the ship service bus cause a lagging power factor the power conditioner can correct this condition by delivering power with a leading power factor thus providing power factor correction.
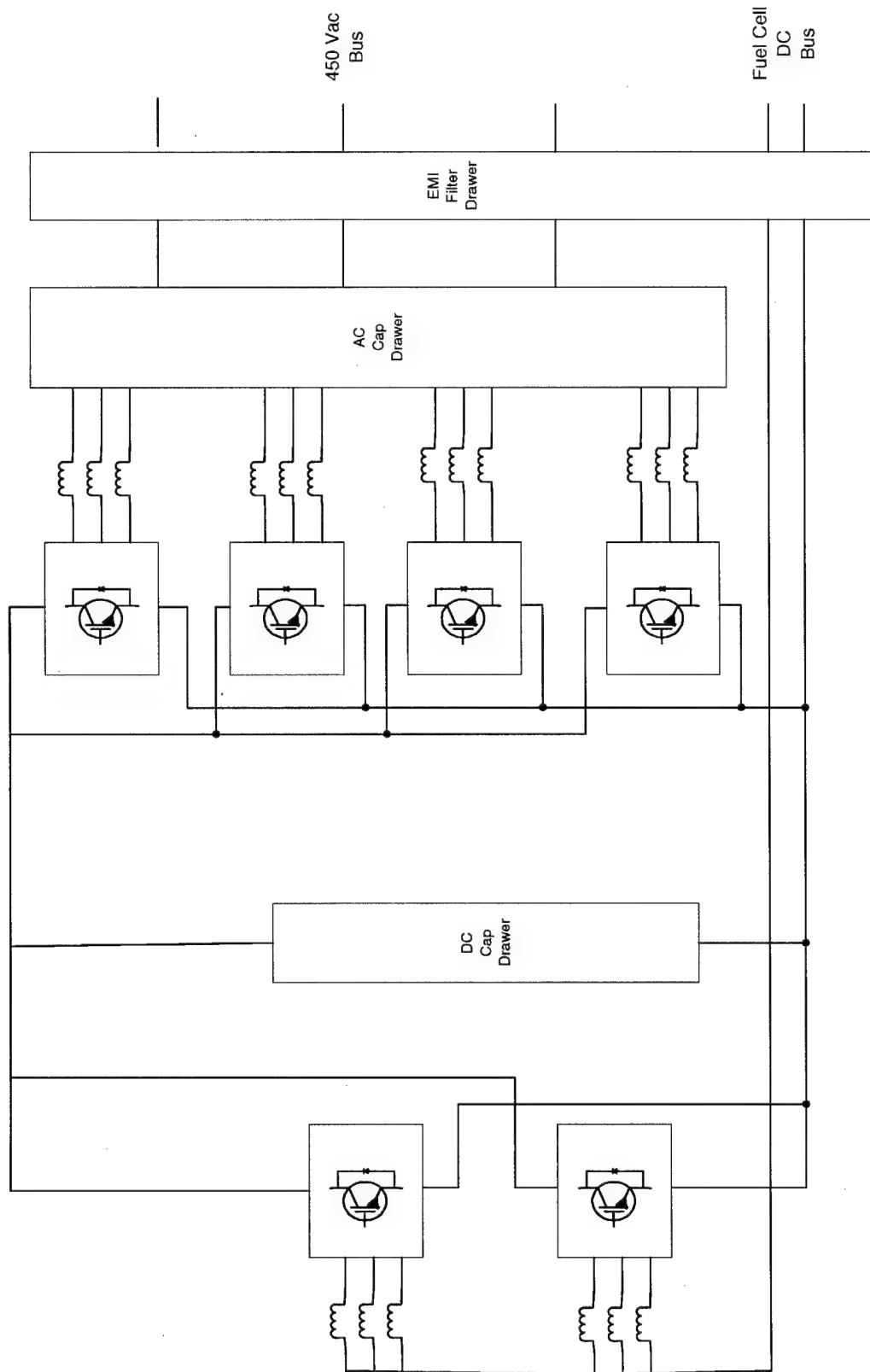
FIGURE A-4. ELECTRICAL ONE-LINE DIAGRAM OF THE POWER CONVERTER IN THE PCS

## 3.0 MECHANICAL SYSTEM

The mechanical system for the 625 kW module, shown in Figure A-5, desulfurizes the NATO F-76 fuel. It then pre-reforms the fuel with steam to a methane-rich gas which is reformed internally and then electrochemically converted to DC power by the direct carbonate fuel cells. The mechanical system also includes provisions to supply air to the fuel cells, manage waste heat within the system, and recover water produced in the fuel cells for use in the fuel conversion process.
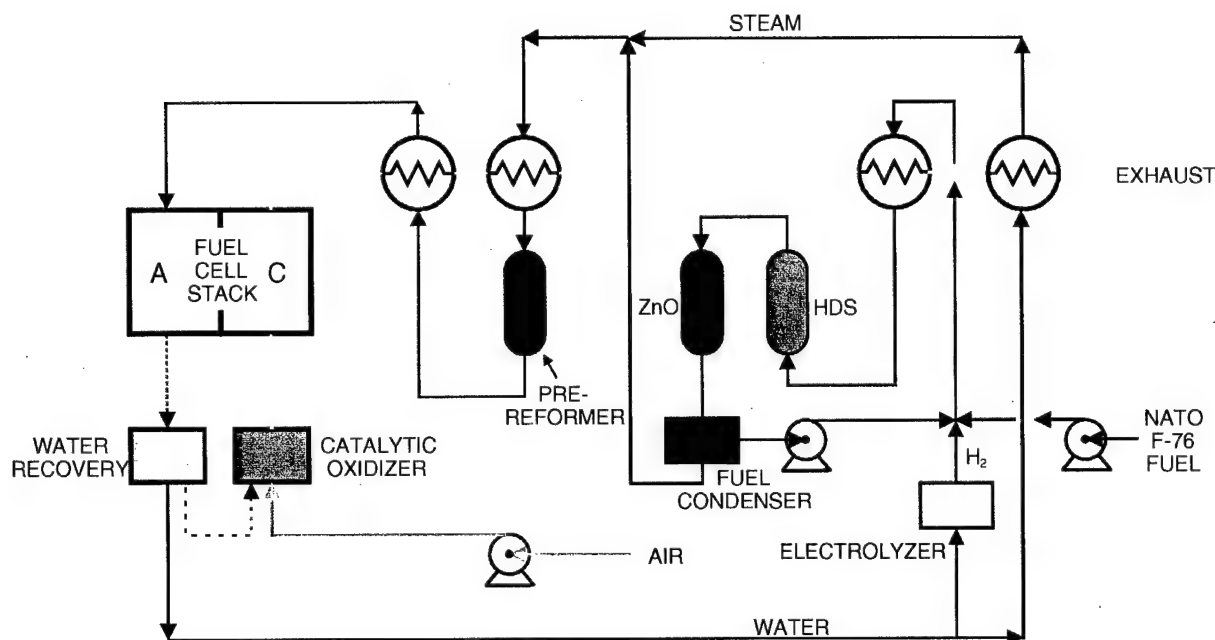


**Figure A-5. Mechanical System Diagram**

The 625 kW power plant module system components are located within an enclosure. Mechanical interfaces with the ship include NATO F-76 supply and drain, air intake, exhaust, and sea water supply and return for cooling.

NATO F-76 fuel is pumped to 700-1000 psia and mixed with recirculated hydrogen and a small amount of makeup hydrogen from an electrolyzer. The heated stream flows through a catalyst bed where sulfur in the fuel reacts with the hydrogen forming $H_2S$. The stream then passes through a chloride guard bed and a bed of ZnO. The $H_2S$ reacts with the ZnO forming ZnS, which remains as a solid in the bed. The stream is then cooled and the desulfurized F-76 is condensed, separated from the hydrogen, which is recirculated, and the liquid desulfurized F-76 is collected in a holding tank. To accommodate sulfur levels in the F-76 fuel up to 1% by weight, the design includes two ZnO beds that can be switched during operation. One bed adsorbs the sulfur while the other bed is being regenerated in situ. This is accomplished by passing a small flow of system exhaust through the bed to oxidize the ZnO forming $SO_2$, which is vented from the system.

The desulfurized F-76 is mixed with steam and flows to an adiabatic pre-reforming reactor where the F-76 is converted to a methane rich stream. This approach to processing of the NATO F-76 provides a high quality methane rich fuel to the DFC stacks.

In the fuel cell stacks the methane rich fuel is reformed with water vapor to hydrogen and carbon oxides. Most of the hydrogen reacts electrochemically in the fuel cells producing DC power. The remaining hydrogen, together with water formed in the cells and $CO_2$ electrochemically transferred from the cell cathodes, is vented from the fuel cell anodes. The anode vent stream is cooled and dried in a condenser where the product water formed in the cells is recovered. The dried anode vent stream then flows to a catalytic oxidizer where it reacts and heats the incoming process air. The stream from the catalytic oxidizer flows to the fuel cell cathodes supplying the oxygen and $CO_2$ completing the fuel cell electrochemical reaction. Exhaust from the fuel cell cathodes provides heat to raise steam and heat fuel processing streams, and is exhausted from the system.

## 4.0 CONTROL SYSTEM AND STRATEGY

The control system is designed for automatic unattended operation. It includes a microprocessor controller with the balance of plant process control algorithms and truth table logic for sequencing between operational states. The control system includes provisions for monitoring and alarms on key process parameters and shutdown actuation for safety and equipment protection, as well as data logging. In addition, the control system has provisions for activation and monitoring from a remote location, and a data output terminal for transfer to a portable data logger for system diagnostics.

The fuel cells themselves have response characteristics similar to a battery provided sufficient reactants are available to support the load current drawn from the cells. During load reduction transients there is a temporary excess of reactants for the decreased load which may be directed to the vent burner while the reactant supply systems decrease flows to the cells proportional to the reduced current demand. During steady-state conditions the fuel system supplies excess fuel to the cells. The unused fuel flows to the catalytic burner, which heats the process air. During increased load steps the excess fuel is available to the cell to partially meet instantaneous current demand while the fuel system increases flow. A fast acting anode flow control valve adjusts fuel to the cells in response to a DC load current signal. Supply of fuel is from the pre-reforming stage of the fuel processing system, which operates at 330 psig and provides an inventory of fuel available to meet demand while process flows to the prereformer are increased. The supply of steam to the prereformer is very rapid by design of the boiler as a once-through type with low fluid inventory. Preliminary analysis of the boiler design indicates a lag of only five seconds to reestablish rated thermal conditions from a 10 percent initial flow condition.

The reactant supply to the cell cathodes operates with excess oxygen and $CO_2$, which is available to support instantaneous current demand while the reactant flow to the cathodes is increased to meet the new current demand. The supply system, which

provides oxygen and $CO_2$ to the cell cathodes, includes variable speed process air and anode recycle blowers.

# APPENDIX B.

# MARINE FUEL CELL — MANEUVERING SURVEY REPORT

# MARINE FUEL CELL — MANEUVERING SURVEY REPORT

## EXECUTIVE SUMMARY

This report documents a survey of U.S. and international regulatory body, commercial, and military sources for existing requirements, ship simulation and model test data, and ship full scale trial data for ship acceleration and stopping capabilities. These data are then used in various regression analyses to determine a correlation between the applicable ship capability and one or more of the ship's characteristics and establish maneuvering requirements for the candidate ship.

This survey is part of the larger effort to develop installation requirements to integrate fuel cells into a candidate ship for ship service and propulsive electric power generation. The candidate ship used in this study is the USCGC VINDICATOR (T-AGOS 3), which has been used in prior and ongoing studies to investigate the operational and cost impacts of integrating fuel cells into the USCG fleet. The report identifies an overall approach, which may be taken to impose various levels of requirements on the candidate ship.

Based on the data gathered and the analysis in the report, the following performance guidelines are recommended, listed in order from the most general, representing minimum acceptable requirements, to the most specific, representing additional, owner-driven requirements:

1) Minimum acceptable stopping distance based on the IMO requirement. No minimum requirement for acceleration can be established.

2) Stopping distance based on "good ship" maneuvering characteristics, as ascertained in the analysis. Due to limited available data, no acceleration requirement can be established.

3) More stringent requirements based on ships of similar type or on the specific ship the candidate ship is replacing.

4) Additional requirements based on a need for higher performance than in previous ships to address a maneuvering deficiency or based on a specific mission requirement.

In the absence of existing trial data and any overriding mission requirements for the candidate ship, T-AGOS 3, subparagraph no. 2 above is used to establish a stopping requirement. Based on the analysis, for a 2295-ton ship with diesel-electric drive and FP propellers, a minimum requirement of ten ship lengths for stopping distance is set. Based on the same criteria and changing from FP to CPP, a requirement of four ship lengths is set. A lack of trial data prevents establishment of an acceleration requirement.

Due to the limited amount of data made available to the authors, the study results and recommendations herein are preliminary in nature and an update is recommended once additional data are gathered.

# TABLE OF CONTENTS

# 1.0 INTRODUCTION

This report documents a survey of existing requirements and data for ship acceleration and stopping capabilities and the development of a database containing specific requirements, simulation predictions, and actual trial data. These data are then used in various regression analyses to determine a correlation between the applicable ship capability and one or more of the ship's characteristics, such as displacement, length, or maximum speed.

This survey is required as part of the larger effort to develop installation requirements to integrate fuel cells into a candidate ship for ship service and propulsive electric power generation. The report identifies an overall approach that may be taken to impose various levels of requirements on the candidate ship. The use of these requirements is twofold, namely, the requirements would apply to the candidate ship for trial performance verification and they would also be used to represent the target maneuvering capabilities for development of the fuel cell propulsion plant simulation model during the design integration phase.

In order to develop requirements that represent minimum acceptable expected/required levels of ship performance, the survey concentrated on mechanical drive low speed and medium speed diesel propulsion plants. Former types of propulsion plants typically employ fixed pitch propellers and require propeller and engine coast down before engines can be stopped and restarted in the astern direction. Therefore, it is expected that the stopping ability is considerably less than for comparable low or medium speed diesel plants with controllable-pitch propellers. Also, diesel plants typically have less installed power available for boost operation than gas turbine propulsion plants, resulting in less power which may be applied astern for stopping.

The candidate ship used in this study is the USCGC VINDICATOR (T-AGOS 3), which has been used in prior and ongoing studies to investigate the operational and cost impacts of integrating fuel cells into the USCG fleet.

# 2.0 BACKGROUND AND APPROACH

Stopping is a maneuver of interest primarily with regard to the avoidance of collisions and groundings. Generally, the stopping distance from harbor speeds (usually 12 to 15 knots) is taken to be the most important criterion for determining the backing power of ships. Collisions at higher speeds are usually avoided by executing the turning maneuver. As ship speed is reduced, the stopping maneuver becomes more important and the turning maneuver becomes less significant. However, in this case, the goal is to ultimately recommend a stopping requirement that will be used to examine the most extreme demands on the fuel cell propulsion system. Therefore, the crash-stop distance from full-ahead speed is taken as the relative measure of stopping ability.

Acceleration is important for ships such as high-endurance cutters, medium-endurance cutters, patrol boats, and other types of ships that may be required to change position rapidly when operating in a fleet or task force. This maneuver also places extreme demands on ship propulsion systems.

In some cases, ship maneuvering requirements are governed by specific ship missions. These mission requirements address such capabilities as mine avoidance for surface combatants, dynamic positioning and track keeping for oceanographic survey ships, and the turning ability of large ships to navigate in restricted waters.

The approach taken in the survey is to research available sources of information, including regulatory requirements, computer simulation and model test data, design reports, building specifications, and builders and acceptance trial data. These requirements and data are then analyzed to determine which ship parameters, such as displacement, length, or speed, would best predict the ship's expected maneuvering characteristics. The predicted characteristics are then written as performance requirements for the candidate ship.

## 3.0 RESEARCH AND ANALYSIS

In general, U.S. and international regulatory body requirements (References 1 to 9) address ship maneuvering trial procedures, minimum acceptable performance in general terms, and documentation of ship maneuvering capabilities and its availability to ship operators.

The International Maritime Organization (IMO) uses a fairly simple mathematical model to indicate the stopping ability of ships:

$$S = A \log_e (1+B) + C$$

where S is the stopping distance in ship lengths and A, B, and C are coefficients dependent on the type of ship and hull form, amount of astern power available, and the time to reverse engines, respectively. The IMO requirement for stopping distance is 15 ship lengths. See Reference 6.

Harold E. Saunders, in *Hydrodynamics in Ship Design*, makes a recommendation for a head reach of 3 ship lengths on high-speed combatant craft to 6, 8, or 10 ship lengths on low-powered cargo ships. See Reference 10.

An examination of numerous existing ship specifications and circulars of requirements (CORs) (references 11 to 27) revealed almost no maneuvering performance requirements. The absence of these data can be attributed to the fact that by the time the specification becomes a contractual instrument, the hull form is fully defined and the choice of propulsion prime movers and propellers has already been made. Hence, maneuvering performance characteristics are not explicit, but rather the result of the hull form and propulsion plant specified.

The available body of government and commercial ship trial performance data applicable to U.S. Navy, U.S. Coast Guard, and Military Sealift Command (MSC) ships was also researched. Contacts with the U.S. Navy produced ship trial data for a various surface combatants, primarily gas turbine powered. Contacts with both the U.S. Coast Guard and MSC were initiated but data held by these organizations have not been located at this time.

The two best sources of data and insight proved to be the Maneuvering Performance of the T-ADC(X) report (Reference 28) and USCG Navigation and Vessel Inspection Circular No. 6-95 (Reference 6). The first document provided simulation-based stopping distance requirements,

based on the actual trials data of several commercial and Naval ships. This background trial data was incorporated into the database of ship maneuvering data for this report. The second document contained The Interim Standards for Ship Maneuverability (MSC/Circ.644), Appendix 3 – Stopping Ability of Very Large Ships, which provided the theoretical background for the IMO standard for ship stopping distance. Though the focus of this document is for large commercial ships, the background consideration of ship length, displacement, top speed, type of prime mover, and time delay in applying thrust astern in formulation of the stopping distance equation was insightful.

Analysis of the data focused on determining upon which parameters ship acceleration and stopping ability depend. An effort was taken to identify as many parameters as necessary to obtain a coherent relationship, without reducing the size of the parameter subgroups to so few points as to be meaningless.

Preliminary analysis of stopping distance focused on the following primary ship parameters:

a. Displacement

. Prime mover type

.. Propeller type

Appendix A contains the results of this analysis and the background data. Ship trial displacements ranged from 700 to 52,374 long tons. Prime movers included diesel engines, gas turbines, electric motors, and steam turbines. Propellers included fixed pitch (FP) and controllable pitch (CP) propellers. The best-fit curves represent a mean performance. Acceptable performance may be considered to be within a band above and below this line. The scatter in the data from each of these lines can be attributed to the following secondary parameters:

a. Installed propulsion power

b. Time delay from the stop command to applying power astern

c. Number of propulsors.

Time delay includes mechanical delay in the propulsion system for stopping of diesel engines and reversing FP propeller rotation and for reversing the controllable reversible pitch propeller. Furthermore, limiters built into the control system impose a delay before current can be reversed in electric motors. Lack of more detailed trial data and the small pool of ships prevented further investigation into additional relationships that could be formed using these secondary parameters.

A second approach was to use R.A. Norbby's nondimensional head reach parameter from the 1983 SNAME paper, "Design and Verification for Adequate Ship Maneuverability," (Reference 29),

$$R' = R_h / LBP / F^2$$

$$= R_h \times g / V^2$$

where $R_h$ is head reach, F is initial full speed Froude number, and V is initial full speed. Appendix B contains the results of this analysis and the background data. This parameter was plotted versus the ship displacement. The plots were divided into FP propeller and CPP groups. The survey data plot also shows a best-fit line through the two data groups.

Principles of Naval Architecture, Reference 32, includes stopping data for older commercial type ships. These data are included in Appendix C for information.

Analysis of acceleration was hindered by lack of data. However, the ship parameters as identified above for ship stopping also contribute to ship acceleration. Additional data are required to formulate a coherent relationship between one or more of these parameters.

## 4.0 RESULTS AND RECOMMENDATIONS

Due to the limited amount of data made available to the authors, the curves herein are preliminary in nature. Therefore, it is recommended that these curves be updated and refined as more data points are gathered.

In the meantime, to formulate a set of requirements which ship designers may use, the following performance guidelines are recommended, listed in order from the most general, representing minimum acceptable requirements, to the most specific, representing additional, owner-driven requirements:

- Minimum acceptable stopping distance based on the IMO requirement (see Reference 6). No minimum requirement for acceleration can be established.

- Stopping distance based on "good ship" maneuvering characteristics, as ascertained in the analysis (see Appendix A). Due to limited available data, no acceleration requirement can be established.

- More stringent requirements based on ships of similar type or on the specific ship the candidate ship is replacing.

- Additional requirements based on a need for higher performance than in previous ships to address a maneuvering deficiency or based on a specific mission requirement.

In the absence of existing trial data and any overriding mission requirements for the candidate ship, T-AGOS 3, subparagraph no. 2 above, may be used to establish a stopping requirement. Using the curves in Appendix A, for a 2295 ton ship with diesel-electric drive and

FP propellers, a minimum requirement of ten ship lengths for stopping distance may be set. Based on the same criteria and changing from FP to CPP, a requirement of four ship lengths may be set. Once again, the lack of trial data prevents establishment of an acceleration requirement.

## 5.0 REFERENCES

1) IMO Resolution A.751(18), 4 Nov 1993

2) SOLAS, Consolidated Edition, 1997

3) ABS Rules for Building and Classing Steel Vessels, 1997-1999

4) Lloyd's Register of Shipping, Provisional Rules for the Classification of Naval Ships, July 1999

5) Rules for Classification, Det Norske Veritas, Jan 1999

6) Navigation and Vessel Inspection Circular No. 6-95, "Maneuvering Standards," U.S. Coast Guard, 21 Jul 1995 (incl. IMO A 18/Res. 751, 22 Nov 1993 and MSC/Circ.644, 6 Jun 1994)

7) Code of Federal Regulations, Title 46-Shipping, Chapter 1-Coast Guard, US Department of Transportation

8) SNAME T&R Bulletin 3-47, Guide for Sea Trials, 1989

9) INSURVINST 4720.1A, Dept. of the Navy, 15 Nov 1993

10) Saunders, Harold E. Hydrodynamics in Ship Design, Volume III, 1965

11) General Specifications for T-Ships, 1991

12) General Specifications for Ships of the United States Navy, 1995

13) System Specification for the Auxiliary Dry Cargo Carrier, T-ADC(X), 8 Sept 1999

14) Specifications for Building Fleet Oiler T-AO 187 Class, 17 Aug 1982

15) COR for New Construction, Commercial Strategic Sealift Ships, COM-20, 22 Apr 1992

16) COR for Conversion of Existing Ships to Strategic Sealift Ships, CSP/S-24, 22 Apr 1992

17) Low Endurance Fisheries Research Vessel Circular of Requirements, Oct 1994

18) NOAA Low Endurance LMR, Circular of Requirements, Mar 1993

19) T-AGS Ocean (Ice) Circular of Requirements, 18 Apr 1991

20) T-AGS 51/52 Specification, July 1990

21) T-AGS 51/52 Circular of Requirements, May 1990

22) FF 21 Ship Specification, 1992-1993

23) LHD 5 Ship Specification, Mar 1999

24) LPD 17 Ship Specification, 8 Apr 1996

25) MHC 51 Ship Specification, Dec 1987

26) MHC 53 Ship Specification, Mar 1989

27) T-AGS 60 Circular of Requirements, 18 Aug 1989

28) Maneuvering Performance of the ADC(X) Ship, Rev. A, 13 Feb. 1997

29) "Design and Verification for Adequate Ship Maneuverability", Transactions of the Society of Naval Architects and Marine Engineers, June 1983

30) "Using Simulation to Determine the Maneuvering Performance of the WAGB-20," Naval Engineers Journal, Jan 1998

31) Electric Propulsion for a Cruise Ship, presented at Propulsion '96 Conference, 24 Sep 1996

32) Mandel, Philip, "Ship Maneuverability and Control," Principles of Naval Architecture, 1967

## 6.0 POINTS OF CONTACT

The following personnel were primary points of contact used for research during the study:

Mr. Robert Kalmus
Chief, Auxiliary Machinery Branch (025)
U.S. Coast Guard Engineering Logistics Center
2401 Hawkins Point Road
Baltimore, MD 21226
410-762-6749

Mr. Kevin Danahy
U.S. Coast Guard Engineering Logistics Center
2401 Hawkins Point Road
Baltimore, MD 21226
(410) 762-6799

Mr. Dick Middleton
U.S. Coast Guard Engineering and Logistics Center
2401 Hawkins Point Road
Baltimore, MD 21226
410-762-6711

Mr. Ed French
Military Sealift Command
Ship Introduction Group
202-685-5568

Mr. Hasan Pehlivan
Naval Sea Systems Command
Ship Propulsion Group, SEA 03Z11
703-602-6101

Mr. Ernst Jung
Wartsila NSD North America, Inc.
One Blue Hill Plaza, PO Box 1544
Pearl River, NY 10965
914-623-1212

Ms. Margaret Holland
Librarian, JJMA
4300 King Street, Suite 400
Alexandria, VA 22302
703-418-0100

# APPENDIX B-ANNEX A

# STOPPING DISTANCE USING DISPLACEMENT
# AND PROPULSION PLANT TYPE

**Ship Reach vs. Displacement**
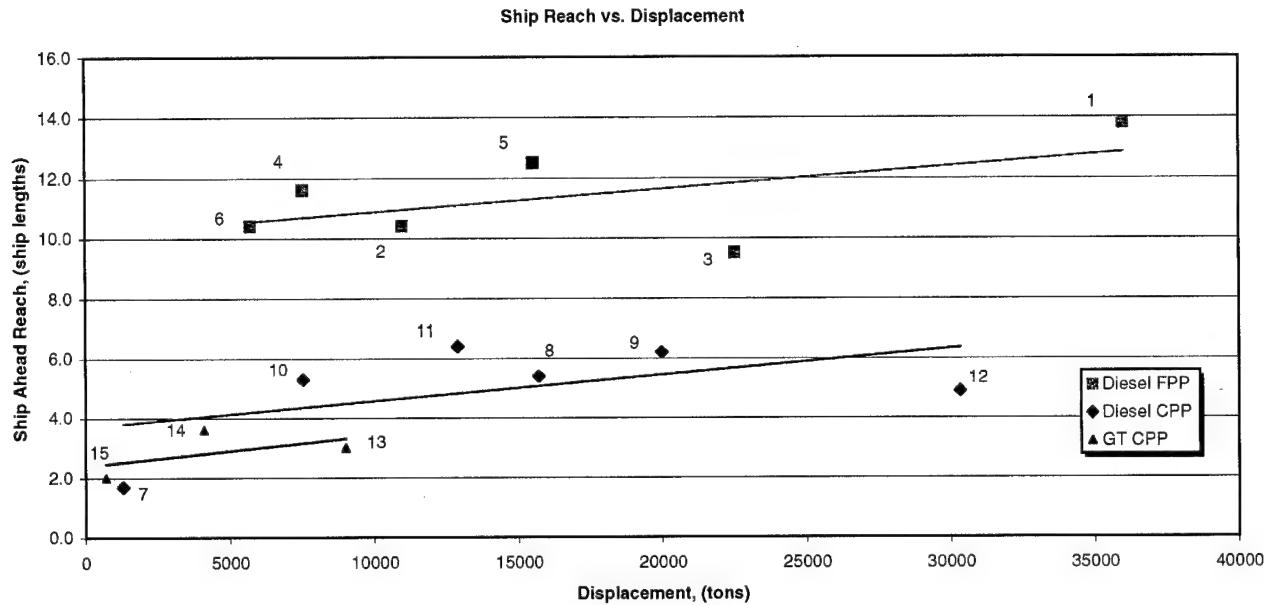


## STOPPING DISTANCE SHIP DATABASE

| ID | SHIP | DISPLACEMENT LTONS | TRIAL DISPL. LTONS | LENGTH FT | SPEED KT | ENGINE | PROP | STOP DISTANCE REACH/SHIP LENGTH |
|----|------|--------------------|--------------------|-----------|----------|--------|------|---------------------------------|
| 1 | CONTAINERSHIP | 35996 | 35996 | 697 | 22.0 | DIESEL | FPP | 13.8 |
| 2 | GENERAL | 17538 | 10980 | 481 | 17.3 | DIESEL | FPP | 10.4 |
| 3 | CONTAINERSHIP | 52374 | 22520 | 735 | 24.0 | DIESEL | FPP | 9.5 |
| 4 | GENERAL | 11900 | 7542 | 441 | 20.5 | DIESEL | FPP | 11.6 |
| 5 | CONTAINERSHIP | 24700 | 15523 | 574 | 22.4 | DIESEL | FPP | 12.5 |
| 6 | GENERAL | 11300 | 5724 | 433 | 19.0 | DIESEL | FPP | 10.4 |
| 7 | MINEHUNTER | 1300 | 1300 | 215 | 14.0 | DIESEL | CPP | 1.7 |
| 8 | LANDING SHIP | 15700 | 15700 | 575 | 24.0 | DIESEL | CPP | 5.4 |
| 9 | RORO | 27790 | 19979 | 574 | 21.4 | DIESEL | CPP | 6.2 |
| 10 | GENERAL | 11900 | 7542 | 441 | 20.5 | DIESEL | CPP | 5.3 |
| 11 | CONTAINERSHIP | 20215 | 12901 | 551 | 21.5 | DIESEL | CPP | 6.4 |
| 12 | CRUISE SHIP | 31338 | 30327 | 607 | 22.3 | DIESEL | CPP | 4.9 |
| 13 | DESTROYE | 9000 | 9000 | 465 | 30.0 | GT | CPP | 3.0 |
| 14 | FRIGATE | 4100 | 4100 | 410 | 28.0 | GT | CPP | 3.6 |
| 15 | MISSILE | 700 | 700 | 100 | 38.0 | GT | CPP | 2.0 |

# APPENDIX B – ANNEX B

# STOPPING DISTANCE ANALYSIS
# USING NON-DIMENSIONAL HEAD REACH PARAMETER
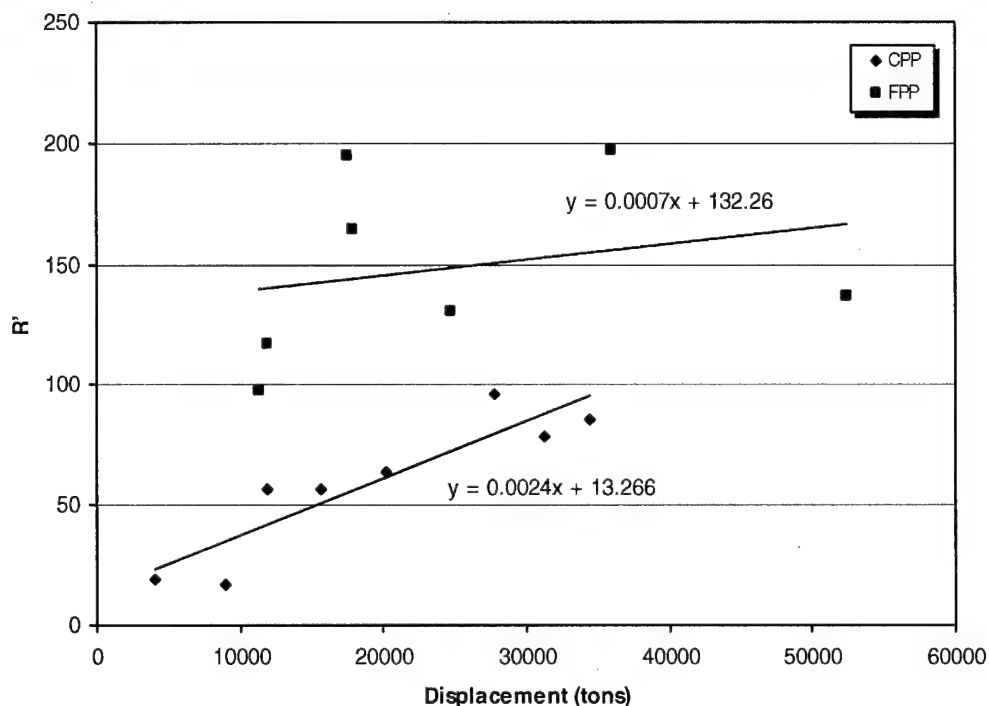


NON-DIMENSIONAL HEAD REACH, R' COMPUTATION

$$R' = R_H / LBP / F_N^2$$

| SHIP | $R_H$/LBP | INITIAL V (KTS) | INITIAL V (FT/S) | LBP (FT) | $F_N$ | R' | D (TONS) |
|---|---|---|---|---|---|---|---|
| DESTROYER | 3.00 | 30.2 | 51.0 | 465 | 0.417 | 17.3 | 9000 |
| FRIGATE | 3.60 | 29.7 | 50.1 | 410 | 0.436 | 18.9 | 4100 |
| LANDING SHIP | 5.40 | 24.9 | 42.0 | 575 | 0.309 | 56.6 | 15700 |
| AUXILIARY CARGO | 4.62 | 20.0 | 33.8 | 656 | 0.232 | 85.6 | 34400 |
| RORO | 6.22 | 20.5 | 34.6 | 574 | 0.255 | 96.0 | 27790 |
| GENERAL CARGO | 5.29 | 21.6 | 36.5 | 441 | 0.306 | 56.5 | 11900 |
| CONTAINERSHIP | 6.35 | 24.9 | 42.0 | 551 | 0.316 | 63.8 | 20215 |
| CRUISE LINER | 4.86 | 20.6 | 34.8 | 607 | 0.249 | 78.6 | 31338 |
| AMPHIBIOUS SHIP | 9.44 | 19.0 | 32.1 | 556 | 0.240 | 164.3 | 17900 |
| CONTAINERSHIP | 13.77 | 23.5 | 39.7 | 699 | 0.264 | 196.9 | 35996 |
| GENERAL CARGO | 10.35 | 17.0 | 28.7 | 481 | 0.231 | 194.7 | 17538 |
| CONTAINERSHIP | 9.51 | 24.0 | 40.5 | 735 | 0.263 | 137.2 | 52374 |
| GENERAL CARGO | 11.57 | 22.2 | 37.5 | 441 | 0.314 | 117.0 | 11900 |
| CONTAINERSHIP | 12.50 | 24.9 | 42.0 | 574 | 0.309 | 130.7 | 24700 |
| GENERAL CARGO | 10.39 | 22.8 | 38.5 | 433 | 0.326 | 97.8 | 11300 |
| TANKER | 6.96 | 16.0 | 27.0 | 909 | 0.158 | 279.3 | 161706 |
| MINESWEEPER | 1.70 | 5.8 | 9.8 | 215 | 0.118 | 122.8 | 1300 |

# APPENDIX B-ANNEX C

# HEAD REACH PARAMETERS OF VARIOUS SHIP TYPES

Table 31  Head Reach for Fifteen Types of Ships
(From Principles of Naval Architecture)

| Vessel | Displacement (tons) | Speed (knots) | ehp | Percent Torque | Head Reach S, (ft) | S/L |
|---|---|---|---|---|---|---|
| C1-B | 12,900 | 14 | 2550 | 75 | 3610 | 9.16 |
| | | 12 | 1550 | 75 | 2930 | 7.43 |
| | | 14 | 2550 | 56.5 | 4325 | 10.98 |
| | | 12 | 1550 | 56.5 | 3565 | 9.05 |
| C1-M-AV1 | 7,400 | 11 | 1065 | 100 | 1910 | 5.97 |
| | | 11 | 1065 | 113 | 1760 | 5.50 |
| C2-S-B1 | 13,900 | 15.5 | 3720 | 75.5 | 3650 | 8.38 |
| | | 12 | 1580 | 75.5 | 2500 | 5.75 |
| | | 15.5 | 3720 | 58 | 4310 | 9.90 |
| | | 12 | 1580 | 58 | 3050 | 7.01 |
| C3 | 16,725 | 16.5 | 5000 | 75 | 3690 | 7.94 |
| | | 12 | 1850 | 75 | 2310 | 4.97 |
| | | 16.5 | 5000 | 56 | 4460 | 9.80 |
| | | 12 | 1850 | 56 | 2860 | 6.15 |
| C4-S-A4 | 19,900 | 17 | 5870 | 75 | 4260 | 8.58 |
| | | 12 | 1930 | 75 | 2560 | 5.16 |
| | | 17 | 5870 | 56 | 5150 | 10.38 |
| | | 12 | 1930 | 56 | 3200 | 6.45 |
| C4-S-1A Mariner | 18,674 | 20 | 9590 | 75.5 | 3780 | 7.16 |
| | | 12 | 1815 | 75.5 | 1720 | 3.26 |
| | | 20 | 9590 | 57 | 4530 | 8.59 |
| | | 12 | 1815 | 57 | 2170 | 4.11 |
| EC2-S-C1 Liberty | 14,200 | 11 | 1208 | 100 | 2840 | 6.82 |
| | | 11 | 1208 | 120 | 2480 | 5.96 |
| VC2-S-AP2 | 14,800 | 15.5 | 3820 | 74.8 | 3745 | 8.60 |
| | | 12 | 1700 | 74.8 | 2610 | 6.00 |
| | | 15.5 | 3820 | 54.5 | 4580 | 10.50 |
| | | 12 | 1700 | 54.5 | 3270 | 7.50 |
| VC2-S-AP3 | 14,800 | 17 | 5400 | 76 | 3535 | 8.11 |
| | | 12 | 1700 | 76 | 2155 | 4.95 |
| | | 17 | 5400 | 61 | 4070 | 9.35 |
| | | 12 | 1700 | 61 | 2540 | 5.83 |
| L6-S-B1 | 21,000 | 10.5 | 1390 | 100 | 3620 | 5.99 |
| | | 10.5 | 1390 | 122 | 3140 | 5.19 |
| P2-S1-DN3 | 17,700 | 19.2 | 8400 | 74.8 | 3790 | 7.58 |
| | | 12 | 1800 | 74.8 | 1890 | 3.78 |
| | | 19.2 | 8400 | 54.5 | 4640 | 9.29 |
| | | 12 | 1800 | 54.5 | 2405 | 4.81 |
| P2-S2-R2 | 20,700 | 19 | 8800 | 76.5 | 3750 | 6.55 |
| | | 12 | 2135 | 76.5 | 1860 | 3.25 |
| | | 19 | 8800 | 65.5 | 4110 | 7.17 |
| | | 12 | 2135 | 65.5 | 2085 | 3.64 |
| P2-SE2-R1 | 22,400 | 19 | 9500 | 124 | 2790 | 4.87 |
| | | 12 | 2300 | 124 | 1340 | 2.34 |
| P3-S2-DL2 | 30,100 | 22.5 | 20000 | 75 | 4090 | 6.47 |
| | | 12 | 2070 | 75 | 1580 | 2.50 |
| | | 22.5 | 20000 | 56 | 4940 | 7.81 |
| | | 12 | 2070 | 56 | 2000 | 3.16 |
| T2-SE-A1 | 21,900 | 14.5 | 3970 | 120 | 3120 | 6.20 |
| | | 12 | 2090 | 120 | 2340 | 4.65 |

# APPENDIX C.

# DYNAMIC SIMULATION RESPONSE CURVE GENERATION

# DYNAMIC SIMULATION RESPONSE CURVE GENERATION

The fuel cell subsystem Simulink™ model was provided by FCE. The model is designed to generate the fuel cell internal flow time histories as well as the corresponding DC and AC electric output power histories. The diagrams of the actual Simulink™ model modules are depicted in Figure C-1. It can be subdivided into four sub-models:

1) The Inverter Control model (Figure C-2),
2) The 625 kW Ship Service Fuel Cell Module model (Figure C-3),
3) The Process Control model (Figure C-4), and
4) The Process Measurement model (Figure C-5).

### SIMULINK ™MODEL OF THE 625 KW FUEL CELL SYSTEM
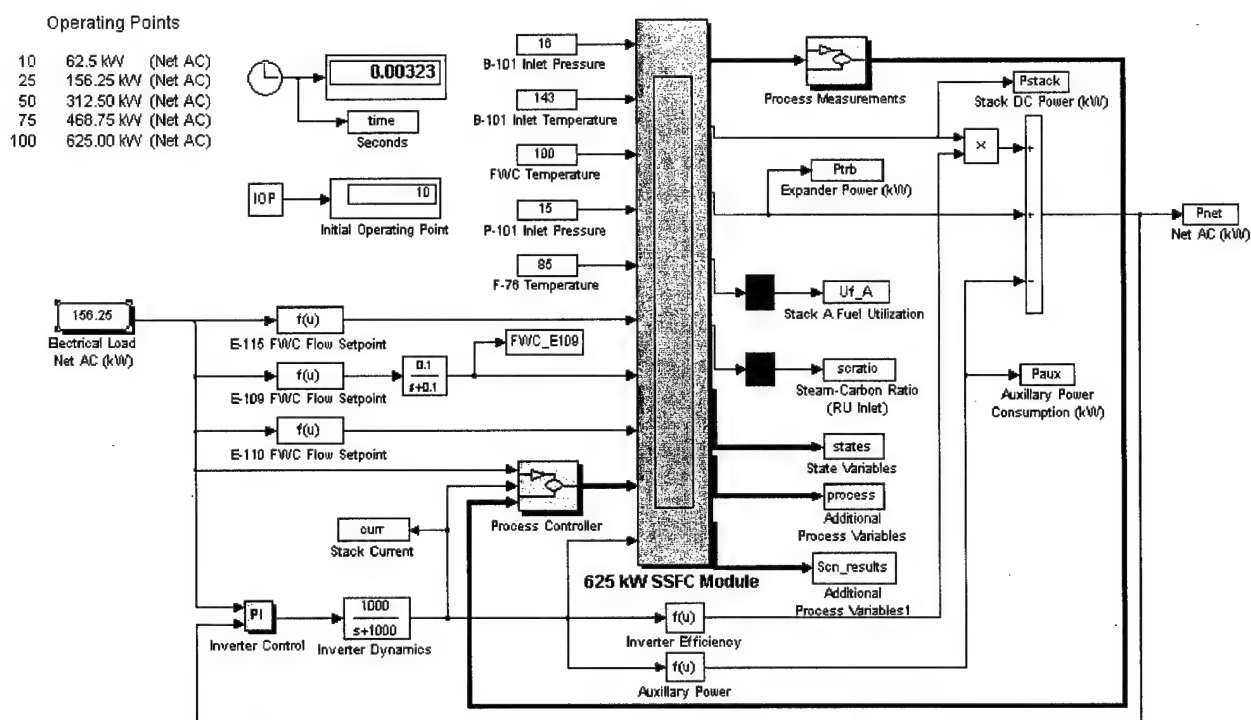


Dynamic Simulation Model for Ship Service Fuel Cell

Figure C-1. Simulink™ Model Modules

### SIMULINK MODEL OF THE INVERTER CONTROL MODULE
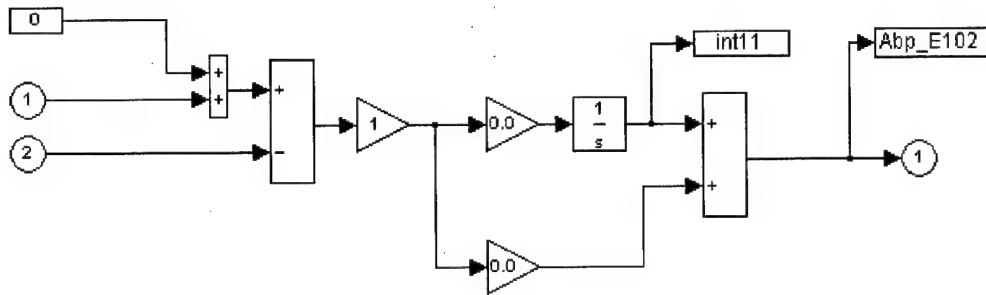


Figure C-2.  Inverter Control Module

The 625 kW SSFC model (Figure C-3) contains all mathematical function required to simulate the transient and steady-state responses of the fuel cell system.  The Process Control model (Figure C-4) contains all the control schematic diagrams needed for operating the 625 kW SSFC module system in a stable and fast response manner.  The Process Measurement model (Figure C-5) samples the operational parameters required for the control of the system and transfers their values from the 625 kW SSFC module to the Inverter control module.  The Inverter control model contains all the control routines needed for the inversion of the fuel cell DC power into AC power.
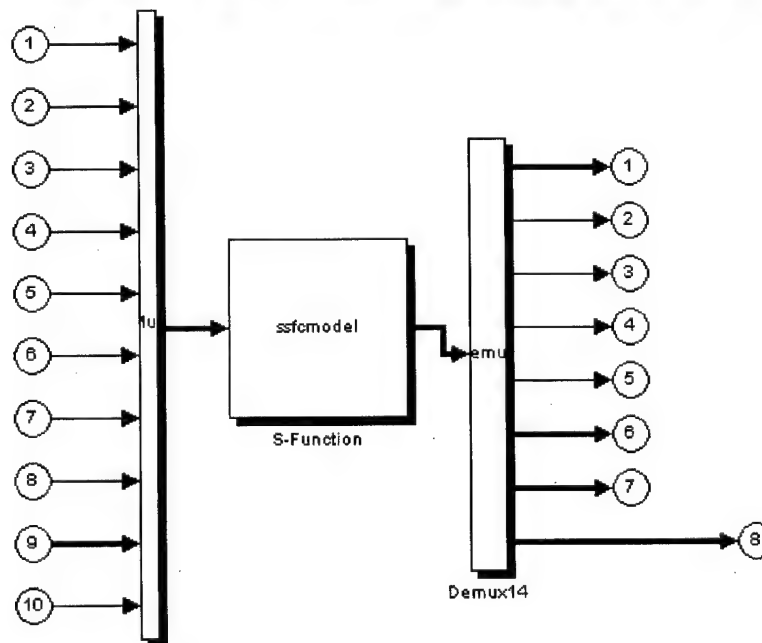


Figure C-3.  625 kW SSFC Module Model

## SIMULINK™ MODEL OF THE PROCESS CONTROL MODULE
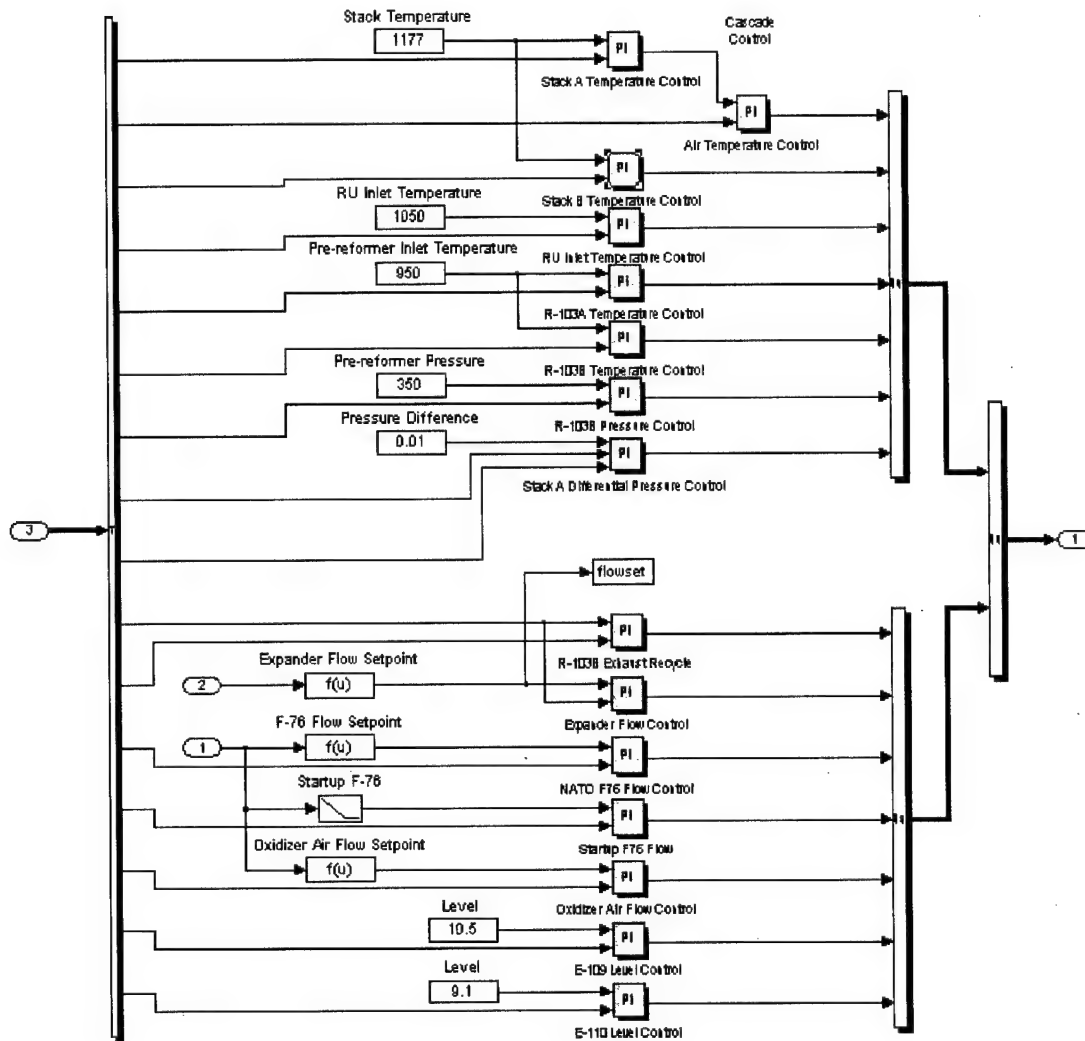
Figure C-4.  Process Control Model

## SIMULINK ™OF THE PROCESS MEASUREMENT MODEL
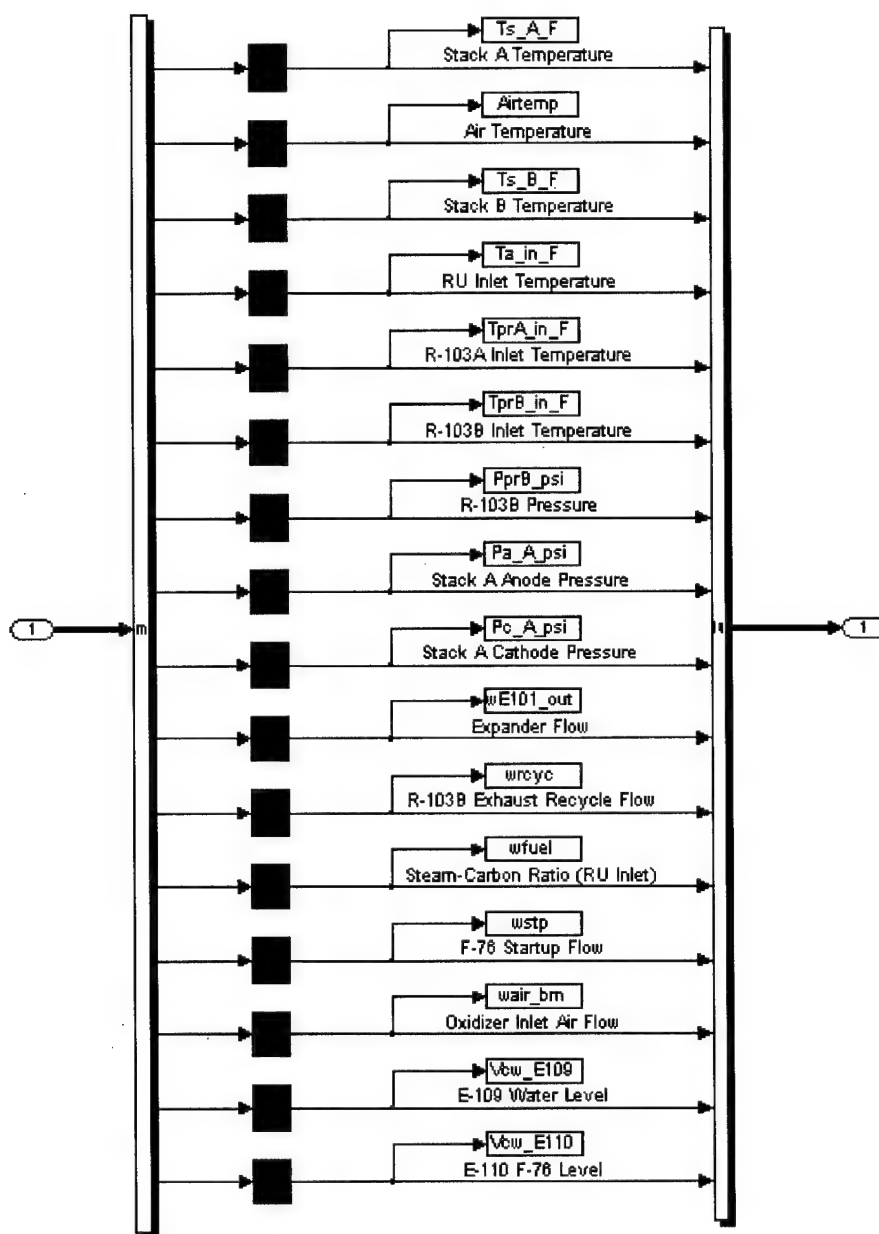


Figure C-5.  Process Measurement Model

Due to the nature of the Simulink™ simulator, the model is incapable of producing results in real-time.  Therefore, for the purpose of incorporating it in the real-time simulation performed with SIMSMART™, its code was modified so that the transient response curves of selected variables can be captured and generated off-line.  For the purpose of testing the modified Simulink™ model, the following variables were extracted:

- Simulation Time (sec)

- AC Net Power Out from FC (kW)

- Mass Flow through the heat recovery unit System (lbm/hr)

- Fuel Mass Flow Rate(lbm/hr)

- Cooling water flow rate at inlet of E116 (lbm/hr)

- Cooling water Temperature at inlet of E116 (°F)

- Prereformer A inlet molar flow (lbmol/hr)

- Prereformer A outlet molar flow (lbmol/hr)

- Prereformer A Temperature (°F)

- Prereformer B inlet molar flow (lbmol/hr)

- Prereformer B outlet molar flow (lbmol/hr)

- Prereformer B Temperature (°F)

The major interest for the SIMSMART$^{TM}$ simulation is the fuel cell net AC power output transient response from a given level to a demand level. The fuel cell system is non-linear. Therefore, the shape of each power transient response curve depends on the values of its initial and terminal power load levels which means that in general, curves which correspond to different initial power levels may intersect. Nevertheless, for the purpose of assessing the performance of the fuel cell as a propulsion power generator, there is a need to cover the whole range of the initial-terminal power level paths. Due to the fact that the curves, which have a given starting power level never intersect, they can be used to generate the time response surface for a given starting power level. To cover the whole range of starting levels, the process has to be repeated in intervals of 5 percent of full power starting with 10 percent.

For each starting power level, four curves corresponding to equally spaced terminal levels are generated. The curves are then approximated by 20$^{th}$ order polynomials by means of curve fitting in the least squares sense. Then, for each time instant, the curve corresponding to a given intermediate terminal power level is obtained by a weighted average of the values of the computed curves and the constant initial power curve at the given time instant via:

$$P(t) = \sum_{i=1}^{5} W_i P_i(t) \tag{1}$$

The interpolation weights, $W_i$, are assumed to be constant from time zero to steady-state for all terminal power levels which are all larger than or all smaller than the initial power level and thus, they are computed from the power interpolation at steady-state. Therefore, the resulting weights are given by:

$$W_1 = \frac{\left(P(\infty)-P_2(\infty)\right)\left(P(\infty)-P_3(\infty)\right)\left(P(\infty)-P_4(\infty)\right)\left(P(\infty)-P_5(\infty)\right)}{\left(P_1(\infty)-P_2(\infty)\right)\left(P_1(\infty)-P_3(\infty)\right)\left(P_1(\infty)-P_4(\infty)\right)\left(P_1(\infty)-P_5(\infty)\right)} \tag{2}$$

$$W_2 = \frac{\left(P(\infty) - P_1(\infty)\right)\left(P(\infty) - P_3(\infty)\right)\left(P(\infty) - P_4(\infty)\right)\left(P(\infty) - P_5(\infty)\right)}{\left(P_2(\infty) - P_1(\infty)\right)\left(P_2(\infty) - P_3(\infty)\right)\left(P_2(\infty) - P_4(\infty)\right)\left(P_2(\infty) - P_5(\infty)\right)} \tag{3}$$

$$W_3 = \frac{\left(P(\infty) - P_1(\infty)\right)\left(P(\infty) - P_2(\infty)\right)\left(P(\infty) - P_4(\infty)\right)\left(P(\infty) - P_5(\infty)\right)}{\left(P_3(\infty) - P_1(\infty)\right)\left(P_3(\infty) - P_2(\infty)\right)\left(P_3(\infty) - P_4(\infty)\right)\left(P_3(\infty) - P_5(\infty)\right)} \tag{4}$$

$$W_4 = \frac{\left(P(\infty) - P_1(\infty)\right)\left(P(\infty) - P_2(\infty)\right)\left(P(\infty) - P_3(\infty)\right)\left(P(\infty) - P_5(\infty)\right)}{\left(P_4(\infty) - P_1(\infty)\right)\left(P_4(\infty) - P_2(\infty)\right)\left(P_4(\infty) - P_3(\infty)\right)\left(P_4(\infty) - P_5(\infty)\right)} \tag{5}$$

$$W_5 = \frac{\left(P(\infty) - P_1(\infty)\right)\left(P(\infty) - P_2(\infty)\right)\left(P(\infty) - P_3(\infty)\right)\left(P(\infty) - P_4(\infty)\right)}{\left(P_5(\infty) - P_1(\infty)\right)\left(P_5(\infty) - P_2(\infty)\right)\left(P_5(\infty) - P_3(\infty)\right)\left(P_5(\infty) - P_4(\infty)\right)} \tag{6}$$

The process is repeated for other internal variables as well.

Figures C-6 and C-7 show the results obtained by running the Simulink$^{TM}$ simulation model for increasing and decreasing load demand levels for various initial steady-state conditions, respectively. The curves in Figure C-8 are examples of the calculated intermediate demand curves, which were obtained by applying the interpolation scheme described by Equations one through six. Figure C-9 presents same type curves for an internal parameter, the hot box total voltage (DC) output as function of time for varying steps in load variations.
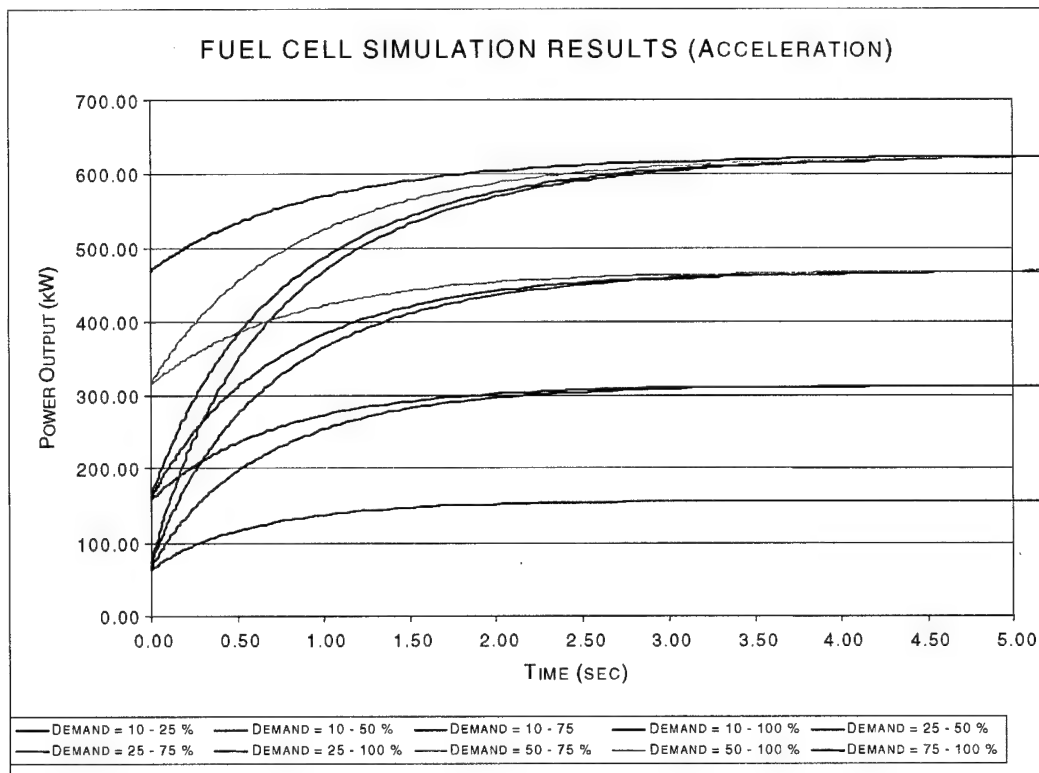
Figure C-6.  Load Demand Increase
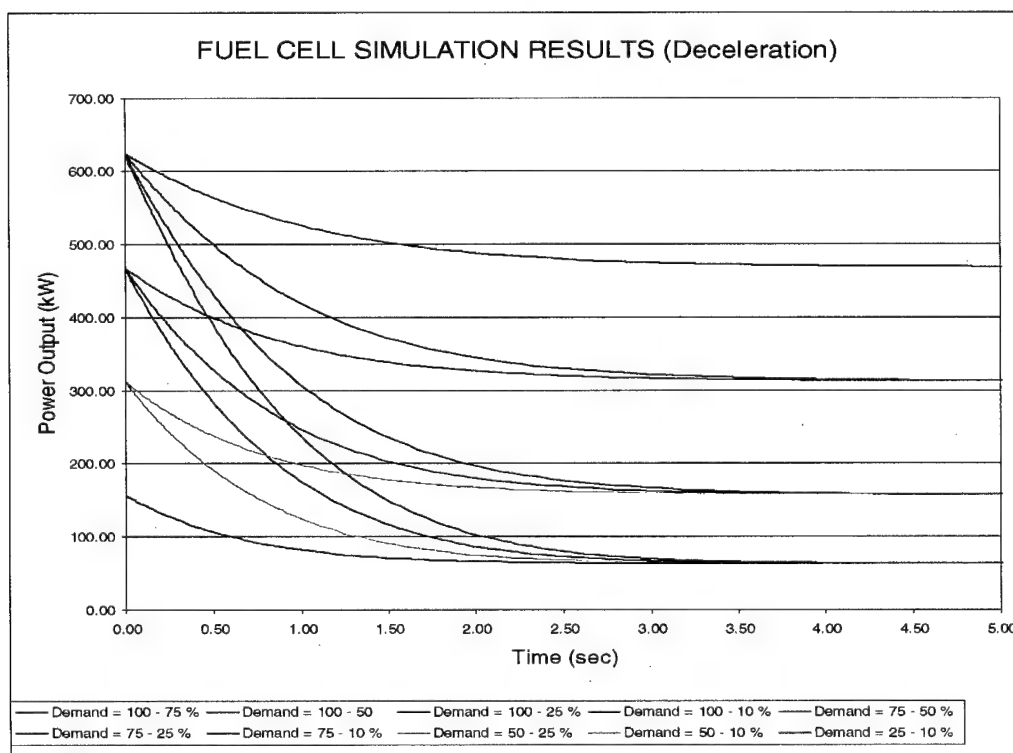


Figure C-7.  Load Demand Decrease
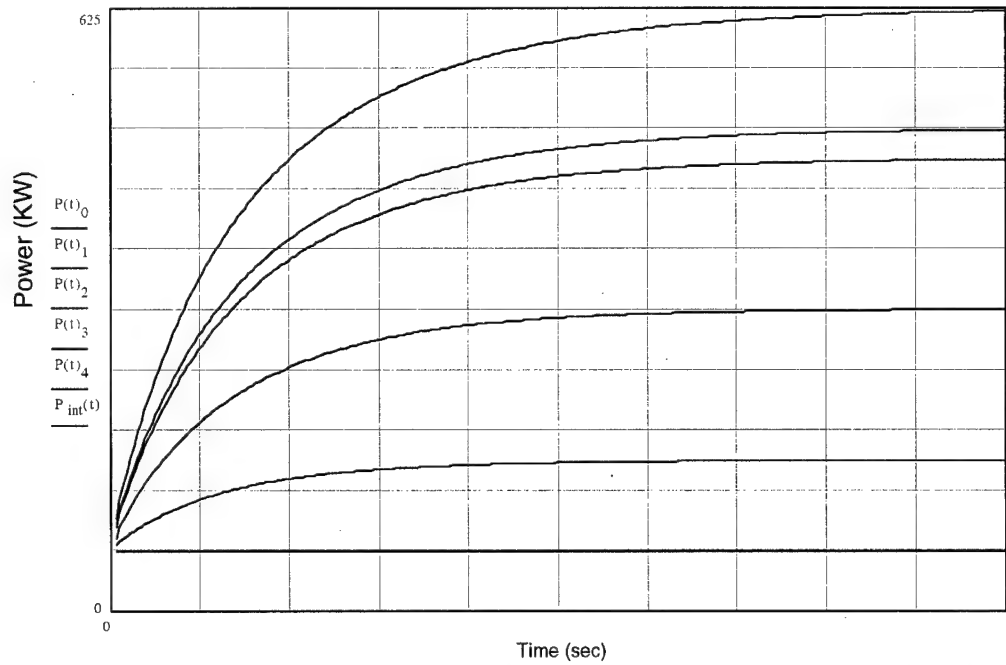
Figure C-8. Interpolated Curve for 500 kW for Increased Demand from 62.5 kW
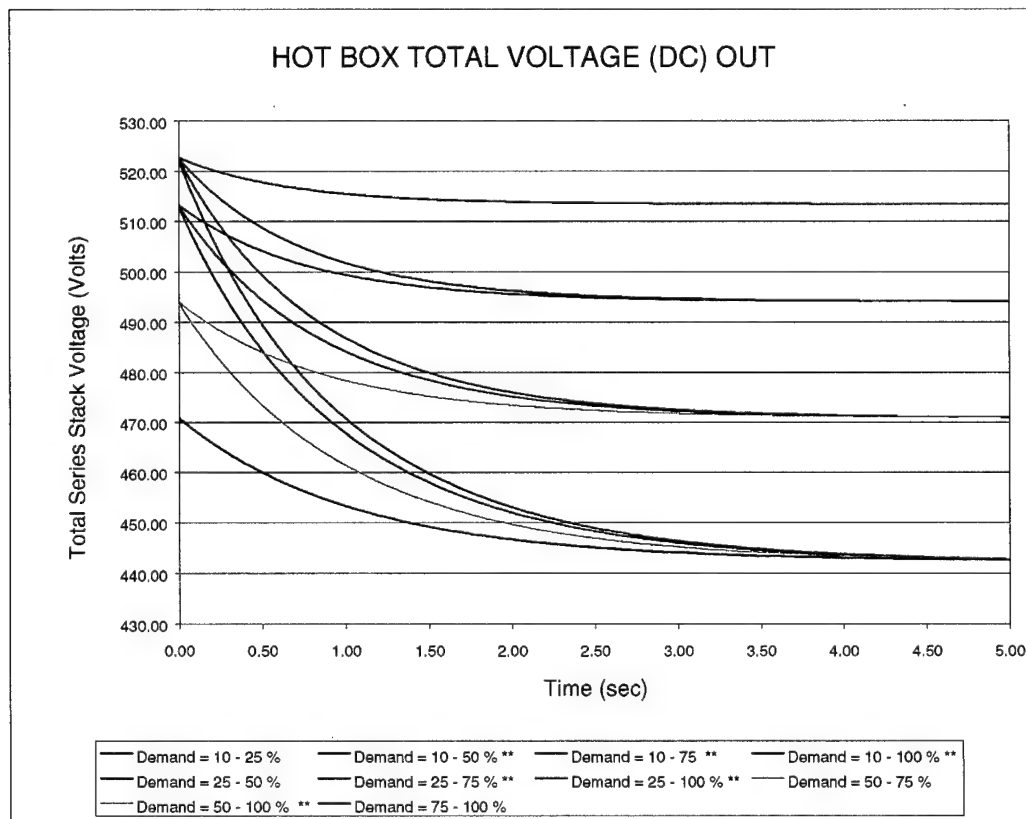


Figure C-9. Hot Box Total Voltage (DC) Output

# APPENDIX D.

# FUEL CELL POWERED SHIP -
# INTEGRATED DYNAMIC SIMULATION - FORMULATION

# FUEL CELL POWERED SHIP
# INTEGRATED DYNAMIC SIMULATION - FORMULATION

## 1.  INTRODUCTION

The purpose of the simulation described herein is to assess the applicability of fuel cells as a power source for integrated electric propulsion plants for ships.  The criteria for successful application are the ability at least to fully perform the maneuvering requirements from the vessel.

For the purpose of this work, a maneuver is defined as the operation of changing the speed of the ship from an initial value to a prescribed terminal value within a prescribed distance (usually, measured in number of ship lengths).

The propulsion actuator considered for the application is an electric AC synchronous motor. The motor is expected to deliver torque for the range of angular speeds spanning from zero to the maximum speed allowed for the propeller (e.g., due to cavitation and/or strength).  Existing synchronous motor models have the major shortcoming of not allowing for finite torque at zero rotational speed.  A new synchronous motor model that has been developed that overcomes this inconsistency.

In the following sections, the models utilized and/or developed for each of the components of the propulsion system are described.  Also, the procedures used in the execution of the maneuvers are detailed.

## 2.  SHIP COMPONENT MODELS

The models used to represent the ship and its propulsion system components are described in detail in the following subsections.

### 2.1  Fuel Cell

The simulation is performed on the real-time network simulator SIMSMART™.  Therefore, the fuel cell model has to be incorporated into the SIMSMART™ network model of the ship and its propulsion systems.  However, the fuel cell model cannot be integrated in a real-time computation algorithm due to the large computational time it necessitates.  Therefore, the temporal responses of the fuel cell principal variables with respect to various characterizing inputs were extracted and used to define the fuel cell behavior.

#### 2.1.1   The Fuel Cell Variables

The temporal response curves of the fuel cell variables for given step power demand changes were extracted from the FC Simulink™ assuming initial steady-state.  The following table lists the variables that were extracted from the Simulink™ model:

| Name | Description |
|------|-------------|
| Pnet | AC Net Power Out from FC (kW) |
| Whru | Mass Flow through the heat recovery unit System (lbm/hr) |
| wF76 | Fuel F76 in (lbm/hr) |
| NprA_in | Preformer A inlet molar flow (lbmol/hr) |
| NprAo | Preformer A outlet molar flow (lbmol/hr) |
| NprB_in | Preformer B inlet molar flow (lbmol/hr) |
| NprBo | Preformer B outlet molar flow (lbmol/hr) |
| Volt_t | Total Series Stack Voltage |

These curves were then used to construct temporal response surfaces, which were generated by means of polynomial curve fitting and interpolation.

The construction of a temporal response surface was accomplished by generating transient response curves between starting power levels (in increments of 10 percent of rated power) to various steady-state power levels. The curves were then separated into power-up and power-down scenario groups. For each group, the curves which started at a given power level were collected together and were used to compute the curve for intermediate steady-states by means of polynomial interpolation (this way the curves to be interpolated never cross one another).

The curve fitting was performed in the sense of least squares by utilizing approximations of up to 28th order polynomials of the form:

$$V(t) = \sum_{i=0}^{N} V_i \ln^i(t) \qquad (1)$$

with, $N$, the order of the polynomial. The natural log transformation of the time axis was utilized due to the small radius of curvatures present in the original curves. Applying the ln operator reduced the order of the required polynomial; thus, helping to reduce the wiggling present in the fitted curve along the segments where the required curvature was small. After the transformation of the data sampling points (in time), the order $N$ of the fitted polynomial was selected by observation so as to minimize the maximum local least squares error. The values of the coefficients of the approximating polynomial were calculated by solving the following least squares matrix equation:

$$(T^T T)C = T^T V \qquad (2)$$

where, $T$ is the $MxN$+1 sample matrix ($M$ is the number of time samples with $M>N$) of the form:

$$T = \begin{bmatrix} 1 & t_1 & t_1^2 & \cdots & t_1^N \\ 1 & t_2 & t_2^2 & \cdots & t_2^N \\ \vdots & \vdots & \vdots & \ddots & \vdots \\ 1 & t_M & t_M^2 & \cdots & t_M^N \end{bmatrix},$$

$C$ is the polynomial coefficient vector, and $V$ is the variable data vector.

The power curve for a given initial power level and any terminal power level is obtained from the interpolation of a few curves having the same initial power level. The interpolation of the curves is executed at a given time instant. The assumptions made in the interpolation process are:

5) The value of a variable at any given time instant, $t=t^*$, is a weighted sum of the values of the response curves at that given instant,

6) The weights equal to the values of the corresponding interpolation shape functions obtained at steady-state (i.e., the interpolation is "similar" for all time instants),

7) The interpolation is a fifth order polynomial,

8) The curve corresponding to constant power is included.

$$P\left(t^*\right) = \sum_{i=1}^{5} P_i\left(t^*\right) W_i\left(P\right) \qquad (3)$$

where,

$$W_i\left(P\right) \doteq N_i\left(P, P\left(t = \infty\right)\right)$$

with,

$$N_1\left(P\right) = \frac{\left(P - P_2\left(\infty\right)\right)\left(P - P_3\left(\infty\right)\right)\left(P - P_4\left(\infty\right)\right)\left(P - P_5\left(\infty\right)\right)}{\left(P_1\left(\infty\right) - P_2\left(\infty\right)\right)\left(P_1\left(\infty\right) - P_3\left(\infty\right)\right)\left(P_1\left(\infty\right) - P_4\left(\infty\right)\right)\left(P_1\left(\infty\right) - P_5\left(\infty\right)\right)}$$

$$N_2\left(P\right) = \frac{\left(P - P_1\left(\infty\right)\right)\left(P - P_3\left(\infty\right)\right)\left(P - P_4\left(\infty\right)\right)\left(P - P_5\left(\infty\right)\right)}{\left(P_2\left(\infty\right) - P_1\left(\infty\right)\right)\left(P_2\left(\infty\right) - P_3\left(\infty\right)\right)\left(P_2\left(\infty\right) - P_4\left(\infty\right)\right)\left(P_2\left(\infty\right) - P_5\left(\infty\right)\right)}$$

$$N_3\left(P\right) = \frac{\left(P - P_1\left(\infty\right)\right)\left(P - P_2\left(\infty\right)\right)\left(P - P_4\left(\infty\right)\right)\left(P - P_5\left(\infty\right)\right)}{\left(P_3\left(\infty\right) - P_1\left(\infty\right)\right)\left(P_3\left(\infty\right) - P_2\left(\infty\right)\right)\left(P_3\left(\infty\right) - P_4\left(\infty\right)\right)\left(P_3\left(\infty\right) - P_5\left(\infty\right)\right)}$$

$$N_4\left(P\right) = \frac{\left(P - P_1\left(\infty\right)\right)\left(P - P_2\left(\infty\right)\right)\left(P - P_3\left(\infty\right)\right)\left(P - P_4\left(\infty\right)\right)}{\left(P_4\left(\infty\right) - P_1\left(\infty\right)\right)\left(P_4\left(\infty\right) - P_2\left(\infty\right)\right)\left(P_4\left(\infty\right) - P_3\left(\infty\right)\right)\left(P_4\left(\infty\right) - P_5\left(\infty\right)\right)}$$

$$N_5\left(P\right) = \frac{\left(P - P_0\left(\infty\right)\right)\left(P - P_1\left(\infty\right)\right)\left(P - P_2\left(\infty\right)\right)\left(P - P_3\left(\infty\right)\right)}{\left(P_5\left(\infty\right) - P_1\left(\infty\right)\right)\left(P_5\left(\infty\right) - P_2\left(\infty\right)\right)\left(P_5\left(\infty\right) - P_3\left(\infty\right)\right)\left(P_5\left(\infty\right) - P_4\left(\infty\right)\right)}$$

Figure D-1 depicts, as an example, the power output interpolated curve for power-up from 10% power to 80% power (500KW) using the fitted curves for power-up from 10% to: 10% (constant power), 25%, 50%, 75%, and 100% power, as data.
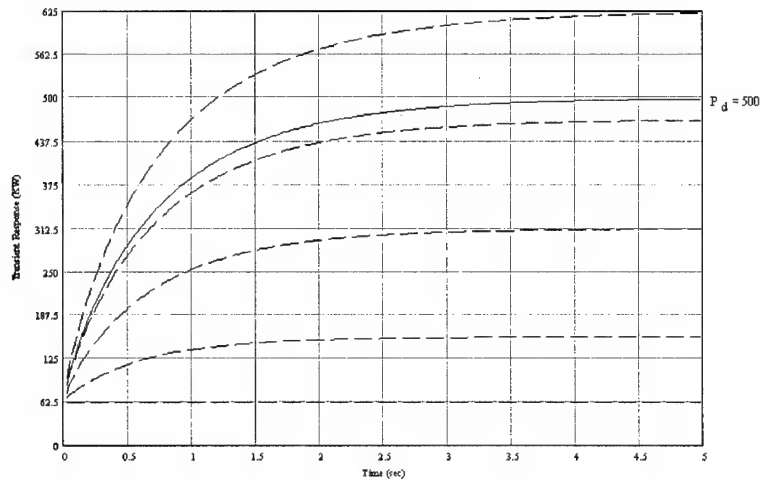


Figure D-1.  The Interpolated 62.5kW to 500kW Curve

### 2.1.2   Fuel Cell Power Characteristics Evaluation

The fuel cell Simulink$^{TM}$ model was tested and studied in order to determine its characteristics and applicability to operations that require power demand changes.  Toward this end, the model was run between two power levels with and without the assumption of steady-state conditions at the beginning of the power demand change.

The power change conditions simulated and the results for each are summarized below.

The following curves were generated (see Figure D-2):

- *"10% to 100% Power Out"* - Assumes steady-state conditions at 10% and reaches steady-state condition at 100%.
- *" 50% to 100% (From Steady-State)"* - Assumes steady-state conditions at 50% and reaches steady-state condition at 100%.  This curve was plotted with a constant time shift with respect to the *"10% to 100% Power Out"* curve such that its starting point is at 50% power of the latter.
- *"50% to 100% (From Actual Conditions)"* - Assumes actual conditions at 50% (the initial variable values for this scenario corresponds to the terminal variable values of *the "10% to 100% Power Out"* scenario at 50%) and reaches steady-state condition at 100%.  This curve was plotted with a constant time shift with respect to the *"10% to 100% Power Out "* curve such that its starting point is at 50% power of the latter.
- *" 25% to 50% (From Steady-State)"* - Assumes steady-state conditions at 25% and reaches steady-state condition at 50%.  This curve was plotted with a constant time shift with respect to the *"10% to 100% Power Out "* curve such that its starting point is at 25% power of the latter.

D-5

- ***"25% to 50% (From Actual Conditions)"*** - Assumes actual conditions at 25% (the initial variable values for this scenario corresponds to the terminal variable values of the ***"10% to 100% Power Out"*** scenario at 20%) and reaches steady-state condition at 50%. This curve was plotted with a constant time shift with respect to the "10% to 100% Power Out" curve such that its starting point is at 20% power of the latter.

As is shown in Figure D-2, all the curves overlap. This means that initial conditions of the fuel cell parameters do not affect the path between two power demand levels.

The conclusions are:

- The above observations indicate that the Simulink™ model of the fuel cell follows linear system transient behavior (which can only be achieved if the control loops within the fuel cell module are very stiff).

- In operations that require stepwise changes of power, the appropriate curve can be traced without the requirement of the attainment of steady-state conditions,

- A reduced set of curves can be used to represent the whole space of scenarios (accomplished by time shifting).
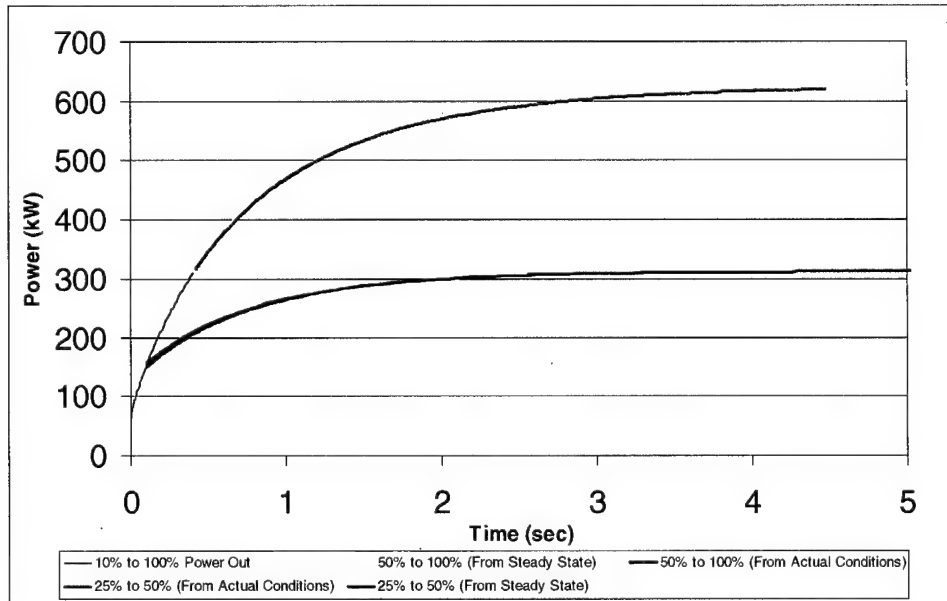


Figure D-2. Power Curves Obtained for Different Initial Conditions

## 2.2 CP and FP Propeller Curves

Propeller thrust and the corresponding propeller torque are modeled according to the following expressions:

$$T_p = \bar{K}_t \rho D^4 N^2 \qquad (4)$$

$$Q_p = \overline{K}_q \rho D^5 N^2 \tag{5}$$

where, $\overline{K}_t = \overline{K}_t(J;\hat{p})$ and $\overline{K}_q = \overline{K}_q(J;\hat{p})$[1] are the thrust and torque non-dimensional coefficients respectively ( $\hat{p} \doteq \dfrac{P}{D}$ is the non-dimensional propeller pitch parameter with, $P$ the pitch of the propeller[2] and $D$ its outer diameter, $J \doteq \dfrac{\mu V}{ND}$ is the non-dimensional variable called the advance ratio where, $V$ is the ship speed (in $^m/_{sec}$), $N$ is the rotational speed of the propeller shaft (in RPS), and $\mu$ is the non-dimensional advance velocity loss factor which is a positive dimensionless constant smaller than unit which accounts for the effect of the ship presence on the flow around the propeller), and $\rho$ is the water density. Therefore, for a given propeller pitch (i.e., $\hat{p}$ ), the propeller performance is prescribed by the thrust and torque coefficients' curves, which are functions of $J$. For a Controlled Pitch Propeller (CPP) the propeller torque and thrust coefficients become families of curves with $\hat{p}$ their parameter.

The simulation allows for the examination of the effect of the propeller pitch on the ship performance. Therefore, the curves that were utilized to represent the propeller model were taken from experimental data of an actual CPP tested at a few pitch values in free flow conditions. The values of the coefficients for any other intermediate $\hat{p}$ value for a given $J$, is obtained from the experimental curves by means of linear interpolation. Then, at $J=J^*$ the values of the thrust and the torque coefficients are calculated by:

$$\overline{K}_{(\square)}(\hat{p};J^*) = N_1(\hat{p})\overline{K}_{(\square)_1}(J^*) + N_2(\hat{p})\overline{K}_{(\square)_2}(J^*) \tag{6}$$

with,

$$N_1(\hat{p}) = \frac{\hat{p} - \overline{p}}{\underline{p} - \overline{p}} \quad , \qquad N_1(\hat{p}) = \frac{\hat{p} - \underline{p}}{\overline{p} - \underline{p}}$$

where, $\overline{p} \geq \hat{p} \geq \underline{p}$ .

Figure D-3 shows the fifth order polynomial fitted curve for the thrust coefficient for 0.2, and =1.0[3] and the corresponding interpolated curve for =0.6.

---

[1] The semicolon symbolizes the fact that $\hat{p}$ is a parameter and not a variable.

[2] The pitch is defined as the distance advanced by the propeller in one turn.

[3] The coefficient curves were fitted by transforming the $J$ values using the ln function (see Eq. 1). Due to the fact that $J$ assumes negative values, the values of the sample points were shifted using a simple translation first.

**CPP Thrust Coefficient Curve**
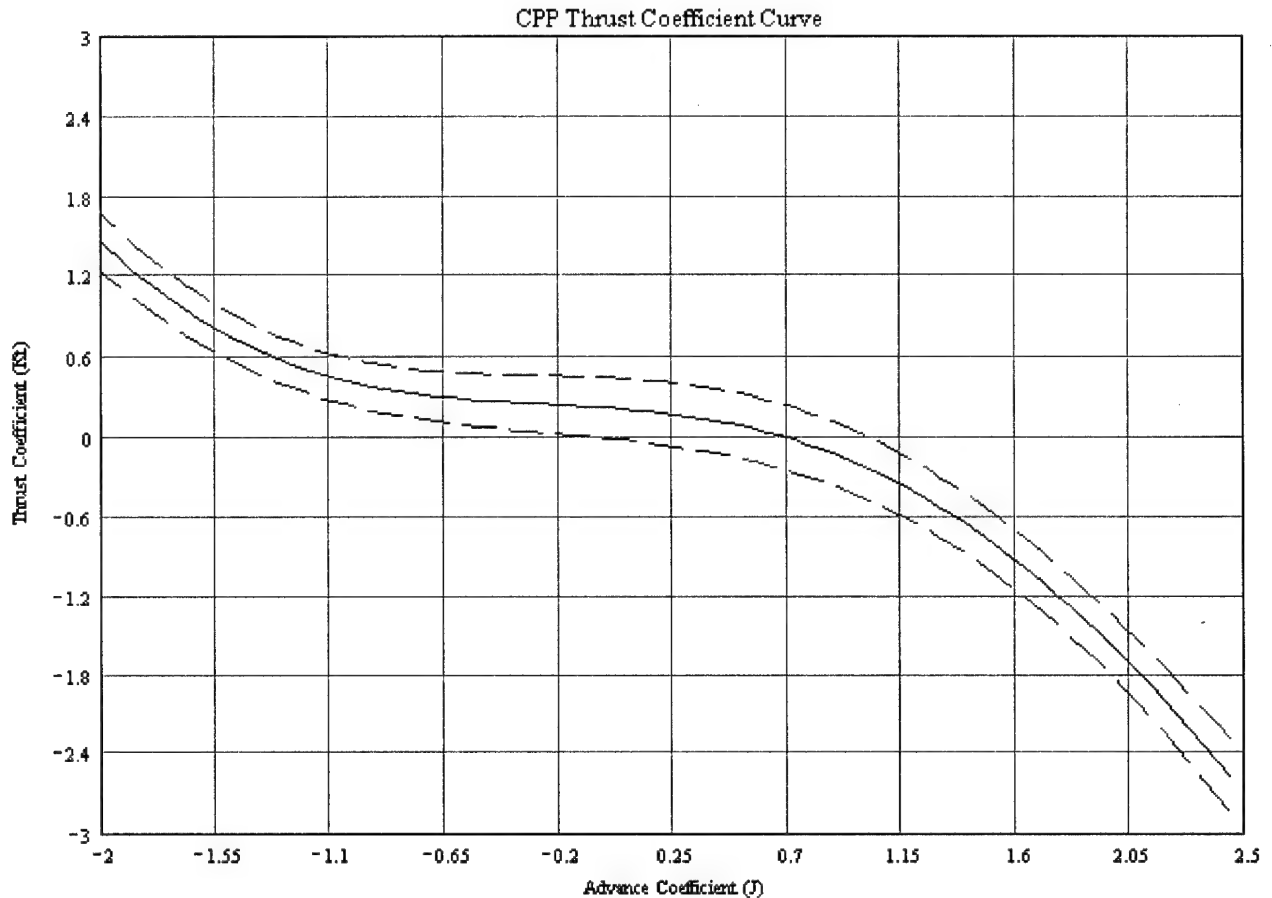
Figure D-3. The Interpolated Thrust Coefficient Curve for P/D =0.6 Using P/D =1.0 and P=0.2

## 2.3 The Motor and Its Control

The propulsion system is a direct drive power train consisting of 3-phase AC synchronous motors. The propulsion motor is a torque source whose torque characteristics are determined by a Variable Speed Drive Control Unit (VSDCU). The propeller uses the motor torque to produce thrust; however, this can only be accomplished by changing the speed of the motor's rotor in conjunction with a change in the source voltage such that the torque angle and the drawn current are kept constant at their maximum allowable values.

### 2.3.1. The Synchronous Motor

Assume that the motor is a Y-connected 3-phase synchronous motor whose three phases are electrically identical. Further, assume that there are no induction windings on the rotor of the motor[4].

The motor angular speed is related to the line frequency by the following relationship:

$$\omega_{Rotor} = \frac{2\pi f}{p/2} = \frac{4\pi f_L}{p} \tag{7}$$

where, $f_L$ is the line frequency, and $p/2$ is the number of pole pairs in the motor stator.

Let the equivalent electric circuit corresponding to one phase of the motor be as illustrated in Figure D-4.
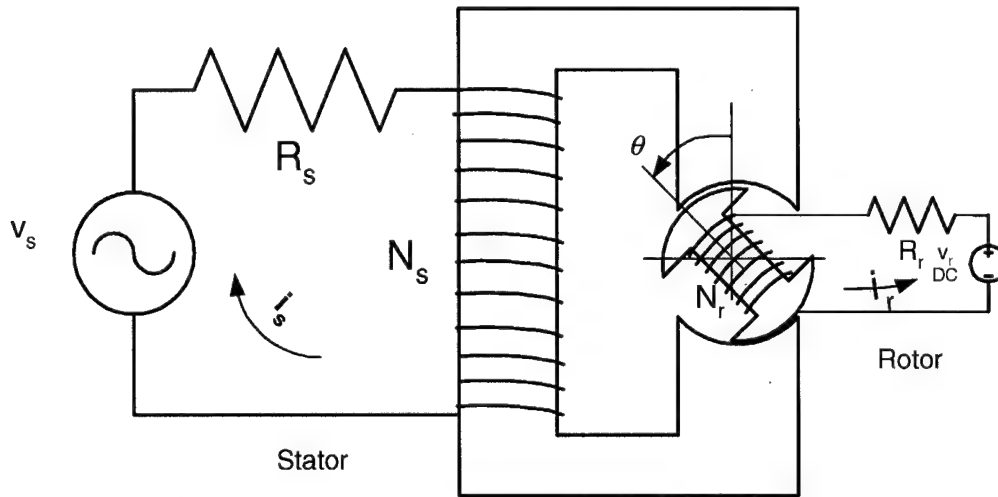


Figure D-4. Equivalent Circuit of One Phase of a Y-Connected Synchronous Motor

Then, in the frame of reference of the stator, the following flux linkages develop:

$$\lambda_s = L_{11}(\theta)i_s + L_{12}(\theta)i_r$$
$$\lambda_r = L_{21}(\theta)i_s + L_{22}(\theta)i_r$$

where, the $L$'s are the apparent inductances representing the rotor and the stator, the $R$'s are their apparent resistances, and the $i$'s are the rotor and stator[5] currents. The current impeding voltages

---

[4] The implication is that the motor stalls whenever the frequency of the source does not match the rotational speed of the rotor.

[5] The term "stator current" used here is comparable to the term "phase current" used in the literature.

that develop across the windings of the stator and the rotor are given by the time rate of change of the flux linkages:

$$e_s = \frac{d\lambda_s}{dt} = L_{11}(\theta)\frac{di_s}{dt} + \frac{\partial L_{11}(\theta)}{\partial \theta}\frac{d\theta}{dt}i_s + L_{12}(\theta)\frac{di_r}{dt} + \frac{\partial L_{12}(\theta)}{\partial \theta}\frac{d\theta}{dt}i_r$$

$$e_r = \frac{d\lambda_r}{dt} = L_{21}(\theta)\frac{di_s}{dt} + \frac{\partial L_{21}(\theta)}{\partial \theta}\frac{d\theta}{dt}i_s + L_{22}(\theta)\frac{di_r}{dt} + \frac{\partial L_{22}(\theta)}{\partial \theta}\frac{d\theta}{dt}i_r$$

Recognizing that the time rate of change of the angle $\theta$ is the angular velocity, $\omega$, of the rotor, the expressions for the induced voltages may be recast in the following matrix form:

$$\begin{Bmatrix} e_s \\ e_r \end{Bmatrix} = \begin{bmatrix} L_{11}(\theta) & L_{12}(\theta) \\ L_{21}(\theta) & L_{22}(\theta) \end{bmatrix} \begin{Bmatrix} \frac{di_s}{dt} \\ \frac{di_r}{dt} \end{Bmatrix} + \omega \begin{bmatrix} \frac{\partial L_{11}(\theta)}{\partial \theta} & \frac{\partial L_{12}(\theta)}{\partial \theta} \\ \frac{\partial L_{12}(\theta)}{\partial \theta} & \frac{\partial L_{22}(\theta)}{\partial \theta} \end{bmatrix} \begin{Bmatrix} i_s \\ i_r \end{Bmatrix} \tag{8}$$

For a constant air-gap between the rotor and the stator, the self-inductance of the rotor and stator are constant with respect to $\theta$. Assuming symmetry, the mutual inductances may be approximated by,

$$L_{12} = L_{21} \approx M\cos\theta$$

with M a constant[6], yielding the following expressions for the induced voltages,

$$\begin{Bmatrix} e_s \\ e_r \end{Bmatrix} = \begin{bmatrix} L_1 & M\cos\theta \\ M\cos\theta & L_2 \end{bmatrix} \begin{Bmatrix} \frac{di_s}{dt} \\ \frac{di_r}{dt} \end{Bmatrix} + \omega \begin{bmatrix} 0 & -M\sin\theta \\ -M\sin\theta & 0 \end{bmatrix} \begin{Bmatrix} i_s \\ i_r \end{Bmatrix} \tag{9}$$

where, for the sake of brevity, the notation $L_{11}=L_1$ and $L_{22}=L_2$ is adapted.

The instantaneous magnetic power induced in the stator for one-phase of the motor is given by:

$$P_{Phase} = \begin{Bmatrix} i_s & i_r \end{Bmatrix} \begin{Bmatrix} e_s \\ e_r \end{Bmatrix} \tag{10}$$

or,

---

[6] Assuming linear material properties.

$$P_{Phase} = \{i_s \quad i_r\} \left[ \begin{bmatrix} L_1 & M\cos\theta \\ M\cos\theta & L_2 \end{bmatrix} \begin{Bmatrix} \dfrac{di_s}{dt} \\ \dfrac{di_r}{dt} \end{Bmatrix} + \omega \begin{bmatrix} 0 & -M\sin\theta \\ -M\sin\theta & 0 \end{bmatrix} \begin{Bmatrix} i_s \\ i_r \end{Bmatrix} \right] \qquad (11)$$

and after multiplying out the terms the power equation becomes,

$$P_p = L_1 i_s \frac{di_s}{dt} + L_2 i_r \frac{di_r}{dt} + M\cos\theta\left( i_r \frac{di_r}{dt} + i_s \frac{di_s}{dt} \right) - 2\omega M \sin\theta i_s i_r \qquad (12)$$

On the other hand, for any fixed rotor position, i.e., $\theta$ held constant, the expression for the induced voltages reduce to,

$$\begin{Bmatrix} e_s \\ e_r \end{Bmatrix} = \begin{bmatrix} L_1 & M\cos\theta \\ M\cos\theta & L_2 \end{bmatrix} \begin{Bmatrix} \dfrac{di_s}{dt} \\ \dfrac{di_r}{dt} \end{Bmatrix} \qquad (13)$$

and, therefore, the corresponding energy stored in the magnetic field of each phase, is given by:

$$W_{Magnetic} = \int \{i_s \quad i_r\} \begin{Bmatrix} e_s \\ e_r \end{Bmatrix} dt = \int \left[ L_1 i_s \frac{di_s}{dt} + L_2 i_r \frac{di_r}{dt} + M\cos\theta\left( i_s \frac{di_r}{dt} + i_s \frac{di_s}{dt} \right) \right] dt$$

$$= \int \left[ L_1 i_s di_s + L_2 i_r di_r + M\cos\theta d(i_s i_r) \right] = \frac{1}{2} L_1 i_s^2 + \frac{1}{2} L_2 i_r^2 + M\cos\theta i_s i_r \qquad (14)$$

The consequent instantaneous power, for $\theta = \theta(t)$, is then given by,

$$P_{Magnetic}(t) = \frac{dW_{Magnetic}}{dt} = L_1 i_s \frac{di_s}{dt} + L_2 i_r \frac{di_r}{dt} + M\cos\theta\left( i_s \frac{di_r}{dt} + i_r \frac{di_s}{dt} \right) - \omega M \sin\theta i_s i_r \qquad (15)$$

The difference between the total power and the power required for the development of the magnetic field should equal the instantaneous mechanical power delivered to the shaft by each phase, i.e.,

$$P_{Q_{Phase}} = P_{Phase} - P_{Magnetic} = Q_{Phase}\omega = -\omega M \sin\theta i_r i_s \qquad (16)$$

The negative sign in Eq. 17 signifies the fact that the direction of the torque is always opposed to the direction of the rotor rotation.

Now, assume synchronous motion. Then, the following time histories can be assumed:

$$\begin{cases} \theta\left(t\right) = \omega t + \theta_0 \\ i_r\left(t\right) = I_r \\ i_s\left(t\right) = I_s \cos\left(\omega t + \theta_0 + \varphi\right) \\ v_r\left(t\right) = V_r \\ v_s\left(t\right) = V_s \cos\left(\omega t + \theta_0 + \delta\right) \end{cases}$$

where, $I_s$ is the amplitude of the phase current, $V_s$ is the amplitude of the phase source voltage, $I_r$ is the DC control current, $V_r$ is the DC control voltage, $\theta_0$ is some rotor initial angle with respect to the stator coordinate system, $\varphi$ is a phase angle between the current and the rotor axis, and $\delta$ is a phase angle between the source voltage and the rotor axis. Therefore, the per phase torque is given by:

$$Q_{Phase} = -MI_s I_r \sin\left(\omega t + \theta_0\right)\cos\left(\omega t + \theta_0 + \varphi\right) \tag{17}$$

Now, the total electric torque produced by the motor is the sum of the contributions of all 3 phases[7], i.e.,

$$\begin{aligned} Q_{Electric}\left(t\right) = &-MI_s I_r \sin\left(\omega t + \theta_0 - \frac{2}{3}\pi\right)\cos\left(\omega t + \theta_0 + \varphi - \frac{2}{3}\pi\right) \\ &-MI_s I_r \sin\left(\omega t + \theta_0\right)\cos\left(\omega t + \theta_0 + \varphi\right) \\ &-MI_s I_r \sin\left(\omega t + \theta_0 + \frac{2}{3}\pi\right)\cos\left(\omega t + \theta_0 + \varphi + \frac{2}{3}\pi\right) \\ = &-\frac{3}{2}MI_s I_r \sin\varphi \end{aligned} \tag{18}$$

which turns to be a time invariant for fixed excitation and source currents.

On the other hand, the characteristic equations governing each of the motor phases can be formulated by applying Kirchoff's law of voltages to the circuit in Figure D-4:

$$-\begin{Bmatrix} E_s \\ E_r \end{Bmatrix} + \begin{Bmatrix} v_s \\ v_r \end{Bmatrix} + \begin{bmatrix} R_s & 0 \\ 0 & R_r \end{bmatrix}\begin{Bmatrix} i_s \\ i_r \end{Bmatrix} = \begin{Bmatrix} 0 \\ 0 \end{Bmatrix} \tag{19}$$

or,

$$\begin{bmatrix} L_1 & M\cos\left(\omega t+\theta_0\right) \\ M\cos\left(\omega t+\theta_0\right) & L_2 \end{bmatrix}\begin{Bmatrix} \frac{di_s}{dt} \\ \frac{di_r}{dt} \end{Bmatrix} + \begin{bmatrix} R_s & -\omega M\sin\left(\omega t+\theta_0\right) \\ -\omega M\sin\left(\omega t+\theta_0\right) & R_r \end{bmatrix}\begin{Bmatrix} i_s \\ i_r \end{Bmatrix} = \begin{Bmatrix} V_s\cos\left(\omega t+\theta_0+\delta\right) \\ V_r \end{Bmatrix} \tag{20}$$

---

[7] See the identities in Section 8.

The first step in obtaining the solutions to Eq. 20 is to substitute the assumed solutions into the dynamics equations. Summing over the three phases (in the same manner as was done in the determination of the total torque output) yields,

$$I_r R_r = V_r \qquad (21)$$

Eq. 21 was obtained from the summation of the second of Eq. 20 while the summation of the first equation is satisfied identically. Then, the solution to the first equation, (i.e., $I_s$), is obtained by applying the Ritz method (see Section 8.2). Due to the fact that the approximated solution contains only one basis function, the corresponding Ritz equation is:

$$\int_0^{\frac{2\pi}{\omega}} \left[ -\omega L_1 I_s \sin\left(\omega t + \theta_0 + \varphi\right) + R_s I_s \cos\left(\omega t + \theta_0 + \varphi\right) - \omega M \sin\left(\omega t + \theta_0 + \varphi\right) \right] \sin\left(\omega t + \theta_0 + \varphi\right) dt$$

$$= \int_0^{\frac{2\pi}{\omega}} V_s \cos\left(\omega t + \theta_0 + \delta\right) \sin\left(\omega t + \theta_0 + \varphi\right) dt \qquad (22)$$

Performing the integrations yields the algebraic equation for the source current amplitude:

$$I_s = \frac{1}{R_s}\left[ V_s \cos\left(\varphi - \delta\right) - \omega M I_r \sin\varphi \right] \qquad (23)$$

Using the fact that for a Y-connection, $I_s$ the amplitude of the phase current is identical to $I_L$, the amplitude of the line current, and substituting Eq. 21 in Eq. 18, yields the electric torque equation for the synchronous motor:

$$Q_{Electric} = -\frac{3}{2}\frac{M I_L V_r}{R_r}\sin\varphi \qquad (24)$$

with, $\varphi$ interpreted as a torque angle. Obviously, the maximum torque that can be delivered by the motor (called the pullout torque) with respect to the torque angle, for all rotational speeds, is obtained when $\sin\varphi$ in the torque equation (Eq. 24) attains the value of one, i.e., $\varphi_{po} = \frac{\pi}{2}$. This yields,

$$Q_{Electric_{po}} = -\frac{3 M I_{L_{po}} V_r}{2 R_r} \qquad (25)$$

Assume that the torque angle be proportional to the torque from zero torque to the pullout torque for all rotational speeds. Then, the torque angle can be written as:

$$\varphi = \frac{\pi}{2Q_{Electric_{po}}} Q_{Electric} \tag{26}$$

thus, rendering the electric torque equation implicit:

$$Q_{Electric} = -\frac{3}{2} \frac{MI_L V_r}{R_r} \sin\left( \frac{\pi R_r}{3MI_{s_{po}} V_r} Q_{Electric} \right) \tag{27}$$

However, the mechanical torque available at the shaft is smaller due to windage, bearing friction, core losses, stray current, among others. Therefore, the mechanical torque available at the shaft is just given by:

$$Q_{mechanical} = \eta_L Q_{Electric} \tag{28}$$

where, $\eta_L$ is a mechanical loss efficiency.

Note that the phase angle difference between the current and the voltage is known as the power angle and it is just given by:

$$\phi = \varphi - \delta \tag{29}$$

yielding, the final expression for the motor phase current in terms of the motor phase voltage:

$$I_s = \frac{1}{R_s}\left[ V_s \cos\phi - \omega M I_r \sin\varphi \right] \tag{30}$$

On the other hand, the total electric power drawn instantaneously (from the three phases) by the motor is given by[8]:

$$\begin{aligned} P_{Electric}(t) &= \sum_{phase=1}^{3} i_{phase}(t) v_{phase}(t) = I_s V_s \cos\left( \omega t + \theta_0 + \varphi + \frac{2}{3}\pi \right) \cos\left( \omega t + \theta_0 + \delta + \frac{2}{3}\pi \right) \\ &\quad + I_s V_s \cos(\omega t + \theta_0 + \varphi) \cos(\omega t + \theta_0 + \delta) \\ &\quad + I_s V_s \cos\left( \omega t + \theta_0 + \varphi - \frac{2}{3}\pi \right) \cos\left( \omega t + \theta_0 + \delta - \frac{2}{3}\pi \right) \\ &= \frac{3}{2} I_s V_s \cos\phi \\ &= \frac{\sqrt{3}}{2} I_L V_L \cos\phi \end{aligned} \tag{31}$$

---

[8] The final expression is obtained by using the relationship between the line voltage and the phase voltage

which means that the total electric power drawn by the motor, for any shaft speed, is time invariable for constant line voltage and current.

The AC power balance on the motor is given by:

$$P_{Electric} = P_{Mechanical} + P_{Total\ Losses} = P_{Mechanical} + P_{Losses} + I_s^2 R_r = \frac{P_{Mechanical}}{\eta_m} + I_s^2 R_s \tag{32}$$

where, $P_{Mechanical}$ is the power at the motor shaft and $\eta_m$ is the motor efficiency. The portion of the power dedicated to the propulsion is the mechanical power. However, the mechanical power is given by:

$$P_{Mechanical} = |\omega Q_{Mechanical}| \tag{33}$$

with, $\eta_s$ the overall propeller shaft efficiency. The above relationships lead to the following for the power balance equation:

$$\frac{\sqrt{3}}{2} I_L V_L \cos\phi = \frac{\eta_L}{\eta_m} |\omega Q_{Electric}| + I_s^2 R_s = \frac{1}{\eta_o} |\omega Q_{Electric}| + I_s^2 R_s \tag{34}$$

where, $\eta_o$ is the motor efficiency due to magnetic and mechanical parasitic effects. It should be noted that additional power is drawn by the motor from its power supply by the DC excitation circuit:

$$P_{DC} = 3 I_r V_r = \frac{3 V_r^2}{R_r}$$

Eqs. 27, 30, and 34 constitute the AC 3-phase synchronous motor model.

The significance of the model developed above lies in the fact that it is consistent. Due to the fact that the torque of the motor is formulated as a function of the source current drawn by the motor, the model can handle a nonzero torque at zero angular velocity. At this condition, the model predicts zero power consumption, which is the result of the fact that under this condition the power angle assumes the value of $\frac{\pi}{2}$.

### 2.3.2 The Variable Speed Drive Control Unit

The major characteristic of an AC synchronous motor is that it is designed to operate under a no-slip condition. In other words, the frequency of rotation of the motor rotor and the frequency of rotation of the magnetic field in the armature are identical. This characteristic allows the motor to be operated and controlled precisely at different rotor speeds. In order to operate an AC synchronous motor under variable speed conditions, the frequency of the AC electrical source must be variable. At the time, other motor parameters such as: line source voltage and current

and DC excitation voltage, must to be controlled during the operation of an AC synchronous motor.

An AC synchronous motor operating at a fixed rotational speed does not deliver more torque unless it draws more power from its electric source. In order for the motor to draw extra power from its source, either a larger torque must be applied to the shaft or, a larger torque angle should be induced in the motor. For propulsion applications, a synchronous motor would not increase its output torque unless the motor torque angle (the constant angular shift between the rotor principal axis and the axis of the rotating magnetic field) is increased. This can only be accomplished by changing the source frequency and its voltage, correspondingly. When a synchronous motor operates as a propulsion motor, its source frequency should be increased at a rate, which will produce a torque angle whose value is always smaller than the pullout condition (corresponding to a torque angle of $90^\circ$). Exceeding the pullout angle will cause a disengagement of the rotor and its driving magnetic field, which will result in a sudden drop in torque (motor stall). Other parameters that need to be controlled during the operation of a synchronous propulsion motor are the source AC voltage, and the DC excitation voltage. The AC source voltage should be increased in a specific manner as the frequency of the source is increased. This allows the motor to draw its maximum allowable AC current in order to produce the maximum torque possible without reaching pullout. In addition, keeping the DC excitation voltage always to its maximum (defined by the excitation field saturation) will increase the pullout torque.

The VSDCU oversees the source current amplitude, and it is programmed to change the rotational frequency in a way that takes the motor from a given initial power level to the final desired level along the most efficient path. Toward this end, the frequency of the electric source of the motor is matched to the rotational speed at which the shaft would have rotated under the actions of the motor torque, the propeller resistance torque, and the inertia of the rotating members in accordance with the motor model and the ship dynamic model. The frequency demand history for a maneuver is therefore, obtained from the dynamics of the ship-propulsion system. Using any other curve, the ship performance may be degraded or the motor might overheat or even stall.

The VSDCU draws 60 Hz AC power from the ship main bus, converts it to DC power, and then inverts it into a variable frequency and variable voltage (not necessarily equal to the bus voltage) AC power, which is fed to the motor. The electric power supplied to the motor matches the power available for propulsion from the main bus of the ship. The power supplied to the motor; however, is not the total power available, rather it is reduced by the VSDCU efficiency:

$$P_{Electric} = \eta_i P_{FC} \qquad (35)$$

with, $\eta_i$ the VSDCU efficiency.

The current-limiting curve for the motor is programmed into the VSDCU. The curve characteristics are determined by the strength of the ship propulsion system components, as well as the motor torque handling capability at each speed (the pullout torque of the motor) or its heat dissipation capability.

The VSDCU/motor reaction time is relatively short with respect to the load demands and the ship maneuvering time constants, and therefore, it is modeled as instantaneous. The set of equations that the VSDCU needs to solve simultaneously to obtain the instantaneous values of the motor control parameters is:

$$
\begin{cases}
\dfrac{1}{R_s}\left(V_s\,\cos(\phi)\,-\,\omega M\,I_{dc}\sin\left(\dfrac{\pi}{2}\dfrac{Q}{Q_{po}}\right)\right)\,-\,I_s = 0 \\[4mm]
\dfrac{3}{2}\,\eta_e M\,I_s\,I_{dc}\sin\left(\dfrac{\pi}{2}\dfrac{Q}{Q_{po}}\right)\,-\,Q = 0 \\[4mm]
\dfrac{3}{2}\,I_s V_s\cos(\phi)\,-\,P_e = 0 \\[4mm]
\Psi = \text{in}\left(\dfrac{\pi}{2}\dfrac{Q}{Q_{po}}\right)
\end{cases}
\tag{36}
$$

Based on the AC synchronous motor operational observations described above, two control schemes have to be utilized to achieve motor maximum instantaneous output torque throughout a complete ship maneuver:

- ***Scheme 1: Instantaneous source power available is equal or larger than the instantaneous motor power demand.*** This control scheme is applied when the instantaneous power demanded by the motor is smaller or equal to the instantaneous power available from the source. In this control scheme, the source frequency and the AC voltage should be increased correspondingly so that the motor torque angle and the instantaneous current drawn from the source are maintained constant to their respective maximum allowable values.

For this control scheme the equations for the AC source voltage, electrical power consumed by the motor, the torque generated at the motor shaft, and motor pullout torque are obtained by solving the equation set (36) maintaining the torque angle and AC source current constant, therefore:

$$
\begin{cases}
V_s = \dfrac{1}{\cos(\phi)}\left(\omega M\,I_{dc}\Psi + I_s R_s\right) \\[4mm]
P_e = \dfrac{3}{2}\,I_s\left(\omega M\,I_{dc}\Psi + I_s R_s\right) \\[4mm]
Q = \dfrac{3}{2}\,\eta_e M\,I_s I_{dc}\Psi \\[4mm]
Q_{po} = \dfrac{3}{4}\,\pi\eta_e M\,I_s I_{dc}\dfrac{\Psi}{\arcsin(\Psi)}
\end{cases}
\tag{37}
$$

- **Scheme 2: Instantaneous source power available is less than the instantaneous power demanded by the motor**. This control scheme is applied when the instantaneous power demanded by the motor is larger than the instantaneous power available from the source. In this control scheme, the AC source frequency and voltage should be increased correspondingly so that the motor torque angle is maintained constant close to its maximum allowable value, while matching the electrical source instantaneous available power.

For this control scheme the equations for the AC source voltage and current, the torque generated at the motor shaft, and motor pullout torque are obtained by solving equation set (36) maintaining the torque angle constant and the electrical power equal to the available electrical power, therefore:

$$
\begin{cases}
V_s = \dfrac{1}{\cos(\phi)}\left(\dfrac{1}{2}\omega M I_{dc}\Psi + \dfrac{1}{6}\sqrt{9\omega^2 M^2 I_{dc}^2 \Psi^2 + 24 P_e R_s}\right) \\[2ex]
I_s = \dfrac{1}{6R_s}\left(-3\omega M I_{dc}\Psi + \sqrt{9\omega^2 M^2 I_{dc}^2 \Psi^2 + 24 P_e R_s}\right) \\[2ex]
Q = \dfrac{1}{4}\ \eta_e \dfrac{M I_{dc}\Psi}{R_s}\left(-3\omega M I_{dc}\Psi + \sqrt{9\omega^2 M^2 I_{dc}^2 \Psi^2 + 24 P_e R_s}\right) \\[2ex]
Q_{po} = \dfrac{1}{8}\ \pi\eta_e \dfrac{M I_{dc}\Psi}{R_s \arcsin(\Psi)}\left(-3\omega M I_{dc}\Psi + \sqrt{9\omega^2 M^2 I_{dc}^2 \Psi^2 + 24 P_e R_s}\right)
\end{cases}
\qquad (38)
$$

Additional control schemes can be developed to match specific propulsion system requirements such as, rotor frequency versus propulsion efficiency curves, torque versus rotor frequency curves, torque versus power consumption curves, power consumption versus frequency curves, among others.

### 2.3.3. Electric Main Bus

The power distribution management is assigned to the ship main bus. The main function of the main bus is to provide a balance between the electrical power demand and supply. Its controller calculates the final total power demand, senses the instantaneous total power demand, and the instantaneous total power supplied. Based on the available instantaneous power, it distributes it according to a load priority. In case of excess instantaneous power the surplus power is diverted to a dissipater load; when the supply is deficient it tries to meet the high priority load demand first and directs the rest to the low priority loads. Based on the final load demand, the bus determines the final power that is required from the sources in accordance with the number of on-line sources.

### 2.3.4. Ship Dynamics

The ship is assumed to be equipped with $n$ motors/propellers, which operate simultaneously and identically. This implies that the dynamics of the ship is one-dimensional. The time constant

of the propulsion system (motor-shaft-propeller) is significant with respect to the time constant of the ship; therefore, its dynamic has to be considered as well.

The model assumes two degrees of freedom for the ship system: the ship location, $x$, and the rotational position of a shaft, $\theta$. The corresponding equations of motion are:

$$\begin{cases} \left(J_m + J_s + J_p + J_{pam}\right)\ddot{\theta} = Q_s - Q_p \\ \left(m_s + nm_p + m_{sam}\right)\ddot{x} = nT_p - R \end{cases} \tag{39}$$

where, $J_m$ is the mass moment of inertia of the rotor of one motor, $J_s$ is the mass moment of inertia of one shaft, $J_p$ is the mass moment of inertia of the propeller, $J_{pam}$ is the propeller added mass moment of inertia (considered as a fixed percentage of the propeller mass moment of inertia), $Q_s$ is the torque available at the shaft, $Q_p$ is the resisting torque due to the propeller, $m_s$ is the mass of the ship, $m_p$ is the mass of one propulsion system (the motor, the shaft, and the propeller), $m_{sam}$ is the ship added mass (considered as a fixed percentage of the ship mass), $T_p$ is the total propulsion thrust (due to both propellers), and $R=R(v)$ is the ship resistance to motion force (see Figure B-5) with $v$ the speed of the ship.

The force of the ship resistance to motion can be fitted by a polynomial (for the whole range of velocities – negative and positive). Then, the resistance force is given by the curve of the form:

$$R(v) = \sum_{k=0}^{K} C_k v^k \tag{40}$$

with, $K$ the order of the polynomial (usually not larger than 3)[9], and the $C_i$'s the interpolation coefficients. It is tacitly assumed that the resistance to the ship motion in the reverse direction is twice that of the resistance to forward motion for the same absolute speed.

Eq. 35 is written explicitly in terms of the ship velocity, $v$, and the shaft rotational angular velocity, $\omega$ to yield:

$$\begin{cases} \dot{\omega} = \dfrac{\eta_s \eta_m}{J_t} Q_{Electric}\left(I_L, Q_{Electric}\right) - \dfrac{1}{4\pi^2 J_t} K_q\left(v, \omega; \hat{p}\right)\rho D^5 \omega^2 \\ \dot{\theta} = \omega \\ \dot{v} = \dfrac{n}{4\pi^2 M_t} K_t\left(v, \omega; \hat{p}\right)\rho D^4 \omega^2 - \dfrac{1}{M_t}\sum_{k=0}^{K} C_k v^k \\ \dot{x} = v \end{cases} \tag{41}$$

---

[9] It should be kept in mind that $R(V)$ is an odd function with respect to the origin.

where, $J_t$ and $M_t$ are the total mass moment of inertia for one shaft and the total mass of the ship, and $Q_s = \eta_s \eta_m Q_{Electric}$ was used[10].

The suitable propeller for the ship is selected by requiring sufficient thrust at full speed, i.e.,

$$R\left(V_{fs}\right) = n T_{fs}$$

where the subscript *fs* stands for "full speed", and $n$ is the number of propellers used. Alternatively, the required torque can be found from,

$$R\left(V_{fs}\right) V_{fs} = Q_{Shaft} \omega_{rated}$$

assuming that the full speed of the ship is attained at the maximum propeller speed which equals the rated speed of the motor.

## 3. NUMERICAL ANALYSIS

The major numerical procedures required in the simulation are as follows:

- Calculation of the motor output torque, and
- Integration of the equations of motion.

### 3.1 Torque Calculation

The calculation for the motor output torque as a function of the source current, requires the solution of an implicit algebraic equation (Eq. 26). Rewriting the Eq. 26 in the following form

$$Q_{Electric} + \frac{3}{2} \frac{M I_L V_r}{R_r} \sin\left( \frac{\pi}{2\alpha Q_{Electric_{rated}}} Q_{Electric} \right) = 0 \tag{42}$$

makes it possible to use zero finding methods to calculate the torque.

Due to its convergence properties, the second order Newton algorithm is utilized to solve the equation. In order to assure convergence, the algorithm is applied in the vicinity of the solution; the approach to the vicinity of the solution is performed by a variable interval sectioning algorithm.

Let the LHS of Eq. 37 be defined as a function whose zero is sought, i.e.,

---

[10] This relationship can be shown to hold from the corresponding power expressions.

$$g\left(Q_{Electric}\right) = Q_{Electric} + \frac{3}{2}\frac{MI_L V_r}{R_r}\sin\left(\frac{\pi}{2\alpha Q_{Electric_{rated}}}Q_{Electric}\right) = 0$$

Then, the algorithm for the second order Newton is:

$$\overline{f}^{(k+1)} = \overline{f}^{(k)} + \left[\frac{g''\left(\overline{f}^{(k)}\right)}{2g'\left(\overline{f}^{(k)}\right)} - \frac{g'\left(\overline{f}^{(k)}\right)}{g\left(\overline{f}^{(k)}\right)}\right]^{-1} \tag{43}$$

where, the prime indicated derivative with respect to $Q_{Electric}$:

$$g'\left(Q_{Electric}\right) = 1 + \frac{3\pi MI_L V_r}{4\alpha R_r Q_{Electric_{rated}}}\cos\left(\frac{\pi}{2\alpha Q_{Electric_{rated}}}Q_{Electric}\right)$$

and,

$$g''\left(Q_{Electric}\right) = -\frac{3\pi^2 MI_L V_r}{8\alpha^2 R_r Q_{Electric_{rated}}^2}\sin\left(\frac{\pi R_r}{3MI_{L_{po}} V_r}Q_{Electric}\right)$$

## 3.2    Numerical Integration

Ship maneuvers are formulated in terms of the required ship displacement between the maneuver starting and completion instances. The control, in the case of a synchronous motor, is twofold: the torque provided by the motor, and the rotational speed of the motor shaft. These variables generate, via the propeller, a thrust force that moves the ship. Due to the fact that the torque and the rotational speed of the motor are independent, the maneuver control should specify the time histories of both the current supplied to the motor, as well as, the frequency of the source. In order not to stall the motor, the instantaneous rotational speed of the motor should match the speed the shaft would have assumed had the shaft been under the influence of the torque and the inertia of the propulsion system. Given the a priori torque time history, the time history of the rotational speed is calculated from the equations of motion.

The equations of motion (Eq. 36) enable the calculation of the time histories of the displacement, speed, and acceleration of the propeller shaft and of the ship. Due to the high level of non-linearity possessed by Eq. 36, their solutions have to be obtained numerically. The method that is used for the integration is the fourth order Runge-Kutta (R-K). Let Eq. 36 be rewritten in the form:

$$\{y\}' = \{F\left(\omega, \theta, v, x\right)\} \tag{44}$$

where,

$$\{y\} = \begin{Bmatrix} \omega \\ \theta \\ v \\ x \end{Bmatrix} \quad , \quad \{F(\omega,\theta,V,x)\} = \begin{Bmatrix} \dfrac{\eta_s \eta_m}{J_t} Q_m(I_s) - \dfrac{1}{4\pi^2 J_t} K_q(v,\omega)\rho D^5 \omega^2 \\ \omega \\ \dfrac{n}{4\pi^2 M_t} K_t(v,\omega)\rho D^4 \omega^2 - \dfrac{1}{M_t}\sum_{k=0}^{K} C_k v^k \\ v \end{Bmatrix}$$

with, $C_m$ the motor constant.

### 3.2.1 <u>Integration Algorithm</u>

The R-K recurrence formula corresponding to Eq. 36 is given by:

$$\{y\}_{(i+1)} = \{y\}_{(i)} + \frac{\Delta t}{6}\left[\{K_1\}_{(i)} + 2\{K_2\}_{(i)} + 2\{K_3\}_{(i)} + \{K_4\}_{(i)}\right] \tag{45}$$

with,

$$\{K_1\}_{(i)} = F\left(t_{(i)},\{y\}_{(i)}\right)$$

$$\{K_2\}_{(i)} = F\left(t_{(i)} + \frac{\Delta t}{2},\{y\}_{(i)} + \frac{\Delta t}{2}\{K_1\}\right)$$

$$\{K_3\}_{(i)} = F\left(t_{(i)} + \frac{\Delta t}{2},\{y\}_{(i)} + \frac{\Delta t}{2}\{K_2\}\right)$$

$$\{K_4\}_{(i)} = F\left(t_{(i)} + \Delta t,\{y\}_{(i)} + \Delta t\{K_3\}\right)$$

Due to the fact that the equations are autonomous, they can be written in the following form:

$$\{K_1\}_{(i)} = F\left(\{y\}_{(i)}\right)$$

$$\{K_2\}_{(i)} = F\left(\{y\}_{(i)} + \frac{\Delta t}{2}\{K_1\}\right)$$

$$\{K_3\}_{(i)} = F\left(\{y\}_{(i)} + \frac{\Delta t}{2}\{K_2\}\right)$$

$$\{K_4\}_{(i)} = F\left(\{y\}_{(i)} + \Delta t\{K_3\}\right)$$

In order to facilitate the real-time calculations, the R-K equations may be written in their explicit form rather then in their functional form[11]. Then, the explicit form of the $K$ terms is as follows:

---

[11] This reduces the number of function calls and therefore, reduces idle storing time.

$$\{K_1\}_{(i)} = \left\{ \begin{array}{l} \dfrac{\eta_s \eta_m}{J_t} Q_{Electric}\left(I_{L_{(i)}}\right) - \dfrac{1}{4\pi^2 J_t} K_q\left(v_{(i)}, \omega_{(i)}\right)\rho D^5 \omega_{(i)}^2 \\[2ex] \omega_{(i)} \\[2ex] \dfrac{n}{4\pi^2 M_t} K_t\left(v_{(i)}, \omega_{(i)}\right)\rho D^4 \omega_{(i)}^2 - \dfrac{1}{M_t}\sum_{k=0}^{K} C_k v_{(i)}^k \\[2ex] v_{(i)} \end{array} \right\} \tag{46}$$

then,

$$\{y\}_{(i)} + \Delta t\big/_2 \{K_1\}_{(i)} = \left\{\begin{array}{l} \omega_{(i)} \\ \theta_{(i)} \\ v_{(i)} \\ x_{(i)} \end{array}\right\} + \dfrac{\Delta t}{2}\left\{\begin{array}{l} \dfrac{\eta_s \eta_m}{J_t} Q_{Electric}\left(I_{L_{(i)}}\right) - \dfrac{1}{4\pi^2 J_t} K_q\left(v_{(i)}, \omega_{(i)}\right)\rho D^5 \omega_{(i)}^2 \\[2ex] \omega_{(i)} \\[2ex] \dfrac{n}{4\pi^2 M_t} K_t\left(v_{(i)}, \omega_{(i)}\right)\rho D^4 \omega_{(i)}^2 - \dfrac{1}{M_t}\sum_{k=0}^{K} C_k v_{(i)}^k \\[2ex] v_{(i)} \end{array}\right\}$$

$$\downarrow$$

$$\left\{\begin{array}{l} \overline{\omega}_{(i)} \\ \overline{\theta}_{(i)} \\ \overline{v}_{(i)} \\ \overline{x}_{(i)} \end{array}\right\} = \left\{\begin{array}{l} \omega_{(i)} + \dfrac{\Delta t}{2}\left(\dfrac{\eta_s \eta_m}{J_t} Q_{Electric}\left(I_{L_{(i)}}\right) - \dfrac{1}{4\pi^2 J_t} K_q\left(v_{(i)}, \omega_{(i)}\right)\rho D^5 \omega_{(i)}^2 \right) \\[2ex] \theta_{(i)} + \dfrac{\Delta t}{2}\omega_{(i)} \\[2ex] v_{(i)} + \dfrac{\Delta t}{2}\left(\dfrac{n}{4\pi^2 M_t} K_t\left(v_{(i)}, \omega_{(i)}\right)\rho D^4 N_{(i)}^2 - \dfrac{1}{M_t}\sum_{k=0}^{K} C_k v_{(i)}^k \right) \\[2ex] x_{(i)} + \dfrac{\Delta t}{2}v_{(i)} \end{array}\right\}$$

$$\Downarrow$$

$$\{K_2\}_{(i)} = \left\{\begin{array}{l} \dfrac{\eta_s \eta_m}{J_t} Q_{Electric}\left(I_{L_{(i)}}\right) - \dfrac{1}{4\pi^2 J_t} K_q\left(v_{(i)}, \omega_{(i)}\right)\rho D^5 \overline{\omega}_{(i)}^2 \\[2ex] \overline{\omega}_{(i)} \\[2ex] \dfrac{n}{4\pi^2 M_t} K_t\left(v_{(i)}, \omega_{(i)}\right)\rho D^4 \overline{\omega}_{(i)}^2 - \dfrac{1}{M_t}\sum_{k=0}^{K} C_k \overline{v}_{(i)}^k \\[2ex] \overline{v}_{(i)} \end{array}\right\} \tag{47}$$

$$\{y\}_{(i)} + \frac{\Delta t}{2}\{K_2\}_{(i)} = \begin{Bmatrix} \omega_{(i)} \\ \theta_{(i)} \\ v_{(i)} \\ x_{(i)} \end{Bmatrix} + \frac{\Delta t}{2}\begin{Bmatrix} \dfrac{\eta_s\eta_m}{J_t}Q_{Electric}\left(I_{L_{(i)}}\right) - \dfrac{1}{4\pi^2 J_t}K_q\left(v_{(i)},\omega_{(i)}\right)\rho D^5 \overline{\omega}_{(i)}^2 \\ \overline{\omega}_{(i)} \\ \dfrac{n}{4\pi^2 M_t}K_t\left(v_{(i)},\omega_{(i)}\right)\rho D^4 \overline{\omega}_{(i)}^2 - \dfrac{1}{M_t}\sum_{k=0}^{K}C_k \overline{v}_{(i)}^{-k} \\ \overline{v}_{(i)} \end{Bmatrix}$$

$$\downarrow$$

$$\begin{Bmatrix} \overline{\overline{\omega}}_{(i)} \\ \overline{\overline{\theta}}_{(i)} \\ \overline{\overline{v}}_{(i)} \\ \overline{\overline{x}}_{(i)} \end{Bmatrix} = \begin{Bmatrix} \omega_{(i)} + \dfrac{\Delta t}{2}\left(\dfrac{\eta_s\eta_m}{J_t}Q_{Electric}\left(I_{L_{(i)}}\right) - \dfrac{1}{4\pi^2 J_t}K_q\left(v_{(i)},\omega_{(i)}\right)\rho D^5 \overline{\omega}_{(i)}^2\right) \\ \theta_{(i)} + \dfrac{\Delta t}{2}\overline{\omega} \\ V_{(i)} + \dfrac{\Delta t}{2}\left(\dfrac{n}{4\pi^2 M_t}K_t\left(v_{(i)},\omega_{(i)}\right)\rho D^4 \overline{\omega}_{(i)}^2 - \dfrac{1}{M_t}\sum_{k=0}^{K}C_k \overline{v}_{(i)}^{-k}\right) \\ x_{(i)} + \dfrac{\Delta t}{2}\overline{v}_{(i)} \end{Bmatrix}$$

$$\Downarrow$$

$$\{K_3\}_{(i)} = \begin{Bmatrix} \dfrac{\eta_s\eta_m}{J_t}Q_{Electric}\left(I_{L_{(i)}}\right) - \dfrac{1}{4\pi^2 J_t}K_q\left(v_{(i)},\omega_{(i)}\right)\rho D^5 \overline{\overline{\omega}}_{(i)}^2 \\ \overline{\overline{\omega}}_{(i)} \\ \dfrac{n}{4\pi^2 M_t}K_t\left(v_{(i)},\omega_{(i)}\right)\rho D^4 \overline{\overline{\omega}}_{(i)}^2 - \dfrac{1}{M_t}\sum_{k=0}^{K}C_k \overline{\overline{v}}_{(i)}^{-k} \\ \overline{\overline{v}}_{(i)} \end{Bmatrix}$$

$$\{y\}_{(i)} + \Delta t\{K_3\}_{(i)} = \begin{Bmatrix} \omega_{(i)} \\ \theta_{(i)} \\ v_{(i)} \\ x_{(i)} \end{Bmatrix} + \Delta t\begin{Bmatrix} \dfrac{\eta_s\eta_m}{J_t}Q_{Electric}\left(I_{L_{(i)}}\right) - \dfrac{1}{4\pi^2 J_t}K_q\left(v_{(i)},\omega_{(i)}\right)\rho D^5 \overline{\overline{\omega}}_{(i)}^2 \\ \overline{\overline{\omega}}_{(i)} \\ \dfrac{n}{4\pi^2 M_t}K_t\left(v_{(i)},\omega_{(i)}\right)\rho D^4 \overline{\overline{\omega}}_{(i)}^2 - \dfrac{1}{M_t}\sum_{k=0}^{K}C_k \overline{v}_{(i)}^{-k} \\ \overline{\overline{v}}_{(i)} \end{Bmatrix}$$

$$\downarrow$$

D-24

$$
\begin{Bmatrix} \overline{\overline{\overline{\omega}}}_{(i)} \\ \overline{\overline{\overline{\theta}}}_{(i)} \\ \overline{\overline{\overline{v}}}_{(i)} \\ \overline{\overline{\overline{x}}}_{(i)} \end{Bmatrix} = \begin{Bmatrix} \omega_{(i)} + \Delta t \left( \dfrac{\eta_s \eta_m}{J_t} Q_{Electric}\left(I_{L_{(i)}}\right) - \dfrac{1}{4\pi^2 J_t} K_q\left(v_{(i)},\omega_{(i)}\right)\rho D^5 \overline{\overline{\omega}}_{(i)}^{\,2} \right) \\ \theta_{(i)} + \Delta t \,\overline{\overline{N}} \\ V_{(i)} + \Delta t \left( \dfrac{n}{4\pi^2 M_t} K_t\left(v_{(i)},\omega_{(i)}\right)\rho D^4 \overline{\overline{\omega}}_{(i)}^{\,2} - \dfrac{1}{M_t}\sum_{k=0}^{K} C_k \overline{\overline{v}}_{(i)}^{\,k} \right) \\ x_{(i)} = \Delta t \overline{\overline{v}}_{(i)} \end{Bmatrix}
$$

$$\Downarrow$$

$$
\{K_4\}_{(i)} = \begin{Bmatrix} \dfrac{\eta_s \eta_m}{J_t} Q_{Electric}\left(I_{L_{(i)}}\right) - \dfrac{1}{4\pi^2 J_t} K_q\left(v_{(i)},\omega_{(i)}\right)\rho D^5 \overline{\overline{\overline{\omega}}}_{(i)}^{\,2} \\ \overline{\overline{\overline{\omega}}}_{(i)} \\ \dfrac{n}{4\pi^2 M_t} K_t\left(v_{(i)},\omega_{(i)}\right)\rho D^4 \overline{\overline{\overline{\omega}}}_{(i)}^{\,2} - \dfrac{1}{M_t}\sum_{k=0}^{K} C_k \overline{\overline{v}}_{(i)}^{\,k} \\ \overline{\overline{v}}_{(i)} \end{Bmatrix}
$$

Note that the propeller coefficients are assumed to be constant throughout the time interval.

### 3.2.2  System Stability Analysis

The fact that the control forces acting on the ship are functions of its kinematic variables renders the system non-conservative. This implies that there is a possibility that the system might have some regions of instability. Obviously, the regions at which instability occurs should be avoided.

The governing equations should reflect the unstable behavior. The first step in the procedure for determining the stability of the equations is to linearize the equations of motion (Eq. 39). Toward this end introduce a small perturbation to the dependant variables $\omega$, $\theta$, $V$, and $x$ in Eq. 41:

$$
\begin{cases} \left(\omega + \overset{\square}{\delta\omega}\right) = \dfrac{K_1}{J}\left(I_s + \delta I_s\right) - \dfrac{1}{4\pi^2 J} K_q\left(v,\omega\right)\rho D^5 \left(\omega + \delta\omega\right)^2 \\[2mm] \left(\theta + \overset{\square}{\delta\theta}\right) = \omega + \delta\omega \\[2mm] \left(v + \overset{\square}{\delta v}\right) = \dfrac{n}{4\pi^2 M} K_t\left(v,\omega\right)\rho D^4 \left(\omega + \delta\omega\right)^2 - \dfrac{1}{M}\sum_{k=0}^{K} C_k \left(v + \delta v\right)^k \\[2mm] \left(x + \overset{\square}{\delta x}\right) = v + \delta v \end{cases} \tag{48}
$$

Using the binomial expansion yields:

$$\begin{cases} \dot{\omega} + \delta\dot{\omega} = \dfrac{K_1}{J}\left(I_s + \delta I_s\right) - \dfrac{1}{4\pi^2 J}K_q\left(v,\omega\right)\rho D^5\omega^2\left(1+2\dfrac{\delta\omega}{\omega}\right) \\[3mm] \dot{\theta} + \delta\dot{\theta} = \omega + \delta\omega \\[3mm] \dot{v} + \delta\dot{v} = \dfrac{n}{4\pi^2 M}K_t\left(v,\omega\right)\rho D^4\omega^2\left(1+2\dfrac{\delta\omega}{\omega}\right) - \dfrac{1}{M}\sum_{k=0}^{K}C_k v^k\left(1+k\dfrac{\delta v}{v}\right) \\[3mm] \dot{x} + \delta\dot{x} = v + \delta v \end{cases} \tag{49}$$

Subtracting Eq. 41 from Eq. 48, one gets the linear equations (in the perturbations),

$$\begin{cases} \delta\dot{\omega} = \dfrac{K_1}{J}\delta I_s - \dfrac{2}{4\pi^2 J}K_q\left(v,\omega\right)\rho D^5\omega\delta\omega \\[3mm] \delta\dot{\theta} = \delta\omega \\[3mm] \delta\dot{v} = \dfrac{2n}{4\pi^2 M}K_t\left(v,N\right)\rho D^4\omega\delta\omega - \dfrac{1}{M}\sum_{k=0}^{K}kC_k v^{k-1}\delta v \\[3mm] \delta\dot{x} = \delta v \end{cases} \tag{50}$$

Now, assuming

$$\begin{cases} \delta\omega = \Delta\omega e^{\lambda t} \\[2mm] \delta\theta = \Delta\Theta e^{\lambda t} \\[2mm] \delta v = \Delta V e^{\lambda t} \\[2mm] \delta x = \Delta X e^{\lambda t} \end{cases} \tag{51}$$

and substituting in Eq. 43 yields:

$$\begin{cases} \lambda\,\Delta\omega = \dfrac{K_1}{J}\delta I_s - \dfrac{2}{4\pi^2 J}K_q\left(v,\omega\right)\rho D^5\omega\Delta\omega \\[3mm] \lambda\,\Delta\Theta = \Delta\omega \\[3mm] \lambda\,\Delta V = \dfrac{2n}{4\pi^2 M}K_t\left(v,\omega\right)\rho D^4\omega\Delta\omega - \dfrac{1}{M}\sum_{k=0}^{K}kC_k v^{k-1}\Delta v \\[3mm] \lambda\,\Delta X = \Delta v \end{cases} \tag{52}$$

In matrix form, Eq. 45 can be written as:

$$\begin{bmatrix} \lambda + \dfrac{2}{4\pi^2 J}K_q\rho D^5\omega & 0 & 0 & 0 \\[3mm] -1 & \lambda & 0 & 0 \\[3mm] -\dfrac{2n}{4\pi^2 M}K_t\rho D^4\omega & 0 & \lambda + \dfrac{1}{M}\sum_{k=0}^{K}kC_k v^{k-1} & 0 \\[3mm] 0 & 0 & -1 & \lambda \end{bmatrix} \begin{Bmatrix} \Delta\omega \\[2mm] \Delta\Theta \\[2mm] \Delta V \\[2mm] \Delta X \end{Bmatrix} = \begin{Bmatrix} \dfrac{K_1}{J}\delta I_s \\[2mm] 0 \\[2mm] 0 \\[2mm] 0 \end{Bmatrix} \tag{53}$$

The eigenvalues of the coefficient matrix indicate that the linearized system is stable as long as the following conditions hold:

$$\begin{cases} K_q \omega > 0 \\ and \\ \sum_{k=0}^{K} k C_k v^{k-1} > 0 \end{cases} \tag{54}$$

These stability conditions are always met for a real ship and matched propeller system.

## 4.  MANEUVER COMPUTATIONS

All ship maneuvers that will be considered belong to one of two types: acceleration of the ship, and deceleration of the ship.  In the acceleration maneuvers, the ship is assumed to initially be cruising at a given constant speed and it is desired to increase it by raising the power to the motors.  In the deceleration maneuvers, the ship is either slowed down or even crash stopped.

From the motor torque equation (Eq. 26), it is clear that the torque is only related to the amplitude of the current supplied to the motor.  On the other hand, the torque developed by the propeller depends on its rotational speed (Eq. 5).  These two variables are independent, as far as both the source and the motor are concerned; however, they are connected through the dynamics of the system, which serves as a constraint for the controller.  The propeller requires change in rotational speed in order to change the torque it delivers, the change time history is determined by the solution to the equations of motion with the torque of the motor being the driving force.  Any other change in rotational speed will either not take advantage of the fuel cell capability when using a slower rate of motor rotation acceleration or, will stall the motor if faster motor rotation acceleration is used.

Due to the fact that the time constant of the ship is much larger than the time constant of the propulsion system, the determining factor in the maneuver is the capability of the fuel cell to provide current.

The fuel cell voltage is assumed to be constant throughout the maneuvers; therefore, the power output is proportional to the torque of the motor.

### 4.1  Fixed Pitch Maneuvers

The current ship-propulsion system model assumes that fixed pitch propellers are utilized.

#### 4.1.1  Acceleration Maneuver

Let the maneuver be defined in terms of the percentage of available power for propulsion.  Then, the maneuver is determined by the final power required from the fuel cell; the motor torque and the motion of the ship follow the fuel cell power curve between the two power levels.

In order to slow down the ship, the maneuver follows the fuel cell power curve to the terminal power level.

The fuel cell available power for consumption by the motors is the power that is supplied beyond the power consumed by the ship services:

$$P_{FC_0} = P_{Services} + P_{FC_{Shaft}}(V_0) = P_{Services} + R(V_0)V_0$$

where, $V_0$ is the steady-state initial velocity of the maneuver.

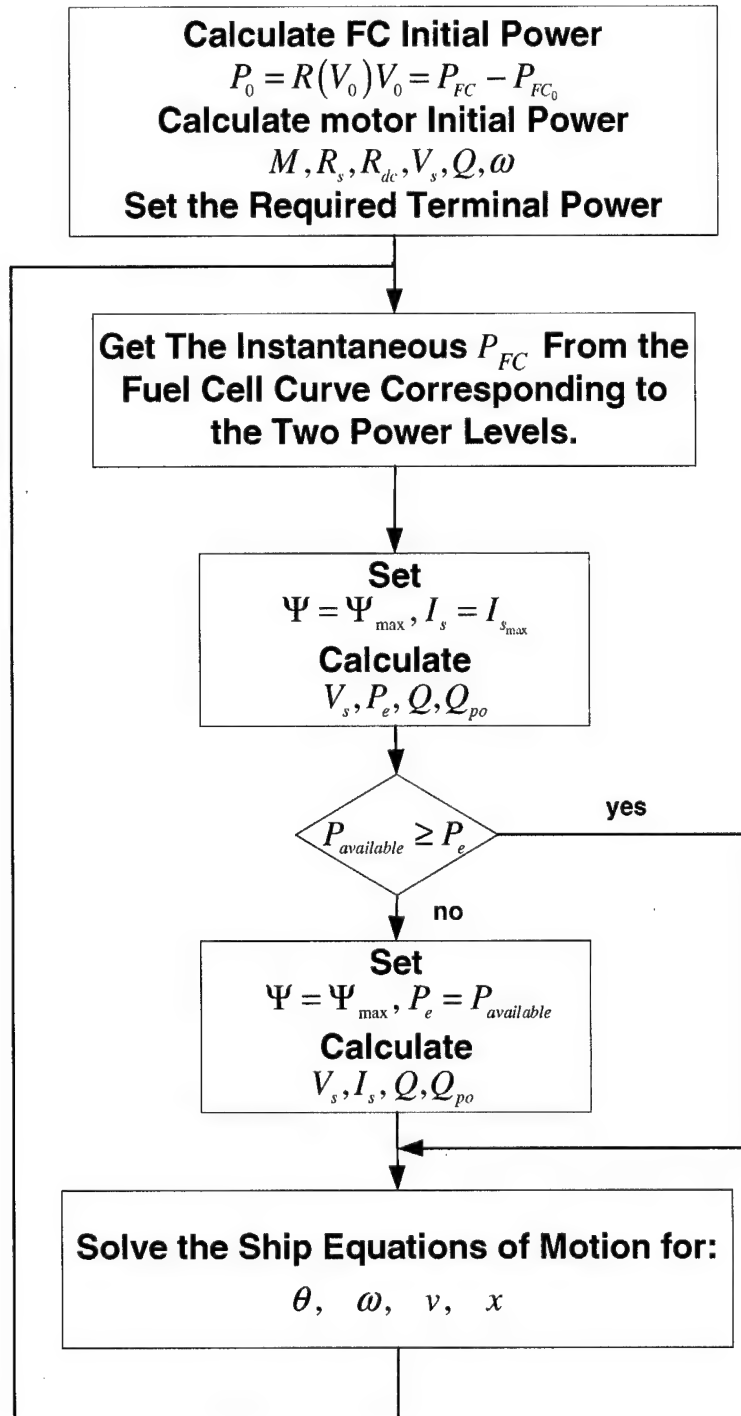The algorithm for the acceleration maneuver is summarized in Figure D-5.

**Calculate FC Initial Power**

$$P_0 = R(V_0)V_0 = P_{FC} - P_{FC_0}$$

**Calculate motor Initial Power**

$$M, R_s, R_{dc}, V_s, Q, \omega$$

**Set the Required Terminal Power**

**Get The Instantaneous $P_{FC}$ From the Fuel Cell Curve Corresponding to the Two Power Levels.**

**Set**

$$\Psi = \Psi_{max}, I_s = I_{s_{max}}$$

**Calculate**

$$V_s, P_e, Q, Q_{po}$$

$$P_{available} \geq P_e$$

**yes**

**no**

**Set**

$$\Psi = \Psi_{max}, P_e = P_{available}$$

**Calculate**

$$V_s, I_s, Q, Q_{po}$$

**Solve the Ship Equations of Motion for:**

$$\theta, \quad \omega, \quad v, \quad x$$

Figure D-5.  The Acceleration/Deceleration Maneuver Algorithm Using *n* Motors

### 4.1.2 Deceleration Maneuver

It is assumed that regeneration is not applied and that venting is not permitted. This way no excess fuel is generated during the deceleration maneuvers.

For deceleration maneuvers with a fixed pitch propeller, there is a need to reverse the direction of rotation of the shaft. Therefore, the maneuver is composed of two sections:

- Reduce torque following the power curve to the idle fuel cell power (zero propulsion power),

- When the propeller rotational speed reaches zero, switch propeller rotational direction and follow the power up curve corresponding to maximum fuel cell power.

The algorithm for the deceleration maneuver is summarized in Figure D-5.

### 4.1.3 Crash Stop Maneuver

In crash stop it is desired to slow down the ship in minimum distance. Using a fixed pitch propeller, there is a need to reverse the direction of rotation of the shaft as soon as possible. Therefore, the maneuver is composed of two sections:

- Disconnect the motor from the AC and DC power supplies,

- Dissipate the power by directing it to an active load,

- When the propeller rotational speed reaches zero, switch propeller rotational direction and follow the power up curve corresponding to maximum fuel cell power.

The algorithm for the crash stop maneuver is summarized in Figure D-6.
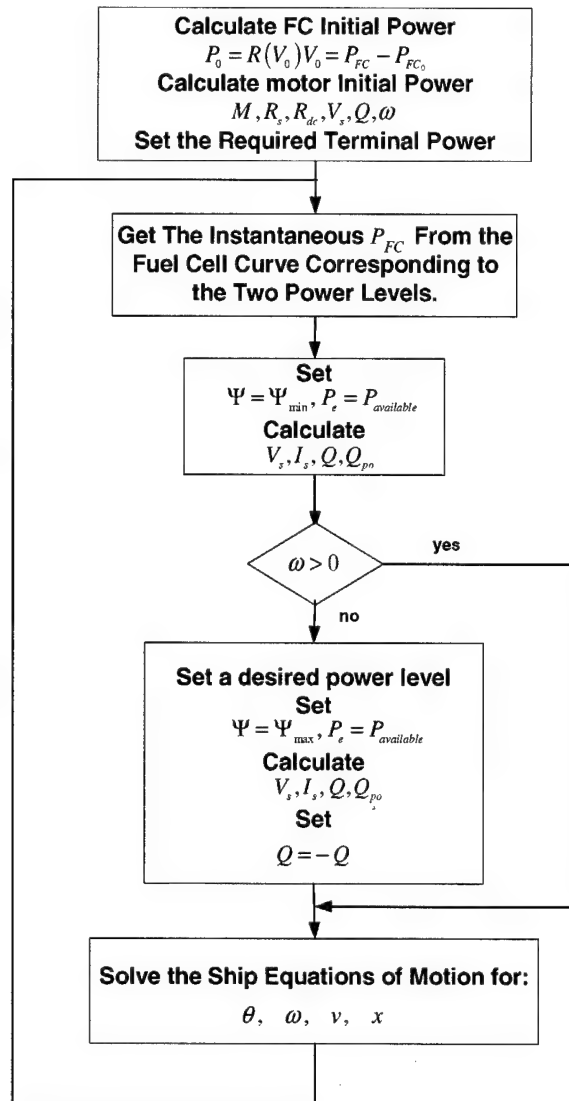
Figure D-6.  The Crash Stop Maneuver Algorithm Using *n* Motors

# 5.  THE INTEGRATED SHIP MODEL

The ship system is modeled as a power network.

## 5.1.  Data Flow Diagram

The network comprises three blocks:

1)  The Fuel Cell Power Unit – the unit is composed of two sub-units:

   - The Fuel Cell and its Controller – provides the transient power-up/power-down characteristics of the fuel cell unit given the initial and terminal power levels,

- The Inverter and its Controller – converts the DC power output of the fuel cell into 3-phase AC power instantaneously and with high efficiency (~98%),

2) AC Motor and its Controller – provides torque and mechanical power at various rotational speeds without exceeding power limitations,

3) The Ship Model

- Provides the dynamics of the ship and the propeller,

- Defines the maneuver demand curve.

Figure D-7 provides the Data Flow Diagram (DFD) for the simulation network, which specifies the routes of data flow between the major blocks of the fuel cell powered propulsion system.
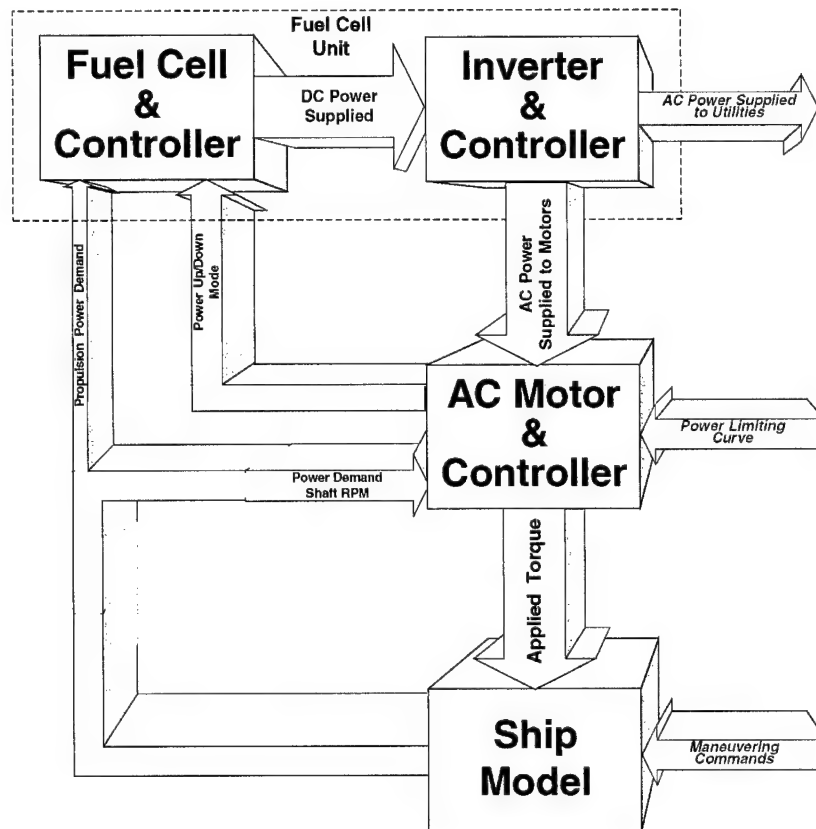


Figure D-7. DFD of the Propulsion System

## 5.2. Network Diagram

It is assumed that the ship is similar in size and weight to a T-AGOS Class size ship. Therefore, the ship parameters are chosen to be similar to the parameters of the T-AGOS Class size ship.

The following component parameters are used in the construction of the SIMSMART™ model:

### 5.2.1    Power Production

Each fuel cell provides 625 kW of DC power, approximately ten percent (62.5kW) of which is consumed by the fuel cell's balance of plant components.  The remainder is converted to 440V 60 Hz AC power and fed to the ship's main bus.  For purposes of the dynamic simulation study, it is assumed that full propulsion power can be generated by two fuel cells, with a third cell providing auxiliary power for hotel and other ship service loads.  The fourth cell is reserved for emergency loads.  This is similar to the existing configuration, where three diesel generators provide propulsion and ship service power, and the fourth is reserved for emergency loads.

### 5.2.2    Power Distribution

The power for the ship to generated by four synchronized[12] fuel cell power plants.  The plants feed power in parallel to a main bus and have a (controlled) constant power factor of 0.8 with respect to the load.  Each motor is equipped with an individual VSDCU.  The VSDCU are connected to the bus and draw the excess current, which is not used by the ship utilities.

The configuration of the system is summarized in Figure D-8.
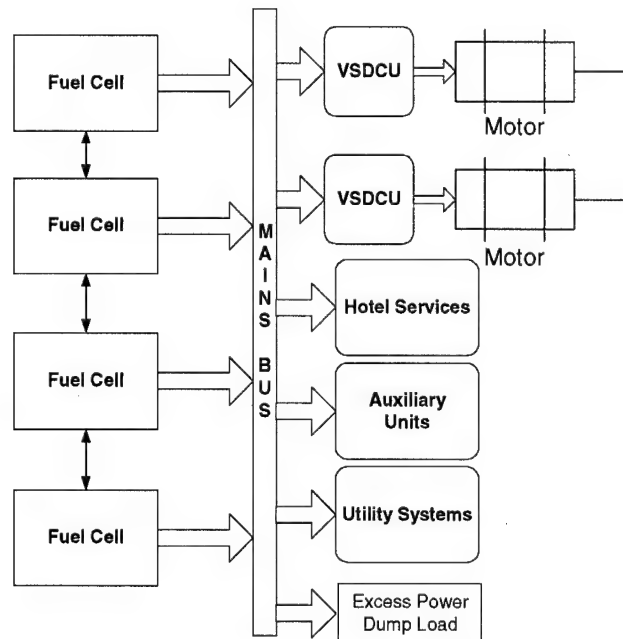


Figure D-8.  Ship power distribution configuration.

---

[12] The synchronization is required so that the voltage and the current amplitudes will add up; lack of synchronization would result in reduced amplitudes.

### 5.2.3   The Main Bus

The Main Bus is controlled so that any excess power generated by the fuel cell and not used by the loads is dumped on a dedicated variable load.

### 5.2.4   The VSDCU

The VSDCU issues power demand to the fuel cells in terms of percentage of power allocated to propulsion.  Due to the fact that all the fuel cells feed a common bus, the demand is distributed equally among the fuel cells and depends on the initial power supplied.  Therefore, the power demand change for each fuel cell is given by:

$$\Delta P_{FC} = \frac{\Delta P_s}{2}$$

where, $0 \leq \Delta P_s \leq 562.5 KW$ is the change in demand at the shaft.  The initial power is simply given by:

$$P_{FC_0} = \frac{1}{4}\left(2P_s + P_{Util}\right)$$

where, $P_{Util}$ is the power consumed by the utilities, hotel services, and the auxiliaries.

**VSDCU** efficiency: $\eta_i = 0.98\%$.

### 5.2.5   The Propulsion Motor

The ship is assumed to be equipped with two DC electric propulsion motors.  Due to the fuel cell control over the power factor it is assumed that the motors are operating at the fixed power factor of 0.8.

Let the following parameters represent the motor:

*   Number: 2,
*   Rated power of each motor: $P_r$=562.5KW,
*   Number of poles in the motor armature: p=10,
*   Rated line voltage (effective): $V_{L_{rated}}^e = 2000V$ ,
*   Rated pullout torque factor: α=1.5,
*   Rating rotational frequency: $f_r$=3Hz,
*   Rated DC control voltage: $V_{r_{rated}} = 2000V$ ,

- Rated DC power: 2.5KW,

- Total efficiency @ rated conditions: $\eta_m$=97%,

- Mass Moment of Inertia of rotor: 1015Kgm$^2$,

- Mass of motor: 8000Kg

The consequences of the above parameters as reflected in the motor model developed above:

- Stator $I^2R_s$ losses: 2.5KW,

- Rotor resistance: R$_r$=6.25$\Omega$,

- Stator resistance: R$_r$=0.052$\Omega$,

- Mutual apparent induction: M=4.0H,

- Rated line current (per phase) effective: $I^e_{L_{rated}} = 200.5A$,

- Rated Pullout torque: $Q_{po\_rated} = 43420\,\text{Nm}$,

- Rated pullout effective current (per phase): $I^e_{L_{po\_rated}} = 255.5\,\text{A}$.

Where, the pullout current is calculated from:

$$\alpha = \frac{Q_{Electric_{po}}}{Q_{Electric_{rated}}} = \frac{I_{L_{po}}}{I_{L_{rated}}} \frac{\sin\left(\frac{\pi R_r}{3MI_{L_{po}}V_r}Q_{Electric_{po}}\right)}{\sin\left(\frac{\pi R_r}{3MI_{L_{po}}V_r}Q_{Electric_{rated}}\right)}$$

$$\Rightarrow I_{L_{po}} = \alpha I_{rated} \frac{\sin\left(\frac{\pi R_r}{3MI_{L_{po}}V_r}\frac{Q_{Electric_{po}}}{\alpha}\right)}{\sin\left(\frac{\pi R_r}{3MI_{L_{po}}V_r}Q_{Electric_{po}}\right)} = \alpha I_{rated} \frac{\sin\left(\frac{\pi}{2\alpha}\right)}{\sin\left(\frac{\pi}{2}\right)} = 1.299 I_{rated}$$

### 5.2.6   The VSDCU

Current limiting curve is a constant about 5% below the rated current: $I^e_{rated} = 190A$,

### 5.2.7   The Ship

- Mass (w/o propulsion system): 3,120,000Kg

- The Resistance Curve is given by (see Figure D-9):

$$R(V) = 1.965 \times 10^4\, V - 1.739 \times 10^3\, V^2 + 307.3 V^3$$

The resistance is given in lbf as a function of the ship speed given in Kts.
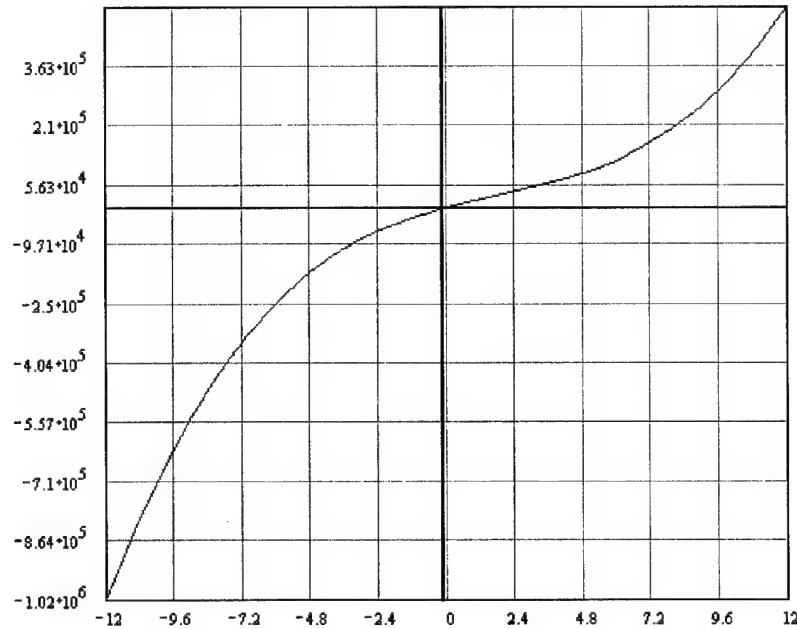


Figure D-9.  The Ship Resistance (lbf) as a Function of Ship Speed (Kt)

## 5.2.8    The Propeller

The model assumes a variable pitch propeller, although a fixed pitch was used for the acceleration and crash stop simulation exercises:

- Number of Propellers: 2,
- Diameter: D=2.457m,
- Pitch: P=3.58m,
- Advance Velocity Loss Factor: $\mu$=0.9,
- Mass Moment of Inertia: 426.6Kgm$^2$,
- Mass: 1,411Kg.

## 5.2.9    The Propulsion Shaft

- Mass Moment of Inertia: 312.9Kgm$^2$
- Mass: 9675Kg
- Efficiency: $\eta_s$=0.9.

## 7. REFERENCES

[1] "Narrative Description of Marine Fuel Cell Module," Fuel Cell Energy, Inc. Report No. 1, Rev. 0, March 2000.

[2] "Descriptions of Steady-State and Dynamic Simulation Models for Marine Fuel Cell System", Fuel Cell Energy, Inc. Report No. 2, Rev. 0, March 2000.

[3] "500KW Molten Carbonate Fuel Cell Demonstration Module - Dynamic Simulation Model Technical Report", JJMA, Oct 1998.

[4] G. McPherson, and R. D. Laramore, **An Introduction Electrical Machines and Transformers**, 2nd Edition, John Wiley & Sons, 1990.

[5] P. C. Krause, O. Wasynczuk, S. D. Sudhoff, **Analysis of Electric Machinery**, 1995.

[6] T. Wildi, **Electrical Machines, Drives, and Power Systems**, Prentice Hall, 1991.

[7] Report 5016-2, Thrust and Torque Coefficients, SSPA, Marine Consulting,

## 7. MATHEMATICAL SUPPLEMENTS

### 7.1 Trigonometric Identities

The following are trigonometric identities used in the derivations of the model of the 3-phase synchronous motor:

4) $\quad \sin\left(\alpha - \dfrac{2\pi}{3}\right) + \sin\alpha + \sin\left(\alpha + \dfrac{2\pi}{3}\right) = 0$

5) $\quad \cos\left(\beta - \dfrac{2\pi}{3}\right) + \cos\beta + \cos\left(\beta + \dfrac{2\pi}{3}\right) = 0$

6) $\quad \sin\left(\alpha - \dfrac{2\pi}{3}\right)\cos\left(\beta - \dfrac{2\pi}{3}\right) + \sin\alpha\cos\beta + \sin\left(\alpha + \dfrac{2\pi}{3}\right)\cos\left(\beta + \dfrac{2\pi}{3}\right) = \dfrac{3}{2}\sin(\alpha - \beta)$

7) $\quad \cos\left(\alpha - \dfrac{2\pi}{3}\right)\cos\left(\beta - \dfrac{2\pi}{3}\right) + \cos\alpha\cos\beta + \cos\left(\alpha + \dfrac{2\pi}{3}\right)\cos\left(\beta + \dfrac{2\pi}{3}\right) = \dfrac{3}{2}\cos(\alpha - \beta)$

### 7.2 The Ritz Method

The Ritz method is a method for calculating the approximate solutions to differential equations. Consider the following ordinary differential equation:

$$L\big(u(t)\big) = f(t)$$

where, $L(\bullet)$ is a differential operator in time. The approximate solution $\hat{u}(t)$ is sought from amongst the family of candidate functions of the form:

$$\hat{u}(t) = \sum_{i=1}^{N} C_i \varphi_i(t)$$

where, the $C_i$'s are unknown constants, and $\varphi_i$'s are linearly independent basis functions. According to the Ritz method, the unknowns are the solution to the following set of algebraic equations:

$$\int_0^T \left[ L(\hat{u}) - f \right] \varphi_i \, dt = 0 \quad , \qquad i = 1, \ldots, N$$

where, in the case of harmonic basis function $T = \dfrac{2\pi}{\omega}$ (the period of one oscillation) where $\omega$ is the angular velocity of the oscillation.

# APPENDIX E.

# USER INTERFACES - DISPLAYS

# USER INTERFACES - DISPLAYS

The fuel cell performance data are prepared prior to the execution of the SIMSMART$^{TM}$ simulation program by running a Matlab$^{TM}$ program that contains the code representing most the building blocks of the fuel cell. Appendix A expands on this subject. SIMSMART$^{TM}$, the commercial program that was selected by NAVSEA for fluid systems simulations, is the principal tool that runs the Dynamic Simulation Model (DSM). Graphic presentation of variables and parameters can be followed on screen, or can be tabulated after a simulation using Excel for plotting "trend" presentations. Samples of the output screens are presented in the following pages.

Figure E-1 presents a screen that contains icons of the ship, the electric motor, the fuel cell and the Balance of plant. These icons are interconnected, and as shown in Figure E-2 flow data can be presented next to the icons of connecting piping.
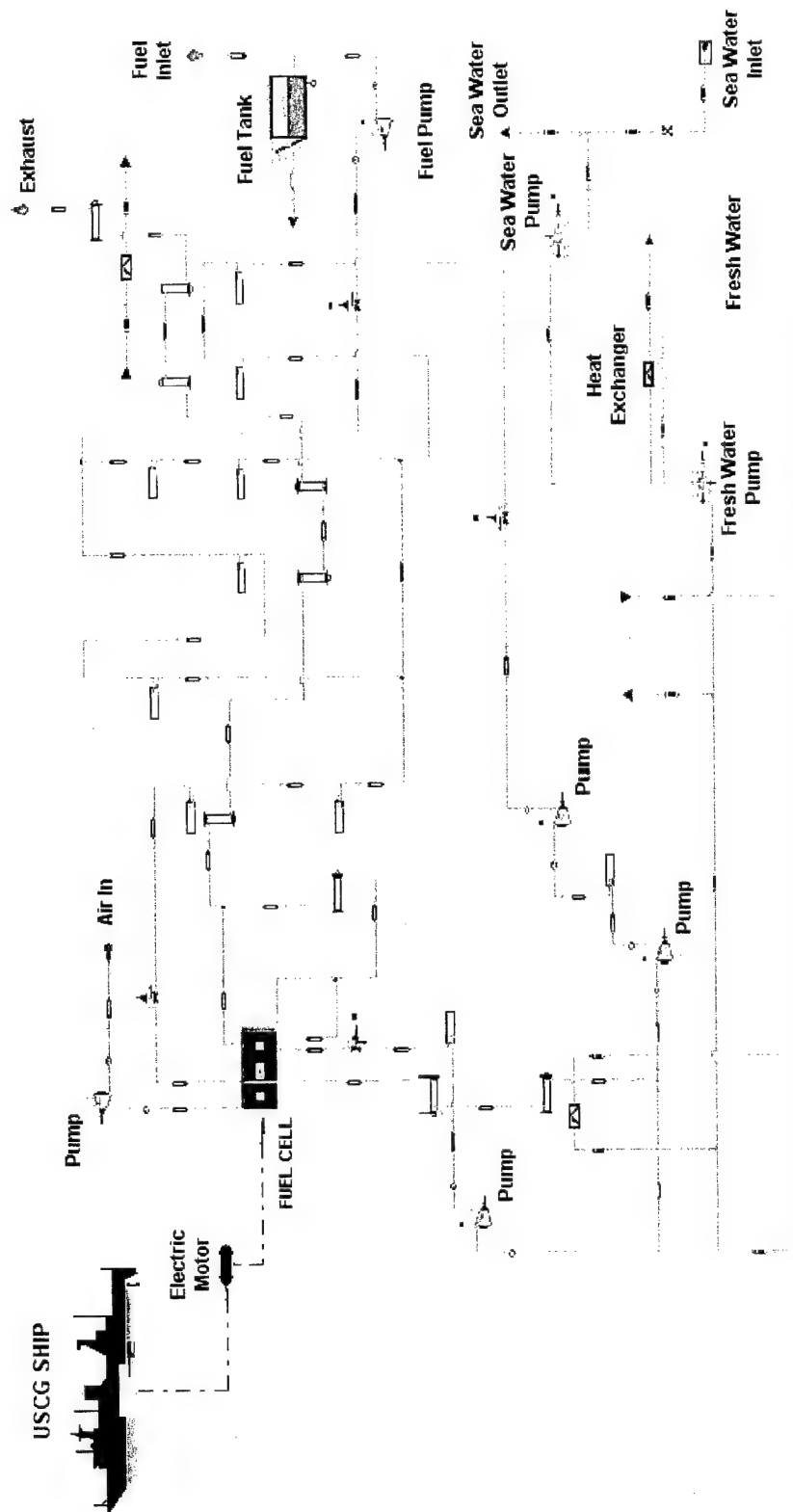
Figure E-1.  SIMSMART™ Screen – Balance of Plant
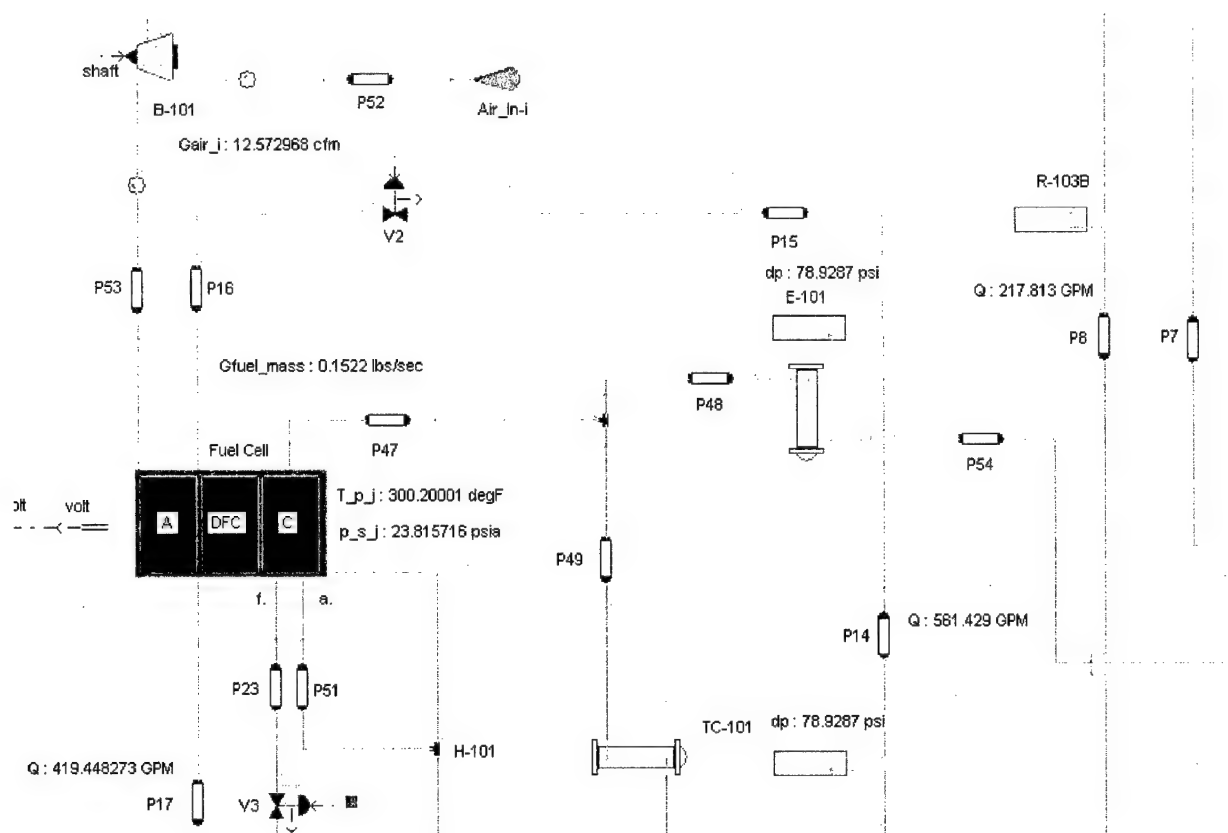
Figure E-2. SIMSMART$^{TM}$ Screen – Close-up about Fuel Cell

Figures E-3 and E-4 show additional modes of on-screen data. Data variables can be presented in groups (see Figure E-3), or a run time Data Access Window can be opened and used to modify data values while running the simulation program (see Figure E-4).

Figure E-5 shows an Access Pull-Down Menu for data manipulation while the simulation program is running.

New and updated icons integrated into the current program are presented in Figures E-6 through E-11. Each icon has imbedded in it a full mathematical description of its dynamic and static characteristics. The ship icon in Figure E-10, for example, has imbedded in it the ship's resistance curves, the propeller curves, the mass inertias of the ship and shafting components, and the equations of motion for the ship and of the shafting.
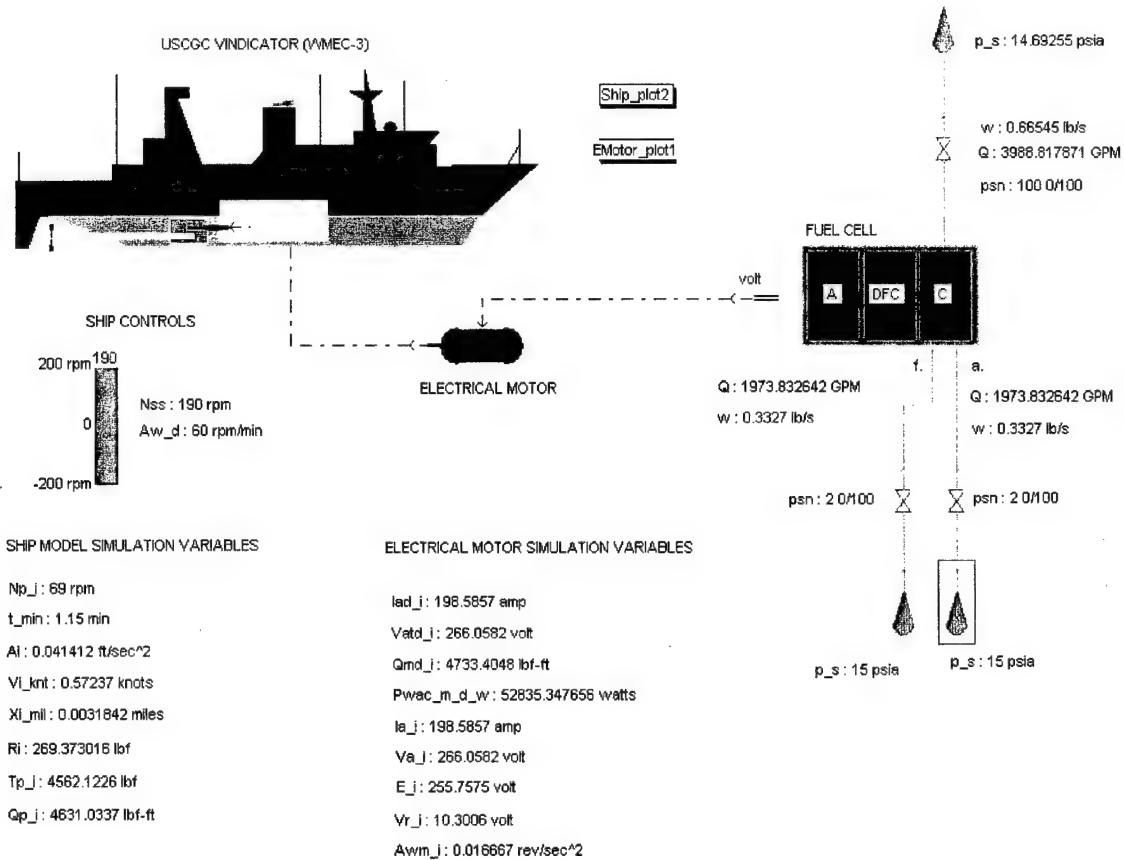
Figure E-3.  SIMSMART$^{TM}$ Screen – Simplified with Simulation Variables
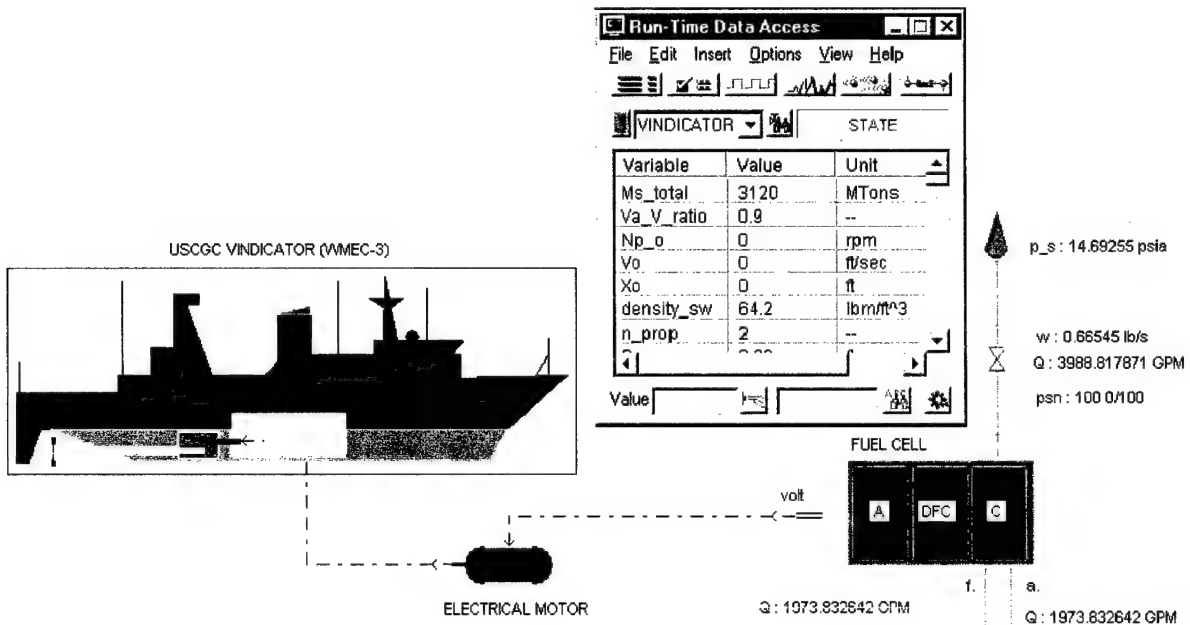


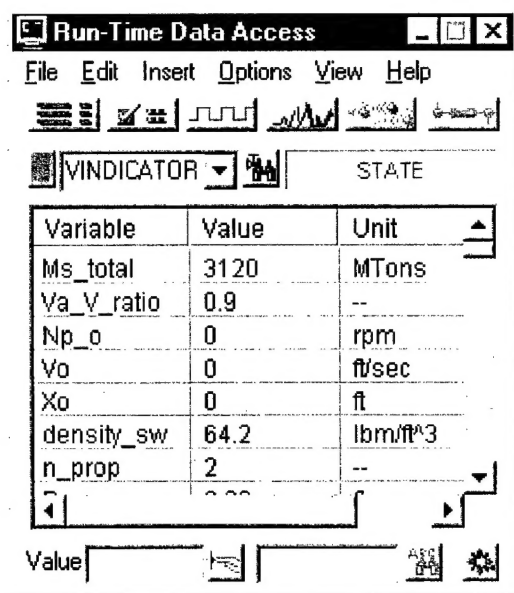Figure E-4.  SIMSMART$^{TM}$ Screen – Simplified System with Run-Time Data

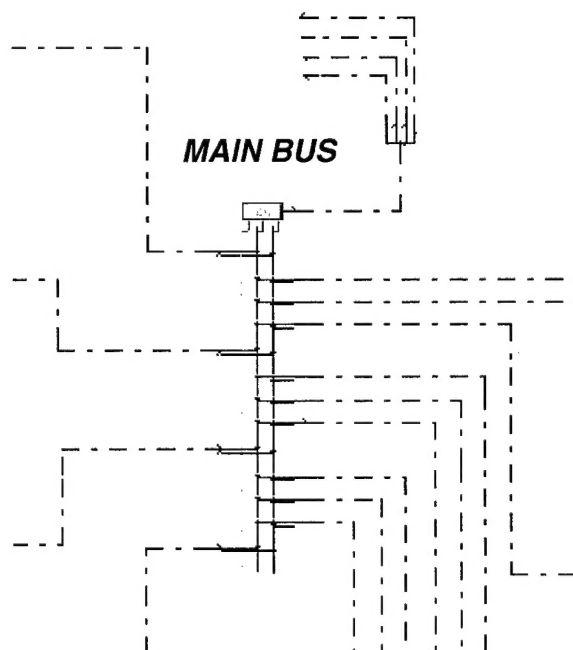Figure E-5. SIMSMART$^{TM}$ Screen – Run-Time Data Access Pull-Down Menu



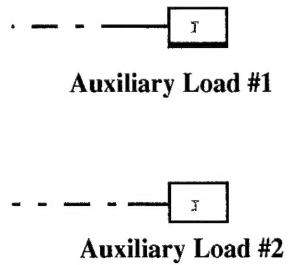Figure E-6. Ship's Main Bus Icon

# SHIP AUXILIARY LOADS

**Auxiliary Load #1**

**Auxiliary Load #2**

Figure E-7. Ship Auxiliary Loads Icon

# RHEOSTAT

**Rheostat**
(Excess Load Dissipated)

Figure E-8.Rheostat Icon

# AC SYNCHRONOUS PROPULSION MOTORS
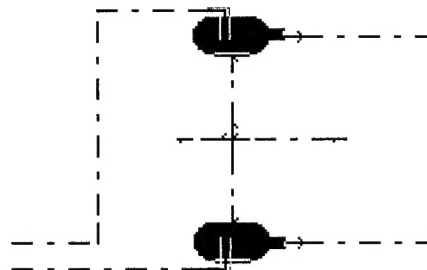
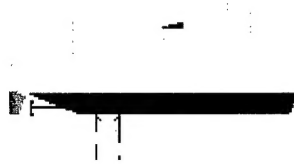Figure E-9. AC Synchronous Propulsion Motors Icon

## *USCG SHIP*

Figure E-10.  USCG Ship Icon

The fuel cell icons, see Figure E-11, have embedded within each icon the dynamic characteristics of the fuel cell.  The data for these icons is pre-generated.  Figure E-12 presents the assembly of the icons used to represent the complete powering system of the ship, including the complete load and control logic system.

## *MARINE FUEL CELL MODULES*

**Marine Fuel Cell #1**

**Marine Fuel Cell #2**

**Marine Fuel Cell #3**
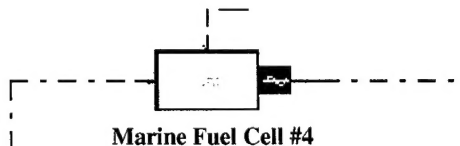
**Marine Fuel Cell #4**

Figure E-11.  Marine Fuel Cell Modules Icon

## REAL TIME DYNAMIC SIMULATION MODEL OF A SHIP
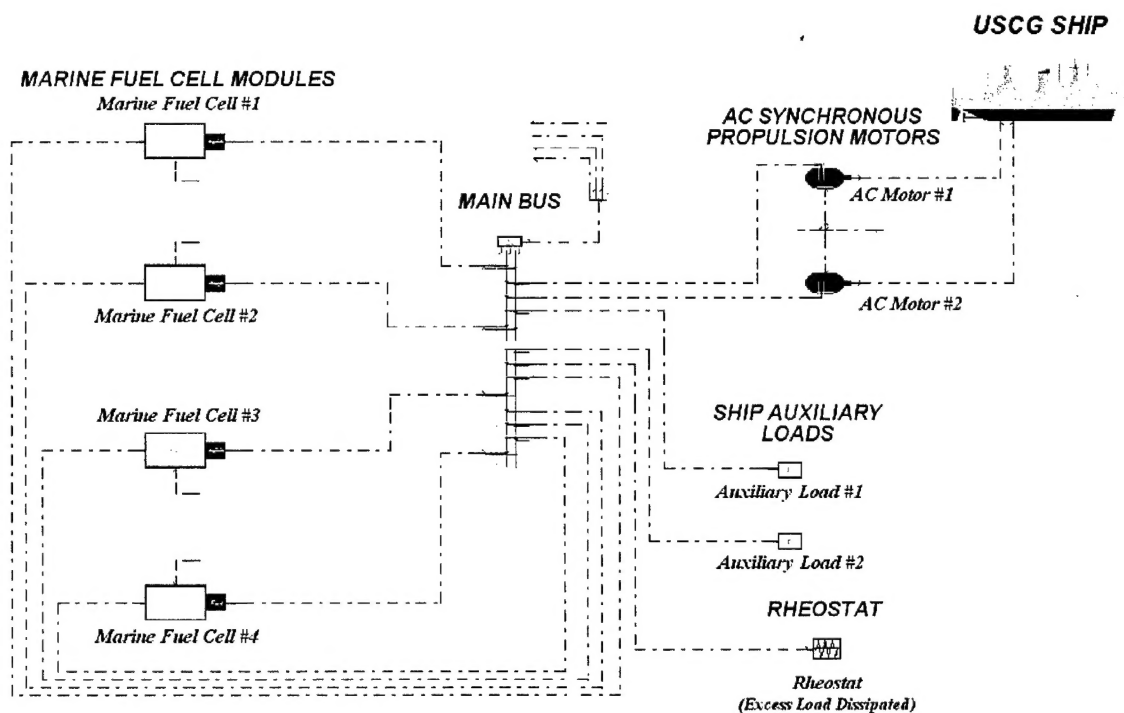## MARINE FUEL CELL POWERED PROPULSION SYSTEM



Figure E-12.  Dynamic Simulation - Marine Fuel Cell Powered Electrical System Assembly